General Disclaimer

One or more of the Following Statements may affect this Document

- This document has been reproduced from the best copy furnished by the organizational source. It is being released in the interest of making available as much information as possible.

- This document may contain data, which exceeds the sheet parameters. It was furnished in this condition by the organizational source and is the best copy available.

- This document may contain tone-on-tone or color graphs, charts and/or pictures, which have been reproduced in black and white.

- This document is paginated as submitted by the original source.

- Portions of this document are not fully legible due to the historical nature of some of the material. However, it is the best reproduction available from the original submission.

Produced by the NASA Center for Aerospace Information (CASI)

Jack M

SD 68-29

MASS-LOADING EFFECTS ON VIBRATION OF RING AND SHELL STRUCTURES

(CONTRACT NAS8-20019, PHASE III)

February 1968

Prepared by

S. Y. Lee
S. S. Tang
J. G. Liyeos

Approved by

S. Y. Lee, Project Engineer

F. C. Hung, Program Manager

Structures & Design Dept., Research, Engineering & Test

SPACE DIVISION
NORTH AMERICAN ROCKWELL CORPORATION

DEC 1968
RECEIVED
NASA STI FACILITY
INPUT BRANCH

N69-13250
(ACCESSION NUMBER) 1
(THRU)
136
(PAGES)
(CODE)
CR 98578
(NASA CR OR TMX OR AD NUMBER)
32
(CATEGORY)
FACILITY FORM 602

SM-53791

SD 68-29

MASS-LOADING EFFECTS ON VIBRATION OF RING AND SHELL STRUCTURES

(CONTRACT NAS8-20019, PHASE III)

February 1968

Prepared by

S. Y. Lee
S. S. Tang
J. G. Liyeos

Approved by

S. Y. Lee, Project Engineer

F. C. Hung, Program Manager

Structures & Design Dept., Research, Engineering & Test

SPACE DIVISION
NORTH AMERICAN ROCKWELL CORPORATION

PRECEDING PAGE BLANK NOT FILMED.

FOREWORD

This report is a description of the third-phase work performed under NASA Contract NAS8-20019, Mass Loading Effects on Localized Vibratory Environments of Rocket Vehicles, by the Space Division (SD) of North American Rockwell Corporation (NR) for the George C. Marshall Space Flight Center, Huntsville, Alabama, during the period of 1 December 1966 to 30 March 1968.

The project was sponsored and administered under the direction of Mr. J. Farrow, Branch Chief, and Mr. R. Schock, Section Chief, of the Vibration and Acoustics Branch, Propulsion and Vehicle Engineering Division, NASA/MSFC.

The work was conducted at NR/SD by S. Y. Lee, Project Engineer and Principal Investigator, who directed the project activities, developed analytical and experimental methods, and solved the mass-loaded and unloaded shell problems; S. S. Tang, who as a staff investigator, performed the free-vibration analysis of the mass-loaded ring structure by transfer matrix approach, assisted in project coordination and was responsible for test specimens design, test monitoring, data reduction, and results comparison; and J. G. Liyeos, also a staff investigator, who was responsible for computer programming and numerical evaluations.

The authors wish to express their appreciation to Messrs. J. Farrow, R. Schock, R. Jewell and C. Lifer of NASA/MSFC for their direction and encouragement, to Mr. C. Bailey of NR/LAD for his assistance in test operations, to Dr. R. Guyan of NR/SD for his contribution in the development of the free vibration analysis of mass-loaded ring structure by the finite-element method, and to Professor M. P. Bienick for his consulation.

TECHNICAL REPORT INDEX/ABSTRACT

ACCESSION NUMBER						DOCUMENT SECURITY CLASSIFICATION	
						UNCLASSIFIED	

TITLE OF DOCUMENT

MASS LOADING EFFECTS ON VIBRATION OF RING AND SHELL STRUCTURES

LIBRARY USE ONLY

AUTHOR(S)

LEE, S.Y. *TANG, S.S. *LIYEOS, J.G.

CODE	ORIGINATING AGENCY AND OTHER SOURCES	DOCUMENT NUMBER
	NORTH AMERICAN ROCKWELL CORP., SPACE DIVISION	SD68-29

PUBLICATION DATE	CONTRACT NUMBER
00FEB68	NAS8-20019

DESCRIPTIVE TERMS

*VIBRATION, *RING, *SHELL, *MASS LOADING EFFECTS

ABSTRACT

THE EFFECTS OF THE ATTACHMENT OF DISCRETE MASSES ON THE VIBRATION CHARACTERISTICS OF RING AND SHELL STRUCTURES WERE STUDIED. ANALYTICAL RESULTS WERE SUBSTANTIATED BY EXPERIMENTAL DATA. ANALYTICALLY, THE SERIES EXPANSION TECHNIQUE WAS USED IN SOLVING THE MASS LOADED SHELL PROBLEM WHILE BOTH THE FINITE-ELEMENT AND TRANSFER-MATRIX METHODS WERE EMPLOYED IN THE ANALYSIS OF MASS LOADED RING STRUCTURES. EXPERIMENTALLY, ALUMINUM RING AND SHELL STRUCTURES LOADED WITH A SERIES OF DISCRETE MASSES WERE EXCITED BY A MAGNETIC INDUCTION METHOD. THE VIBRATORY MOTION WAS MEASURED BY AN AUTOMATICALLY REVOLVING PROXIMITY GAGE. THE INFLUENCE OF THE MASS OF THE EXCITER AND THAT OF THE INSTRUMENTATION, HENCE, WERE ELIMINATED. RESPONSE DATA WERE OBTAINED WITH MINIATURE ACCELEROMETERS AS WELL AS PROXIMITY GAGE FOR COMPARISON PURPOSES. IN ADDITION TO THE AMPLITUDE CHANGES OF THE LOCAL VIBRATION RESPONSE CAUSED BY THE ADDITION OF THE DISCRETE MASSES THE STUDIES ALSO SHOW THE FREQUENCY SHIFTS, THE CHANGE OF MODAL BEHAVIOR AND THE TRANSMISSIBILITY CHARACTERISTICS RESULTED FROM THE INCREASED DISCRETE MASS OF THE STRUCTURE. THE RESULTS SHOW THAT THE PROCEDURE CURRENTLY RECOMMENDED BY NASA/MSFC FOR PREDICTING THE AMPLITUDE REDUCTION OF THE LOCAL VIBRATION RESPONSE OF UNLOADED STRUCTURE TO ACCOUNT FOR THE INFLUENCE OF THE ADDITION OF THE MASSES, PROVIDES A FAIR APPROXIMATION IN THE FIRST VIBRATION MODE BUT IS OVERLY CONSERVATIVE FOR HIGHER MODES.

ABSTRACT

Efficient methods for predicting the effects of attached masses on the vibration characteristics of ring and shell structures were developed and substantiated with experimental data. Analytically, the series expansion technique was used in solving the mass-loaded shell problem, while both the finite-element and transfer-matrix methods were employed in the analysis of mass-loaded ring structures. Experimentally, aluminum ring and shell structures loaded with discrete masses were excited by a electrical induction force, and the vibratory motion was measured by an automatically revolving proximity gage. The influences of the masses of the exciter and of the instrumentation, thus, were eliminated. Response data were obtained with miniature accelerometers and with a proximity gage for comparison purposes. The studies show, in addition to the amplitude changes of the local vibration response caused by the addition of the discrete masses, the frequency shifts, the change of modal behavior, and the transmissibility characteristics resulting from the increased discrete mass on the structure. The results show (1) that the response attenuation for the first mode was somewhat similar to the procedure currently recommended by NASA/MSFC for predicting the amplitude reduction of the local vibration response of unloaded structure to account for the influence of the addition of the mass; (2) that for higher modes, much more amplitude reductions were found, and the rate of amplitude reduction progressed very rapidly; and (3) that the transmissibility characteristics in a function of normal modes, indicated some differences for beams, plates, honeycomb plates, rings, and shells.

PRECEDING PAGE BLANK NOT FILMED.

CONTENTS

Section		Page
1.0	INTRODUCTION	1
2.0	DYNAMIC ANALYSIS OF MASS-LOADED RINGS TRANSFER MATRIX METHOD	5
3.0	DYNAMIC ANALYSIS OF MASS-LOADED RINGS BY FINITE-ELEMENTS METHOD	17
4.0	DYNAMIC ANALYSIS OF MASS-LOADED AND UNLOADED SHELLS	27
5.0	EXPERIMENTAL INVESTIGATION	39
6.0	COMPARISON OF ANALYTICAL AND EXPERIMENTAL RESULTS	53
7.0	CONCLUSIONS	109
8.0	REFERENCES	111
	APPENDIX	115

PRECEDING PAGE BLANK NOT FILMED.

ILLUSTRATIONS

Figure		Page
1	Coordinates and Sign Conventions of Rings	7
2	Lumped-Mass System of Ring	7
3	Beam Element	17
4	Coordinate Transformation	19
5	Computed Mode Shapes of Ring I, Mode 1, n = 2	23
6	Computed Mode Shapes of Ring I, Mode 2, n = 3	24
7	Computed Mode Shapes of Ring I, Mode 3, n = 4	25
8	Computed Mode Shapes of Ring I, Mode 4, n = 5	26
9	Mass-Loaded Shell	29
10	Vibration Test Set-up for Ring	41
11	Vibration Test Set-up for Shell	43
12	Proximity Gage Set-up for Plotting Radial Mode Shapes of Shell	44
13	Accelerometers Set-up for Vibration Test of Mass-Loaded Shell	45
14	Instrumentation Set-up for Vibration Tests of Ring and Shell, Part I	46
15	Instrumentation Set-up for Vibration Tests of Ring and Shell, Part II	47
16	Comparison of Natural Frequencies of Rings, Modes 1, 2, and 3	58
17	Comparison of Natural Frequencies of Rings, Modes 4 and 5	59
18	Comparison of Frequency Ratio of Ring I, Mode 1	60
19	Comparison of Frequency Ratio of Ring I, Mode 2	61
20	Comparison of Frequency Ratio of Ring I, Mode 3	62
21	Comparison of Frequency Ratio of Ring I, Mode 4	63
22	Comparison of Frequency Ratio of Ring I, Mode 5	64
23	Test Data of Mass Loading Effect on Natural Frequencies of Ring II	65
24	Mass-Loading Effect on Vibration Transmissibility of Ring	67
25	Mass-Loading Effect on Acceleration Response of Ring I, Mode 1	68
26	Mass-Loading Effect on Acceleration Response of Ring I, Mode 2	69

Figure		Page
27	Mass-Loading Effect on Acceleration Response of Ring I, Mode 3	70
28	Mass-Loading Effect of Acceleration Response of Ring I, Mode 4	71
29	Mass-Loading Effect of Acceleration Response of Ring I, Mode 5	72
30	Mass-Loading Effect of Acceleration Response of Ring II, Mode 1	73
31	Mass-Loading Effect of Acceleration Response of Ring II, Mode 2	74
32	Mass-Loading Effect of Acceleration Response of Ring II, Mode 3	75
33	Mass-Loading Effect of Acceleration Response of Ring II, Mode 4	76
34	Mass-Loading Effect of Acceleration Response of Ring II, Mode 5	77
35	Typical Mode Shapes of Mass-Loaded Ring	78
36	Mass-Loading Effect on Radial Acceleration Response of Ring II, Mode 1, n = 2	79
37	Mass-Loading Effect on Radial Acceleration Response of Ring II, Mode 2, n = 3	80
38	Mass-Loading Effect of Radial Acceleration Response of Ring II, Mode 3, n = 4	81
39	Mass-Loading Effect of Radial Acceleration Response of Ring II, Mode 4, n = 5	82
40	Mass-Loading Effect of Radial Acceleration Response of Ring II, Mode 5, n = 6	83
41	Mass-Loading Effect on Radial Acceleration of Shell	90
42	Comparison of Natural Frequencies of Shell I	92
43	Mass-Loading Effect on Natural Frequencies of Shell I, Mode 1	93
44	Mass-Loading Effect on Natural Frequencies of Shell I, Mode 2	94
45	Mass-Loading Effect on Natural Frequencies of Shell I, Mode 3	95
46	Mass-Loading Effect on Natural Frequencies of Shell I, Mode 4	96
47	Mass-Loading Effect on Natural Frequencies of Shell I, Mode 5	97
48	Mass-Loading Effect on Natural Frequencies of Shell II	98
49	Mass-Loading Effect on Acceleration Response of Shell I, Mode 1	99

Figure		Page
50	Mass-Loading Effect on Acceleration Response of Shell I, Mode 2	100
51	Mass-Loading Effect of Acceleration Response of Shell I, Mode 3	101
52	Mass-Loading Effect on Acceleration Response of Shell I, Mode 4	102
53	Mass-Loading Effect on Acceleration Response of Shell I, Mode 5	103
54	Mass-Loading Effect on Acceleration Response of Shell II, Mode 1	104
55	Mass-Loading Effect on Acceleration Response of Shell II, Mode 2	105
56	Mass-Loading Effect on Acceleration Response of Shell II, Mode 3	106
57	Mass-Loading Effect on Acceleration Response of Shell II, Mode 4	107
58	Mass-Loading Effect on Acceleration Response of Shell II, Mode 5	108

PRECEDING PAGE BLANK NOT FILMED

TABLES

Table		Page
1	Computed Natural Frequencies and Frequency Ratios of Rings	22
2	Comparison of the Theories of Cylindrical Shells	30
3	Computed Natural Frequencies (CPS) of Shell	36
4	Properties of Attached Masses	40
5	Vibration Test Runs for Unloaded and Mass-Loaded Rings	48
6	Vibration Test Runs for Unloaded and Mass-Loaded Shells Excited by Electroinduction Shaker	50
7	Vibration Test Data of Ring I With One Accelerometer on Ring	54
8	Vibration Test Data of Ring II With 16 Accelerometers on Ring	55
9	Comparison of Natural Frequencies of Rings, Cases 0 to 4	56
10	Comparison of Natural Frequencies of Rings, Cases 5 to 8	57
11	Vibration Test Data of Shell I Excited by Electro-induction Shaker, One Meter on Shell	86
12	Vibration Test Data of Shell I Excited by Electro-induction Shaker (Continued)	87
13	Vibration Test Data of Shell II Excited by Electro-induction Shaker, 20 Accelerometers on Shell	88
14	Vibration Test Data of Shell II Excited by Electro-induction Shaker (Continued)	89
15	Comparison of Natural Frequencies of Shell I	91

1.0. INTRODUCTION

Most aerospace equipment or components are affected by the dynamic behavior of the primary structures which generally consist of rings and shells. During the earlier studies of this program, emphasis was placed on investigations of the mass-loading effects on simple structures; i.e., beams, plates, and honeycomb plates. The present study, which is the third phase of the program, is a combined theoretical and experimental investigation of the mass-loading effects on ring and shell structures. Earlier exploratory studies by Lee (References 1 through 10) and the last two phases of this program (References 11 and 12) provided the background for the present investigation and formed the bases for the methods of approach.

Because of technical and financial considerations, the evolution of aerospace programs has been accompanied by great emphasis on the success of individual components and on the assembly of components and local structures. These components and local structures are subjected to crucial environments of shock, vibration, and acoustics during ground operations and in flight; nevertheless, insufficient design progress has been realized from related experience and practical applications in the areas of vibration, environmental prediction, dynamic analysis, testing, and evaluation.

Dynamic problems increase and, simultaneously, become more critical when local structures serve as supports for other components or pieces of equipment. In such cases, the dynamicist is confronted with two problems. One is the estimation of the effect of the equipment on the response of the supporting structure in order to predict realistically the vibratory environment experienced by the mounted component. The other is the calculation of the vibration response of the combined interacting system for the design of local structures.

In performing dynamic analysis, scientists and engineers have relied on experimental data or assumptions of the quality factor, complex modulus of elasticity, or damping factor in order to compute the vibration response of a structure. With respect to mass-loaded structures, however, two problems arise immediately: (1) the applicability of the experimental data or assumptions for unloaded structures to mass-loaded structures and (2) information to support the new assumptions for mass-loaded structures. In consideration of these two problems, one of the major objectives of this program is to explore the relationship between the transmissibility characteristics of the mass-loaded structures and those of the unloaded structures undergoing forced vibration and free vibration.

In the field of environmental dynamics, Mahaffey and Smith (Reference 14) published their study of the local vibration data of airplane flights in 1960. Eldred, Robers, and White (Reference 15) presented a similar investigation on aircraft and missiles in late 1961. In 1962, Franken (Reference 16) reported the results of his study on the vibration environment of Titan missiles. The data obtained from these studies have been widely used throughout the aerospace industry to predict dynamic environments for missiles and space vehicles. The primary concern during these studies, however, was the statistical regression of the airplane or missile flight vibration data at a given vehicle zone, and mass-loading effects specifically due to the mounted equipment were lacking. Presently, there is no unique method available for predicting mass-loading effects on vibration environment; therefore, another objective of this program study is to investigate these effects on environmental dynamics.

The first documentation of mass-loading effects on vibration environment appears to be Military Specification MIL-E-5272, but the mass-loading provision presented appears to have been determined rather arbitrarily. These mass-loading effects criteria were endorsed and specified in the new specification standards, MIL-STD-810, by an evaluation committee (Reference 17) of shock and vibration specialists consisting of Government and industry dynamics experts selected by the USAF in late 1962. No information could be found, however, regarding the author, the date of initiation, or the technical basis used in establishing the arbitrary mass-loading criteria.

During 1963-68, Schock, Barrett, Jewel, Winter and Lifer (References 18 through 23) of NASA/MSFC, aware of the mass loading phenomenon, introduced an empirical prediction technique that allowed some amplitude reduction of the vibration environment due to the increase of weights. The technique is a result of their statistical study of Saturn firing test data. They also initiated and recommended theoretical and experimental research studies to investigate the dynamic response phenomenon.

At the laboratory of the former Missiles Development Division of North American Rockwell Corporation, mass-loading effects on vibrating structures were observed by Lee in 1956. He later found these phenomena repeatedly in his work in connection with twelve missile and space systems at Douglas Aircraft Company. He initiated the analytical investigation of the vibration characteristics of mass-loaded structures, emphasizing the frequency shifts and modal isolation studies in research papers (References 1 and 6) in 1959 for the University of Southern California. In 1962, a preliminary experimental and theoretical investigation of the mass-loading and coupling problem was launched by Lee at the Space Division of North American Rockwell Corporation (References 3 and 4). A consistent trend of the

mass-loading effect on transmissibility characteristics then became apparent. These basic concepts were followed with further development through the first two phases of this program (References 11 and 12). After Lee's initial contact with NASA/MSFC in 1963, and following a technical presentation, this study program was first authorized in 1965 to correlate all of the aforementioned efforts and to develop a technique for predicting the mass-loading effects for beams, plates, and honeycomb plates. Subsequently, the investigation was expanded to include ring and shell structures. The analytical work of mass-loaded and unloaded shell structures was developed and carried out by Lee in conjunction with his graduate research work. The method of approach for analyzing mass-loaded and unloaded ring structures employing the transfer matrix approach was initiated in 1964 and used in this program (References 8 and 9); however, the ring problem was investigated further to obtain higher mode information by the finite-element computer program developed by Dr. Guyan of North American Rockwell Corporation.

The preliminary study results obtained by Lee and the subsequent findings resulting from this research program on the investigation of mass-loaded beams and plates show that the empirical technique developed by Schock, Barrett, Jewel, Winter and Lifer of NASA/MSFC represents a fair approximation for predicting amplitude attenuation in the first mode of the forced response of unloaded structures to account for the effect of the increase of masses; however, overconservatism is observed for higher modes. The present study includes the investigation of free vibration as well as forced vibration covering the phenomena of frequency shifts, modal behaviors, and transmissibility characteristics of mass-loaded structures as compared with those of the unloaded structures. The final objective of this study phase is to determine whether or not mass-loaded ring and shell structures will exhibit mass-loading phenomena that are identical with those previously established for mass-loaded beams and plates.

PRECEDING PAGE BLANK NOT FILMED.

2.0. DYNAMIC ANALYSIS OF MASS-LOADED AND UNLOADED RINGS BY TRANSFER MATRIX METHOD

The free vibration problem of a mass-loaded ring can be conveniently analyzed by the method of transfer matrix (References 8, 9, and 24). The ring is treated as a lumped-mass system with masses joined together by massless curved-beam elements as shown in Figures 1 and 2.

The nomenclature used in this section is as follows:

a	= width of attached mass
A	= cross-sectional area of ring
A_o	= cross-sectional area of attached mass
b	= length of attached mass
d	= distance between mass center and X-axis
E	= Young's modulus of ring
E_o	= Young's modulus of attached mass
g	= acceleration due to gravity
h	= ring thickness
H	= thickness of attached mass
i, j	= row and column number in matrices
I_x	= mass moment of inertia of ring element about X-axis
I_{x_o}	= mass moment of inertia of attached mass about X-axis
J_x	= area moment of inertia of ring element about X-axis

J_{x_o} = area moment of inertia of attached mass about X-axis

L = axial length of ring

m = mass of ring element

M = attached mass

M_x, M_z = bending moment about x and z axes, respectively

n = station number = 1, 2, 3, - - - r

N = tangential force in y direction

P = point matrix of lumped mass

r = total number of lumped masses or stations

R = radius of the central axis of ring

S = field matrix of elastic, curved-beam element

T = torsional moment about y-axis

u, v, w = ring displacements in x, y, and z direction, respectively

[U] = transfer matrix with elements u_{ij}

V_x, V_z = shearing forces in x and z directions, respectively

$\left|Z\right|$ = column matrix of the state vector

$= \left|v \; -w \; -\psi \; -M_x \; -V_z \; N\right|$

ϕ, ψ, θ = angles of rotation about x, y, and z axes, respectively

ψ = central angle between two stations in radians

γ = weight density of ring

ω = natural circular frequency

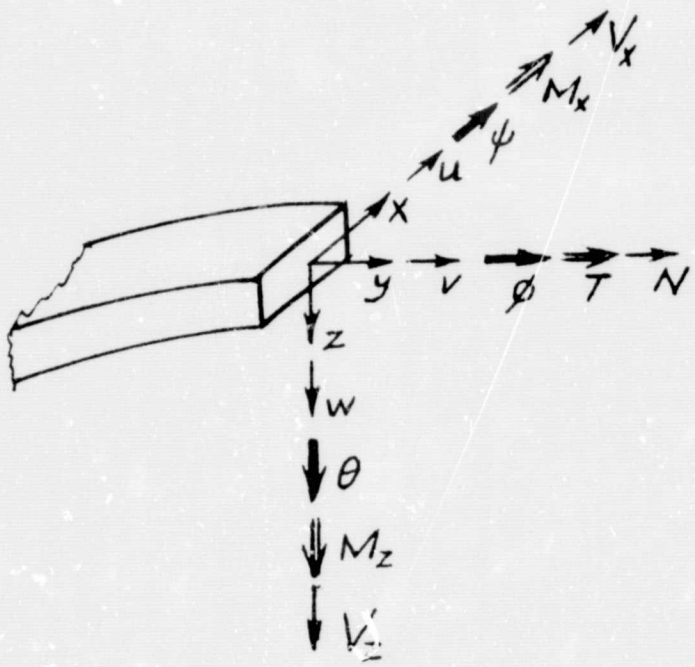


Figure 1. Coordinates and Sign Conventions of Ring

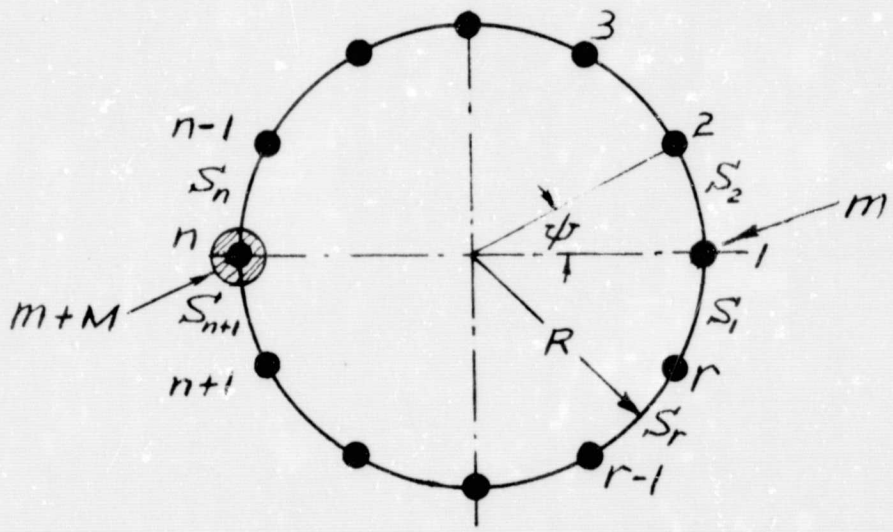


Figure 2. Lumped-Mass System of Ring

During free vibration in the y-z plane, the state vector (displacements, forces, and moments) at any station n can be expressed in terms of the state vector at Station 1 as follows:

$$\left|Z\right|_n = [U]_n \left|Z\right|_1 \qquad (1\text{-}1)$$

where

$$\left|Z\right|_n = \left|v \; -w \; -\psi \; -M_x \; -V_z \; N\right|_n \qquad (1\text{-}2)$$

= column matrix of above 6 quantities at Station n

$[U]_n$ = transfer matrix for Station n.

The transfer matrix $[U]_n$ is the product of two sets of matrices, the point matrix P_n and the field matrix S_n, arranged in the following manner:

$$[U]_n = P_n \, S_n \, P_{n-1} \, S_{n-1} \, - \, - \, - \, P_2 \, S_2 \, P_1 \qquad (1\text{-}3)$$

The point matrix P_n is a 6 x 6 matrix consisting of inertia terms and is given as

$$P_n = \begin{bmatrix} 1 & 0 & 0 & 0 & 0 & 0 \\ 0 & 1 & 0 & 0 & 0 & 0 \\ 0 & 0 & 1 & 0 & 0 & 0 \\ 0 & 0 & -I_x \omega^2 & 1 & 0 & 0 \\ 0 & m\omega^2 & 0 & 0 & 1 & 0 \\ -m\omega^2 & 0 & 0 & 0 & 0 & 0 \end{bmatrix}_n \qquad (1\text{-}4)$$

The elastic field matrix is also a 6 x 6 matrix consisting of stiffness terms and is given as

$$S_n = \begin{bmatrix} \cos\psi & -\sin\psi & -R(1-\cos\psi) & \frac{-R^2}{EJ_x}(\psi-\sin\psi) & S_{15} & \frac{RF_1}{EA}+\frac{R^3F_6}{EJ_x} \\ \sin\psi & \cos\psi & R\sin\psi & \frac{R^2}{EJ_x}(1-\cos\psi) & \frac{1}{EA}+\frac{R^2}{EJ_x} & RF_3 \\ 0 & 0 & 1 & \frac{R}{EJ_x}\psi & \frac{R^2}{EJ_x}(1-\cos\psi) & \frac{-R^2}{EJ_x}(\psi-\sin\psi) \\ 0 & 0 & 0 & 1 & R\sin\psi & -R(1-\cos\psi) \\ 0 & 0 & 0 & 0 & \cos\psi & -\sin\psi \\ 0 & 0 & 0 & 0 & \sin\psi & \cos\psi \end{bmatrix} \qquad (1-5)$$

where

$$S_{15} = S_{26} = \frac{R}{2EA}\Psi\sin\Psi - \frac{R^3F_5}{EJ_x}, \qquad F_5 = 1 - \cos\Psi - \frac{\Psi}{2}\sin\Psi$$

$$F_1 = \frac{1}{2}(\Psi\cos\Psi + \sin\Psi), \qquad F_3 = \frac{1}{2}(\sin\Psi - \Psi\cos\Psi)$$

$$F_6 = \frac{1}{2}(2\Psi + \Psi\cos\Psi - 3\sin\Psi).$$

If any additional mass is attached to Station n, several quantities in the matrices P_n and S_n should be modified to include the effects from the attached mass as follows:

Unloaded Case	Mass-Loaded Case
m	$m + M$
I_x	$I_x + I_{x_o}$
EA	$EA + E_o A_o$
EJ_x	$EJ_x + E_o J_{x_o}$

The formulas for calculation of the quantities m, I_x, I_{x_o}, J_x, and J_{x_o} are given in Appendix A.

The continuity condition requires that the state vectors at Station 1 and Station (r+1) must be equal; i.e.,

$$\left|Z\right|_1 = \left|Z\right|_{r+1} \tag{1-6}$$

but

$$\left|Z\right|_{r+1} = P_1 S_1 \left|Z\right|_r \tag{1-7}$$

and

$$\left|Z\right|_r = [U]_r \left|Z\right|_1 \tag{1-8}$$

where

$$[U]_r = P_r S_r P_{r-1} S_{r-1} - - - P_2 S_2 P_1 \tag{1-9}$$

Substituting Equation 1-8 into Equation 1-7,

$$\left|Z\right|_{r+1} = P_1 S_1 [U]_r \left|Z\right|_1 \tag{1-10}$$

let

$$\left.\begin{aligned} [U]_{r+1} &= P_1 S_1 [U]_r \\ &= P_1 S_1 P_r S_r P_{r-1} S_{r-1} - - - P_2 S_2 P_1 \end{aligned}\right\} \tag{1-11}$$

therefore

$$\left|Z\right|_{r+1} = [U]_{r+1} \left|Z\right|_1 \tag{1-12}$$

From Equations (1-6) and (1-12),

$$\left|Z\right|_1 = [U]_{r+1} \left|Z\right|_1 \tag{1-13}$$

or

$$\left[[U]_{r+1} - [I]\right] \left|Z\right|_1 = 0 \tag{1-14}$$

where

[I] = unit matrix of Order 6.

The frequency determinant is

$$\det \left| [U]_{r+1} - [I] \right| = 0 \tag{1-15}$$

By expansion of Equation 1-15 a polynomial of order $3(r+1)$ in ω^2 will be obtained. The natural frequencies then can be solved. For each frequency ω there is a set of values $\{Z\}_1$, the state vector at Station 1, which can be found from Equation 1-14. The state vectors at other stations then can be calculated by Equation 1-1. The mode shapes are v, w, and ψ, the first three elements of the column matrix $\{Z\}_n$. Of particular interest is the radial motion w. The procedures for obtaining this radial mode shape are as follows:

Let u_{ij} = elements of the transfer matrix $[U]_{r+1}$ of Equation 1-11.

Write Equation 1-14 in expanded form:

$$\begin{bmatrix} (u_{11}-1) & u_{12} & u_{13} & u_{14} & u_{15} & u_{16} \\ u_{21} & (u_{22}-1) & u_{23} & u_{24} & u_{25} & u_{26} \\ u_{31} & u_{32} & (u_{33}-1) & u_{34} & u_{35} & u_{36} \\ u_{41} & u_{42} & u_{43} & (u_{44}-1) & u_{45} & u_{46} \\ u_{51} & u_{52} & u_{53} & u_{54} & (u_{55}-1) & u_{56} \\ u_{61} & u_{62} & u_{63} & u_{64} & u_{65} & (u_{66}-1) \end{bmatrix}_{r+1} \begin{Bmatrix} v \\ -w \\ -\psi \\ -M_x \\ -V_z \\ N \end{Bmatrix}_1 = 0 \tag{1-16}$$

Assume that M_{x_1} is known (e.g., unity); then the other quantities of $\{Z\}_1$ can be solved. Rearranging Equation 1-16 and neglecting the 4th equation, the following equation is obtained.

$$\begin{bmatrix} (u_{11}-1) & u_{12} & u_{13} & u_{15} & u_{16} \\ u_{21} & (u_{22}-1) & u_{23} & u_{25} & u_{26} \\ u_{31} & u_{32} & (u_{33}-1) & u_{35} & u_{36} \\ u_{51} & u_{52} & u_{53} & (u_{55}-1) & u_{56} \\ u_{61} & u_{62} & u_{63} & u_{65} & (u_{66}-1) \end{bmatrix} \begin{Bmatrix} v \\ -w \\ -\psi \\ -V_z \\ N \end{Bmatrix}_1 = M_{x_1} \begin{Bmatrix} u_{14} \\ u_{24} \\ u_{34} \\ u_{54} \\ u_{64} \end{Bmatrix} \quad (1-17)$$

In another form,

$$[C]\{D\}_1 = M_{x_1}\{G\} \quad (1-18)$$

where [C] is the square matrix in Equation 1-17 formed by the co-factor of the element $(u_{44} - 1)$ of the square matrix in Equation 1-16; $\{D\}_1$ is the column matrix on the left side of Equation 1-17; and $\{G\}$ is the matrix on the right side of Equation 1-17. From Equation 1-17 or 1-18, the unknown quantities in $\{D\}_1$ can be found in terms of M_{x_1} as follows:

$$v_1 = \frac{Q_v}{|C|} M_{x_1}, \qquad w_1 = -\frac{Q_w}{|C|} M_{x_1}, \qquad \psi_1 = -\frac{Q_\psi}{|C|} M_{x_1},$$
$$V_{z_1} = -\frac{Q_z}{|C|} M_{x_1}, \qquad N_1 = \frac{Q_N}{|C|} M_{x_1} \quad (1-19)$$

Where $|C|$ = determinant of [C],

$$Q_V = \det \begin{vmatrix} u_{14} & u_{12} & u_{13} & u_{15} & u_{16} \\ u_{24} & (u_{22} - 1) & u_{23} & u_{25} & u_{26} \\ u_{34} & u_{32} & (u_{33} - 1) & u_{35} & u_{36} \\ u_{54} & u_{52} & u_{53} & (u_{55} - 1) & u_{56} \\ u_{64} & u_{62} & u_{63} & u_{65} & (u_{66} - 1) \end{vmatrix}$$

$$Q_W = \det \begin{vmatrix} (u_{11} - 1) & u_{14} & u_{13} & u_{15} & u_{16} \\ u_{21} & u_{24} & u_{23} & u_{25} & u_{26} \\ u_{31} & u_{34} & (u_{33} - 1) & u_{35} & u_{36} \\ u_{51} & u_{54} & u_{53} & (u_{55} - 1) & u_{56} \\ u_{61} & u_{64} & u_{63} & u_{65} & (u_{66} - 1) \end{vmatrix}$$

$$Q_\psi = \det \begin{vmatrix} (u_{11} - 1) & u_{12} & u_{14} & u_{15} & u_{16} \\ u_{21} & (u_{22} - 1) & u_{24} & u_{25} & u_{26} \\ u_{31} & u_{32} & u_{34} & u_{35} & u_{36} \\ u_{51} & u_{52} & u_{54} & (u_{55} - 1) & u_{56} \\ u_{61} & u_{62} & u_{64} & u_{65} & (u_{66} - 1) \end{vmatrix}$$

$$Q_z = \det \begin{vmatrix} (u_{11} - 1) & u_{12} & u_{13} & u_{14} & u_{16} \\ u_{21} & (u_{22} - 1) & u_{23} & u_{24} & u_{26} \\ u_{31} & u_{32} & (u_{33} - 1) & u_{34} & u_{36} \\ u_{51} & u_{52} & u_{53} & u_{54} & u_{56} \\ u_{61} & u_{62} & u_{63} & u_{64} & (u_{66} - 1) \end{vmatrix}$$

$$Q_N = \det \begin{vmatrix} (u_{11} - 1) & u_{12} & u_{13} & u_{15} & u_{14} \\ u_{21} & (u_{22} - 1) & u_{23} & u_{25} & u_{24} \\ u_{31} & u_{32} & (u_{33} - 1) & u_{35} & u_{34} \\ u_{51} & u_{52} & u_{53} & (u_{55} - 1) & u_{54} \\ u_{61} & u_{62} & u_{63} & u_{65} & u_{64} \end{vmatrix}$$

For unit bending moment, the deflections and forces are simplified to

$$v_1 = \frac{Q_v}{|C|}, \qquad w_1 = -\frac{Q_w}{|C|}, \qquad \psi_1 = -\frac{Q_\psi}{|C|}, \qquad M_{x_1} = 1, \tag{1-20}$$

$$V_{z_1} = \frac{Q_z}{|C|}, \qquad N_1 = \frac{Q_N}{|C|}$$

By knowing these quantities for Station 1, the state vector at any station n then can be solved by Equation 1-1. The radial mode shape w_n will be determined from $\left|Z\right|_n$.

A computer program based on this formulation has been provided for evaluation of the natural frequencies and modes of the mass-loaded and unloaded rings. Satisfactory solutions were obtained for the first three modes without difficulty; however, results for the higher modes became less accurate because extremely large numbers were involved in solving the frequency polynomials of very high order. To overcome this problem, a method based on the finite-element/matrix-iteration technique was developed. Details of this method are given in the following section.

PRECEDING PAGE BLANK NOT FILMED.

3.0. DYNAMIC ANALYSIS OF MASS-LOADED RINGS BY FINITE-ELEMENT METHOD

Conventional engineering structures can be visualized as an assemblage of structural elements interconnected at a discrete number of nodal points. If the force-displacement relationships for the individual elements are known, it is possible, by using the direct-stiffness method of structural analysis, to derive the properties and study the behavior of the assembled structure (References 25, 26 and 27).

After a suitable discretized mathematical model of the structural system has been adopted, equations relating nodal forces and nodal displacements for each type of structural element must be derived. These equations take the matrix form

$$\left\{F\right\} = [k] \left\{u\right\}$$

where [k] is known as the element stiffness matrix. For the two-dimensional Euler beam element (Figure 3) the specific equations are as shown in Figure 3.



Figure 3. Beam Element

$$\begin{Bmatrix} A_1 \\ V_1 \\ M_1 \\ A_2 \\ V_2 \\ M_2 \end{Bmatrix} = \begin{bmatrix} \frac{AE}{\ell} & 0 & 0 & -\frac{AE}{\ell} & 0 & 0 \\ 0 & \frac{12EI}{\ell^3} & \frac{6EI}{\ell^2} & 0 & -\frac{12EI}{\ell^3} & \frac{6EI}{\ell^2} \\ 0 & \frac{6EI}{\ell^2} & \frac{4EI}{\ell} & 0 & -\frac{6EI}{\ell^2} & \frac{2EI}{\ell} \\ -\frac{AE}{\ell} & 0 & 0 & \frac{AE}{\ell} & 0 & 0 \\ 0 & -\frac{12EI}{\ell^3} & -\frac{6EI}{\ell^2} & 0 & \frac{12EI}{\ell^3} & -\frac{6EI}{\ell^2} \\ 0 & \frac{6EI}{\ell^2} & \frac{2EI}{\ell} & 0 & -\frac{6EI}{\ell^2} & \frac{4EI}{\ell} \end{bmatrix} \begin{Bmatrix} u_1 \\ v_1 \\ \theta_1 \\ u_2 \\ v_2 \\ \theta_2 \end{Bmatrix}$$

Dynamic response analysis requires a similar set of equations relating nodal forces and nodal accelerations. These may be written

$$\{F\} = [m]\{\ddot{u}\}$$

where [m] is referred to as the element mass or inertia matrix. For the beam, these equations become

$$\begin{Bmatrix} A_1 \\ V_1 \\ M_1 \\ A_2 \\ V_2 \\ M_2 \end{Bmatrix} = \frac{\rho \ell A}{g} \begin{bmatrix} \frac{1}{3} & 0 & 0 & \frac{1}{6} & 0 & 0 \\ 0 & \frac{13}{35} & \frac{11\ell}{210} & 0 & \frac{9}{70} & -\frac{13\ell}{420} \\ 0 & \frac{11\ell}{210} & \frac{\ell^2}{105} & 0 & \frac{13\ell}{420} & -\frac{\ell^2}{140} \\ \frac{1}{6} & 0 & 0 & \frac{1}{3} & 0 & 0 \\ 0 & \frac{9}{70} & \frac{13\ell}{420} & 0 & \frac{13}{35} & -\frac{11\ell}{210} \\ 0 & -\frac{13\ell}{420} & -\frac{\ell^2}{140} & 0 & -\frac{11\ell}{210} & \frac{\ell^2}{105} \end{bmatrix} \begin{Bmatrix} \ddot{u}_1 \\ \ddot{v}_1 \\ \ddot{\theta}_1 \\ \ddot{u}_2 \\ \ddot{v}_2 \\ \ddot{\theta}_2 \end{Bmatrix}$$

The particular form of the mass matrix given here is referred to as a consistent mass matrix, since its derivation is based on the same displacement functions used for the stiffness matrix; therefore, there is no need for arbitrary mass lumping.

Structural element stiffness and mass properties are usually derived with respect to coordinate axes convenient to that element. Prior to assembly of the structural equations, it is necessary to transform each $[\bar{k}]$ and $[\bar{m}]$ so that forces, displacements, and accelerations are referred to a common structural coordinate system. If the barred quantities pertain to the common coordinate system the transformations (Figure 4) required are

$$\{F\} = [B]\ \{\bar{F}\}$$

$$\{u\} = [B]\ \{\bar{u}\}$$

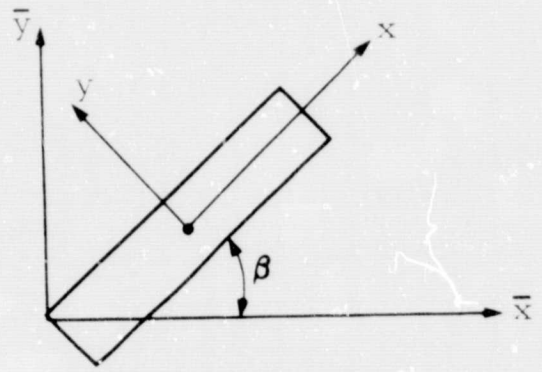


Figure 4. Coordinate Transformation

where

$$[B] = \begin{bmatrix} \cos\beta & \sin\beta & 0 & 0 & 0 & 0 \\ -\sin\beta & \cos\beta & 0 & 0 & 0 & 0 \\ 0 & 0 & 1 & 0 & 0 & 0 \\ 0 & 0 & 0 & \cos\beta & \sin\beta & 0 \\ 0 & 0 & 0 & -\sin\beta & \cos\beta & 0 \\ 0 & 0 & 0 & 0 & 0 & 1 \end{bmatrix}$$

Substitution into the force-displacement equations gives

$$[B] \left| \bar{F} \right| = [k] [B] \left| \bar{u} \right|$$

Since [B] is an orthogonal matrix,

$$\left| \bar{F} \right| = [B]^T [k] [B] \left| \bar{u} \right|$$

The element stiffness matrix in structural coordinates is then identified as

$$[\bar{k}] = [B]^T [k] [B]$$

Similarly, the transformed element mass matrix is

$$[\bar{m}] = [B]^T [m] [B]$$

An overall structure stiffness and mass matrix may now be assembled by superposing individual $[\bar{k}]$ and $[\bar{m}]$ in such a way that all matrix elements associated with the same nodal degree of freedom are added. This procedure, which is the essence of the direct stiffness method, is represented in equation form by

$$[k] = \sum_{i=1}^{n} [\bar{k}]_i$$

$$[M] = \sum_{i=1}^{n} [\bar{m}]_i$$

After forming the system free-free stiffness and mass matrices, all boundary conditions to be imposed are accounted for. In the case of zero constraint conditions, rows and columns of the system matrices corresponding to suppressed degrees of freedom are deleted.

There may also be degrees of freedom present in the system matrices associated with inertia forces which may be neglected in comparison to those that are more dominant. It is then preferable to remove these freedoms from the problem before proceeding with the solution. One such technique for eliminating excess unknowns from the system equations is given in Reference 28.

For modal analysis, the structural equations of the vibration take the form

$$[k] \left|u_o\right| = \omega^2 [M] \left|u_o\right|$$

where $u = u_o \sin \omega t$.

For structures not fully supported, [k] will be singular; and it is preferable to invert [M] to obtain equations in the standard eigenproblem form,

$$[M]^{-1} [k] \left|u_o\right| = \omega^2 \left|u_o\right|$$

It is a matter of numerical efficiency that the coefficient matrix $[M]^{-1} [k]$ be symmetric. This may be accomplished if $[M]^{-1}$ is obtained by a Choleski decomposition and new variables are adopted. Let

$$[M] = [F]^T [F]$$

where [F] is an upper triangular matrix. Then,

$$[M]^{-1} = [F]^{-1} \left([F]^{-1}\right)^T$$

Next, introduce the variables $\left|q\right|$ so that

$$\left|q\right| = [F] \left|u_o\right|$$

Substitution and premultiplication by [F] reduces to the form

$$\left([F]^{-1}\right)^T [k] [F]^{-1} \left|q\right| = [D] \left|q\right| = \omega^2 \left|q\right|$$

in which the dynamic matrix [D] is symmetric. Solution of these equations gives the natural frequencies of the structure, and the modes are obtained by the inverse transformation

$$\left|u_o\right| = [F]^{-1} \left|q\right|$$

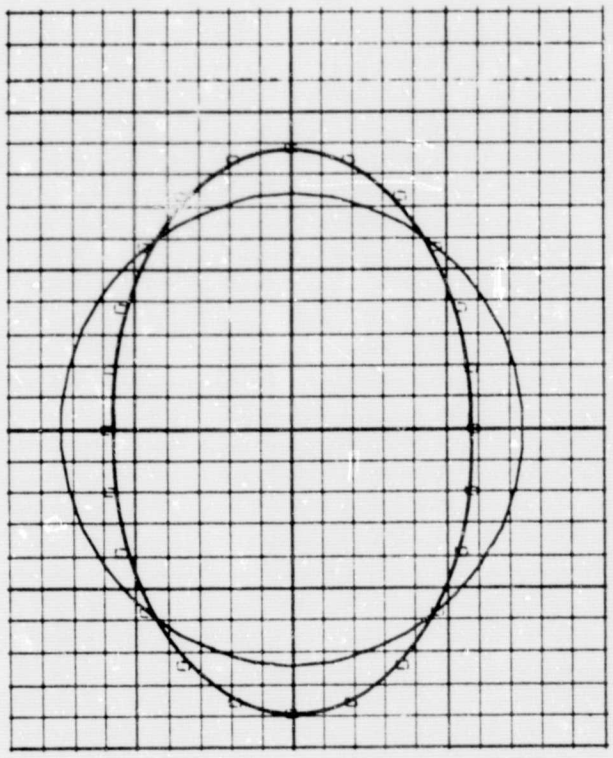
The computed natural frequencies and mode shapes of the first five modes for the ring test model are given in Table 1 and Figures 5 through 8.

Table 1. Computed Natural Frequencies and Frequency Ratios of Rings

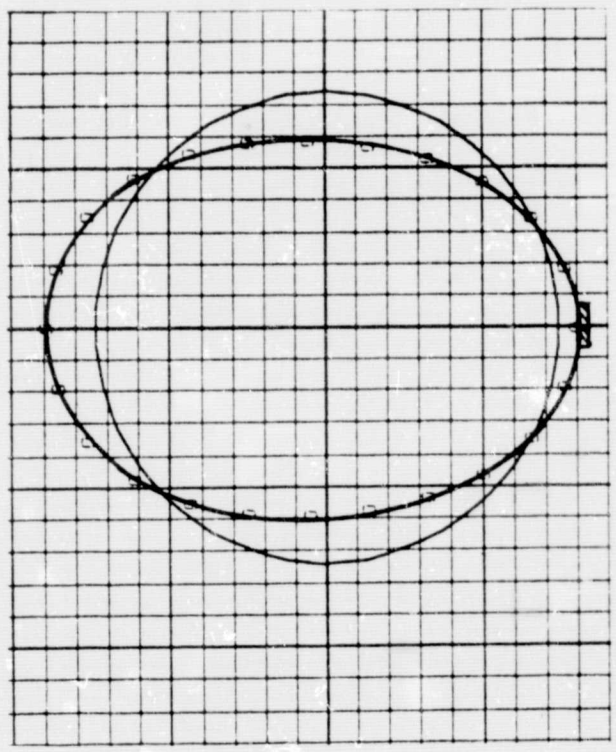
Case Number		0	1	2	3	4	5	6	7	8
M_2/M_1		0	0.16	0.32	0.60	0.82	1.08	1.58	2.54	3.52
Mode 1	Freq.	15.6	14.7	13.8	12.7	12.2	11.8	11.2	10.8	10.6
	f_2/f_1	1.0	0.941	0.885	0.815	0.782	0.756	0.718	.692	0.689
Mode 2	Freq.	44.2	42.0	40.0	38.3	37.6	37.2	36.6	36.1	35.9
	f_2/f_1	1.0	0.950	0.905	0.866	0.850	0.841	0.827	0.816	0.811
Mode 3	Freq.	84.9	81.5	79.0	77.0	76.5	76.0	75.5	75.0	74.7
	f_2/f_1	1.0	0.960	0.930	0.906	0.901	0.895	0.890	0.883	0.880
Mode 4	Freq.	137.5	133.3	130.4	128.7	128.1	127.5	127.0	126.8	126.4
	f_2/f_1	1.0	0.970	0.948	0.935	0.931	0.927	0.923	0.920	0.919
Mode 5	Freq.	202.3	198.0	195.2	193.2	192.8	192.2	192.0	191.5	191.0
	f_2/f_1	1.0	0.978	0.965	0.955	0.952	0.950	0.948	0.946	0.944

Notes: (1) Frequency unit = cps.

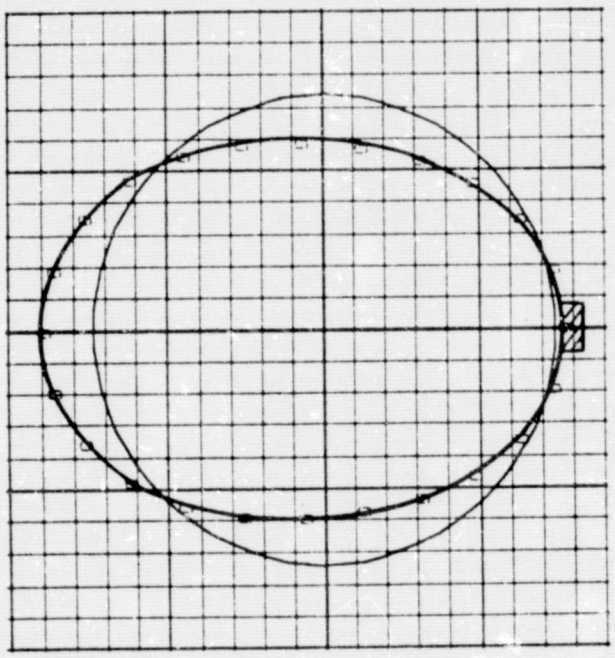
(2) f_1 = frequency of unloaded ring, Case 0.
f_2 = frequency of mass loaded rings, Cases 1 to 8



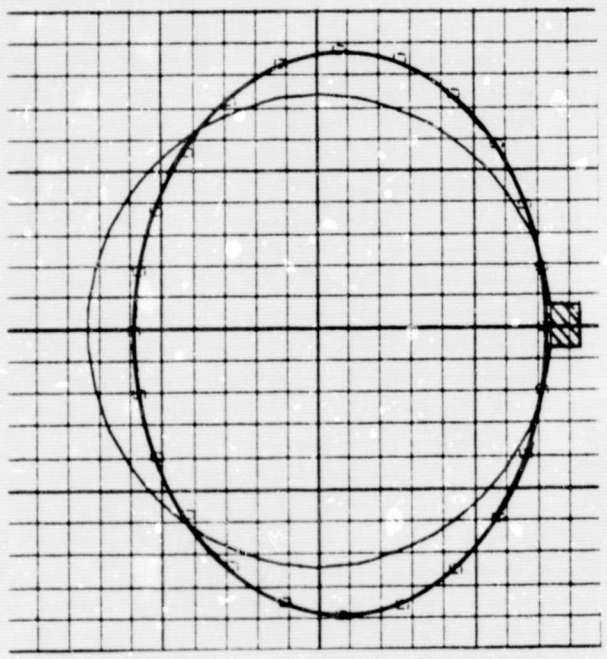
$M_2/M_1 = 0$, f = 15.6 cps



$M_2/M_1 = 0.82$, f = 12.2 cps

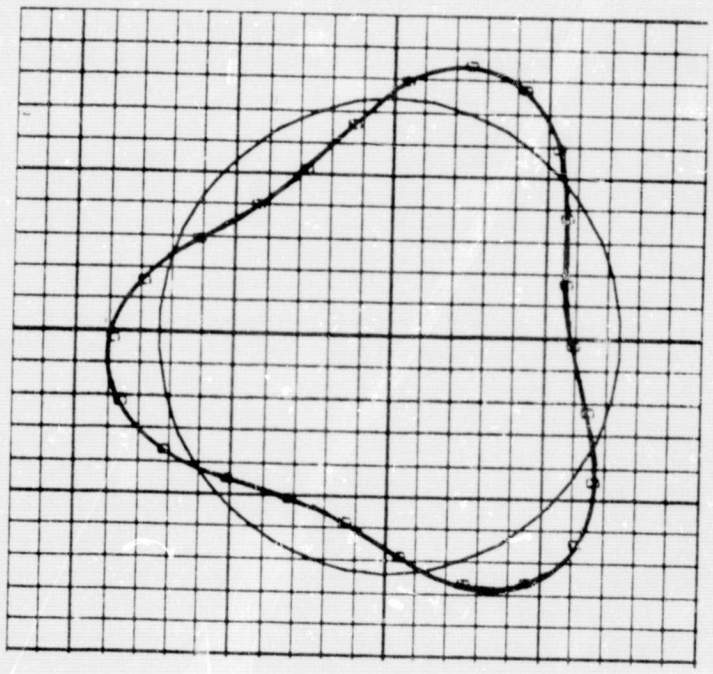


$M_2/M_1 = 1.58$, f = 11.2 cps

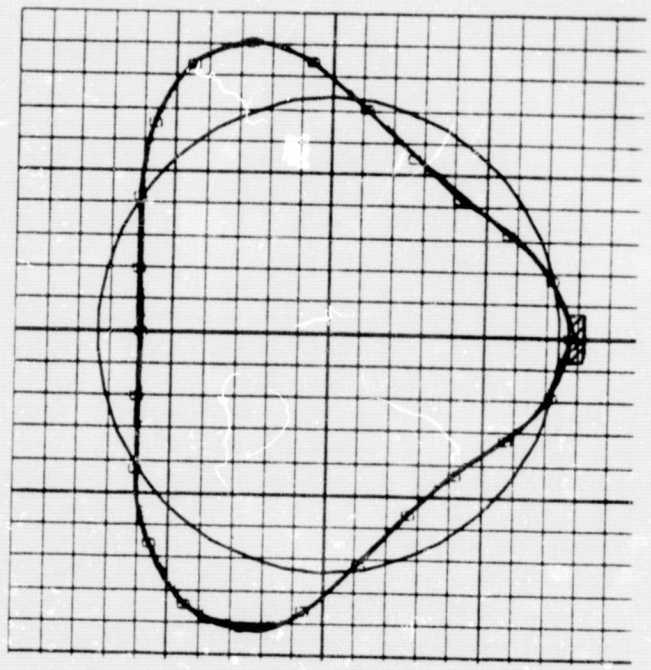


$M_2/M_1 = 3.52$, f = 10.6 cps

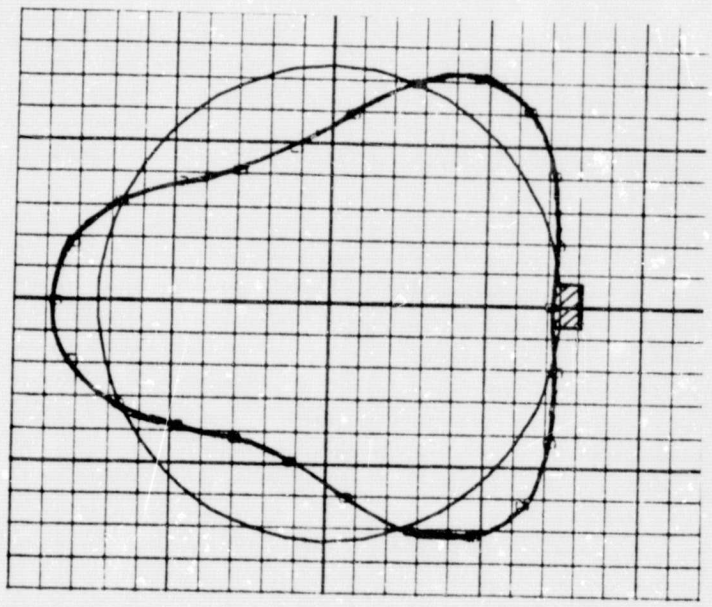
Figure 5. Computed Mode Shapes of Ring I, Mode 1, n = 2



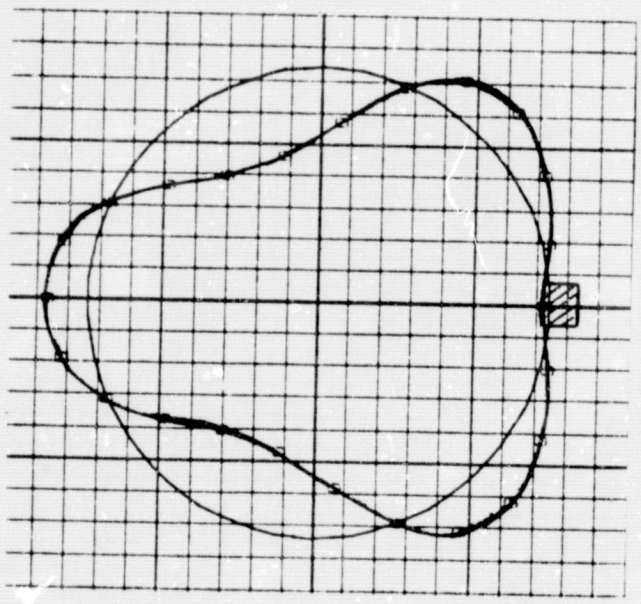
$M_2/M_1 = 0$, f = 44.2 cps



$M_2/M_1 = 0.82$, f = 37.6 cps

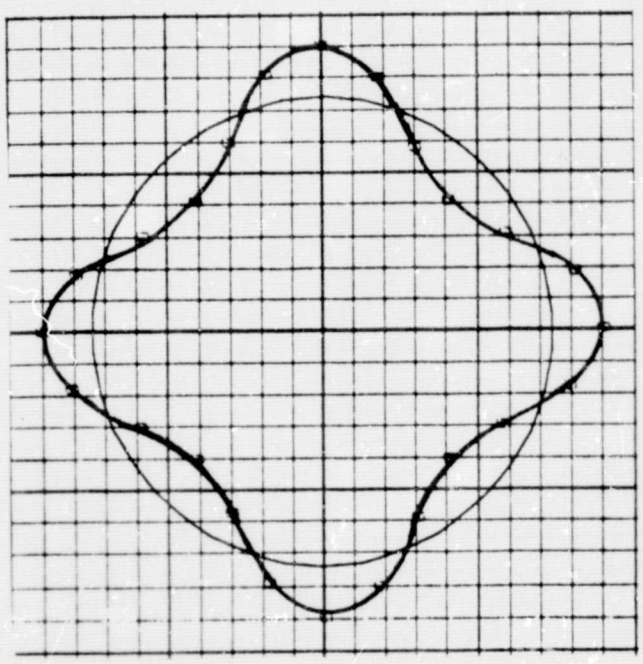


$M_2/M_1 = 1.58$, f = 36.6 cps

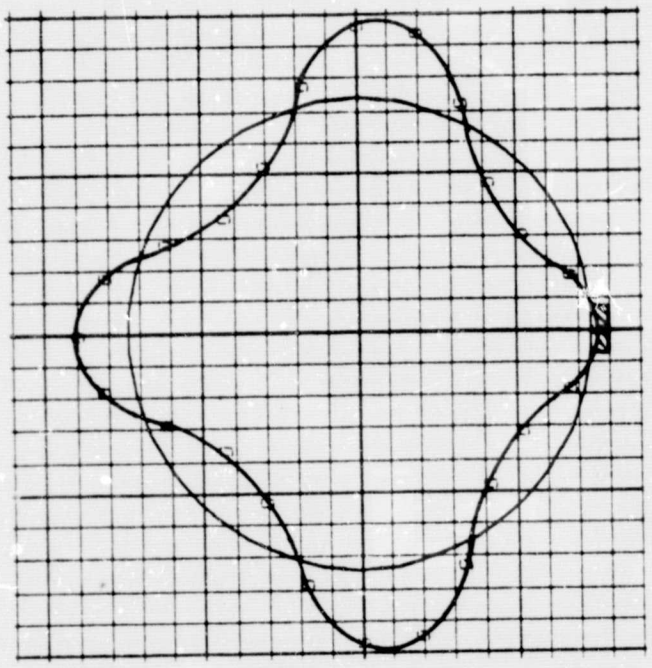


$M_2/M_1 = 3.52$, f = 35.9 cps

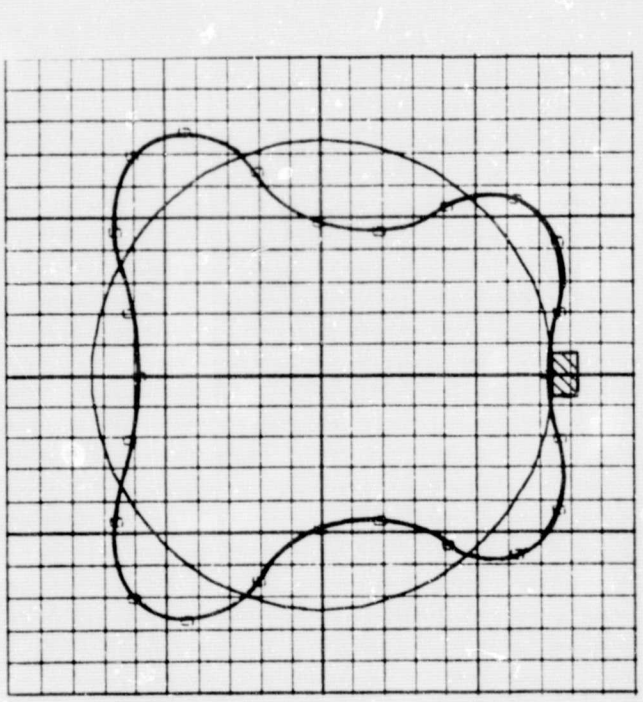
Figure 6. Computed Mode Shapes of Ring I, Mode 2, n = 3



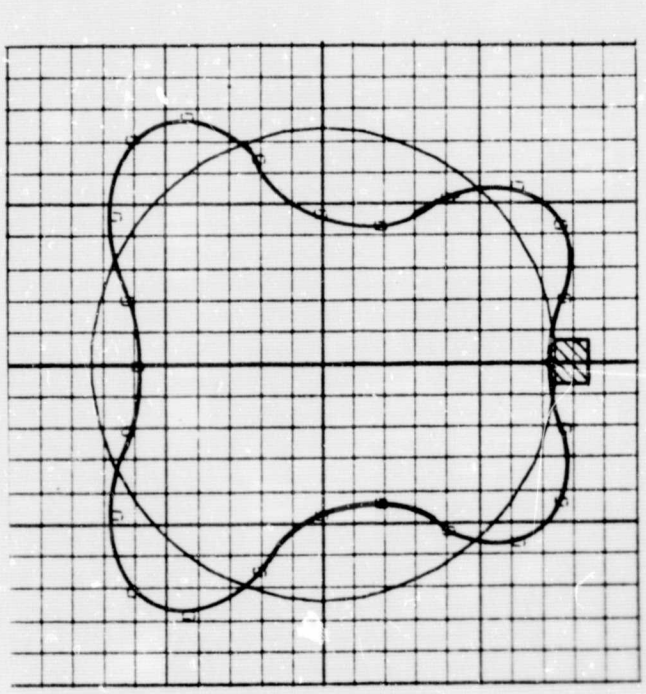
$M_2/M_1 = 0$, f = 84.9 cps



$M_2/M_1 = 0.82$, f = 76.5 cps

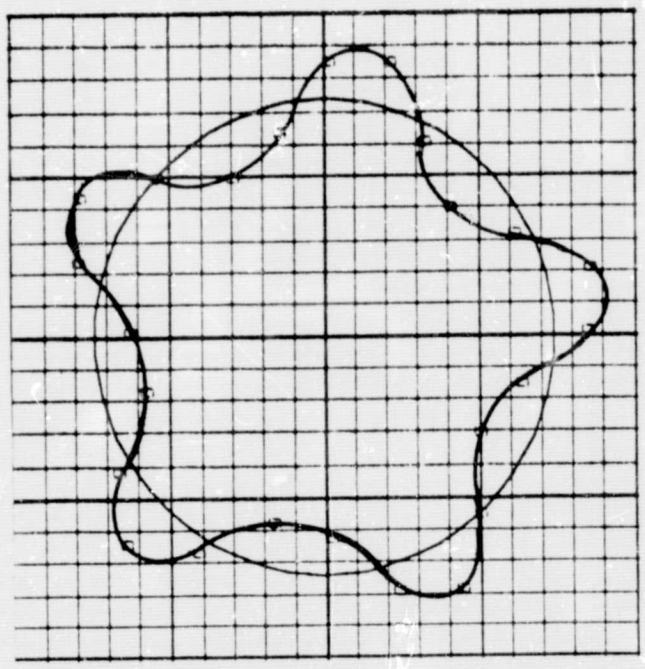


$M_2/M_1 = 1.58$, f = 75.5 cps

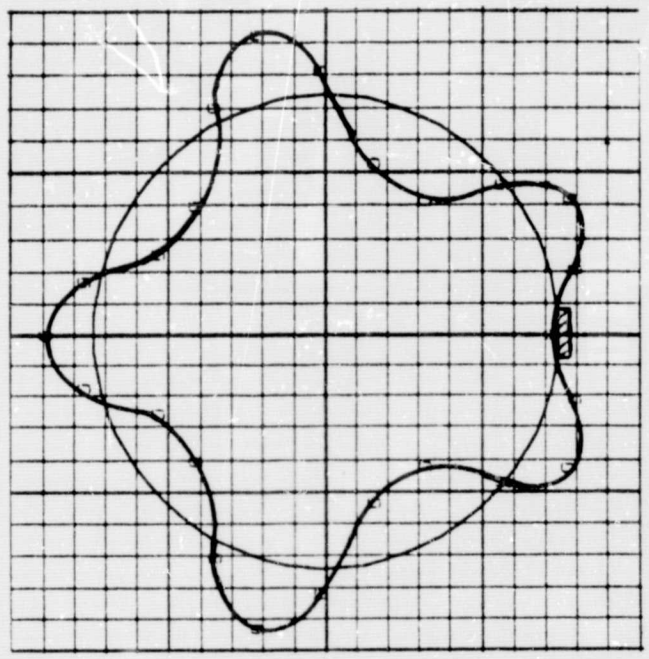


$M_2/M_1 = 3.52$, f = 74.7 cps

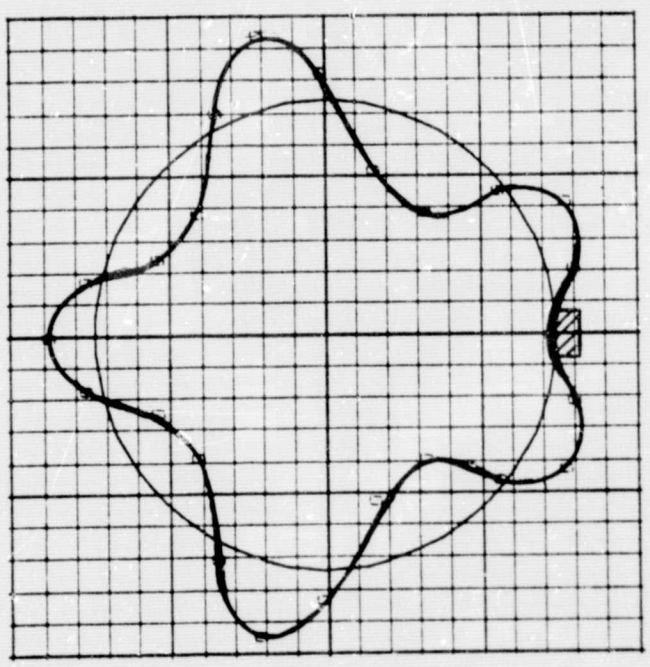
Figure 7. Computed Mode Shapes of Ring I, Mode 3, n = 4



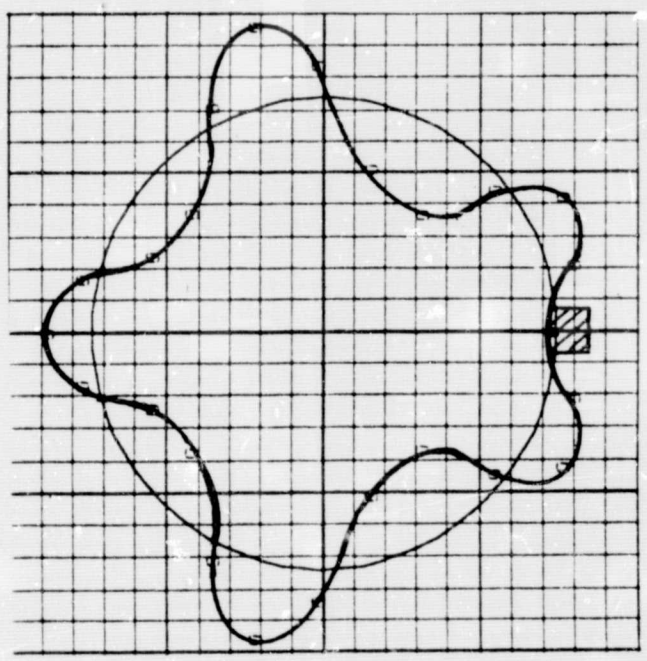
$M_2/M_1 = 0$, f = 137.5 cps



$M_2/M_1 = 0.82$, f = 128.1 cps



$M_2/M_1 = 1.58$, f = 127.0 cps



$M_2/M_1 = 3.52$, f = 126.4 cps

Figure 8. Computed Mode Shapes of Ring I, Mode 4, n = 5

4.0 DYNAMIC ANALYSIS OF MASS-LOADED AND UNLOADED SHELL STRUCTURES

Dynamic analysis of shell structures may be accomplished by a mathematical treatment of the describing partial differential equations of motion, which in very simple cases only, lend themselves to a closed-form exact solution. There are some physical simplification approaches, such as grid-work and finite-element, suggesting a replacement of the shell structure by a set of simplified structural elements on which matrix iteration techniques can be applied. These structural simplification approaches would result in approximate solutions and may require large computer operations for matrix iteration.

In the present study, a shell structure is treated as a continuous system whose motions are described by a set of partial differential equations. Among the many methods for solving this type of problem, the finite-difference and Galerkin techniques can be used to obtain an approximate solution, while the series expansion technique can be employed to find an exact solution and is to be emphasized in this study. An exact and closed-form solution can be obtained only if the assumed series for the displacement functions are sufficiently accurate to satisfy the boundary conditions and the equations of motion. Various sets of differential equations representing shell structures have been developed by different authors with discrepancies in certain minor terms; some of these are compared in Table 2. The series expansion technique may be applied efficiently to these approaches, as well as to those of Donnell, Flügge, Vlasov, and others, for solving the vibration problems of thin, isotropic shell structures. However, it will be a laborious effort in analyzing mass—loaded shell structures and may introduce problems in computer programming. Through the energy approach, the equations of motion can be established in a simple form and solved conveniently by the series expansion technique using simple computer programming and requiring only little computer time.

Nomenclature used in this section is given in the following list, which includes a diagram (Figure 9) of the mass-loaded shell.

A_{mn}, B_{mn}, C_{mn} = Fourier coefficients of displacements u, v, and w

$D_A = \dfrac{E \pi^2 h m}{1.82}$

D_B = $\frac{E \pi^2 h^3 m}{21.84}$

E = Young's modulus

I_x, I_θ = centroidal mass moments of inertia of m_a

L = length of shell

M = largest value for integer m

M_S = mass of shell

N = largest value for integer n

T = kinetic energy

V = strain energy

x_o = length of the mass m_a

a = mean radius of shell

e = eccentric distance between mid-surface of shell to mass m_a

h = skin thickness of shell

h_o = thickness of the mass m_a

m = number of half-waves along longitudinal axis

n = number of circumferential waves along radial direction

m_a = attached mass

t = time

u, v, w = displacements of a pcint on the mid-surface of the shell in the direction of x, θ and z.

x, θ, z = longitudinal, circumferential and radial coordinates

α_m $= \frac{m\pi}{L}$

α_i $= \frac{i\pi}{L}$

λ $= \frac{1}{\omega^2}$

θ_o = width of mass m_a

ν = Poisson's ratio

ρ = mass density

ω = frequency of vibration in cps

Subscripts

i, j = positive integers

s = refer to shell

$\dot{}$ = differentiation with respect to time

i $= \sqrt{-1}$

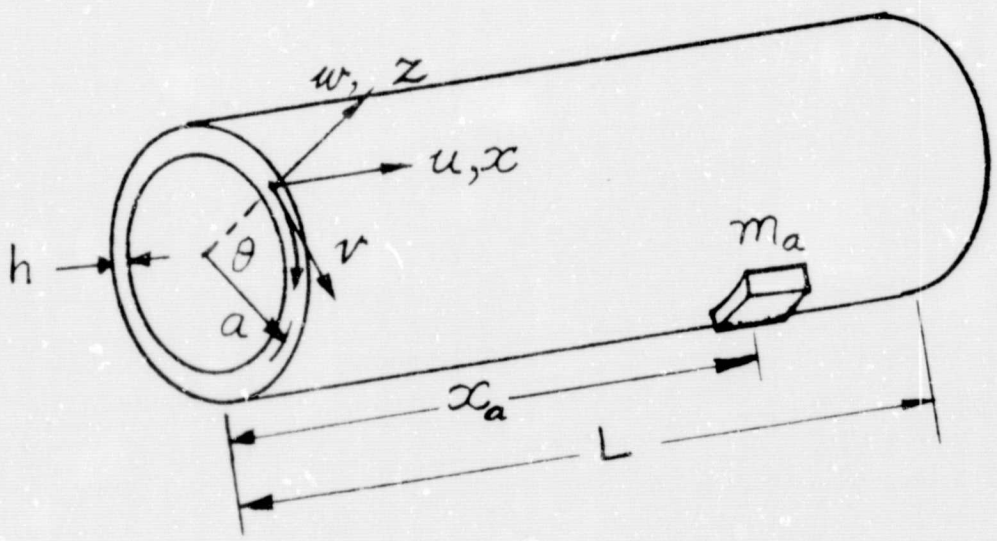


Figure 9. Mass-Loaded Shell

Table 2. Comparison of the Theories of Cylindrical Shells

Characteristic Eq. $\lambda^8 - (4n^2 + A)\lambda^6 + (6n^4 + \frac{1-\nu^2}{K} + B)\lambda^4 - (4n^6 + C)\lambda^2 + n^4(n^2-1)^2 + D = 0$

A	B	C	D	Authors
0	0	0	0	Donnell
-2ν	$-6n^2$	$-2(4-\nu)n^4 + 2(2-\nu)n^2$	0	Flügge and Byrne
-2ν	$-(4+\nu)n^2 + 1$	$-(8-\nu)n^4 + 2n^2$	0	Vlasov
0	$-\frac{4-\nu}{2(1-\nu)}n^2 + \frac{2+\nu}{2(1-\nu)}$	$-\frac{8-8\nu-3\nu^2}{4(1-\nu)}n^2 + \frac{(2+\nu)(2-3\nu)}{4(1-\nu)}$	0	Kennard
0	$-2(2+\nu)n^2$	$-2(3+\nu)n^4 + \frac{1}{2}(5+3\nu)n^2$	0	Naghdi and Berry
0	$-(6+\nu-\nu^2)n^2 + 2(1-\nu^2)$	$-(7+\nu)n^4 + (3+\nu)n^2$	0	Timoshenko
0	$-2(4-\nu^2)n^2 + 4(1-\nu^2)$	$-4(2n^2+1)n^2$	0	Novozhilov
-2	$-6n^2 + 1$	$2(-3n^2+1)n^2$	0	Morley
-2ν	$-6n^2 + 4 - 3\nu^2$	$-2(4-\nu)n^4 + 2(2-\nu)n^2$	0	Biezeno and Grammel
0	$-(6+\nu-\nu^2)n^2$	$-(7+\nu)n^4$	$-p^4$	Bijlaard
Following are additional terms for more accuracy.				
$-\frac{3-\nu}{1-\nu}\gamma p^2$	$-\gamma p^2\left[\frac{3(3-\nu)}{1-\nu}n^2 + \frac{1}{K}\right] + \frac{2}{1-\nu}\gamma^2 p^4$	$-\gamma p^2\left[\frac{3(3-\nu)}{1-\nu}n^4 + 2\frac{n^2}{K} - 2(3+\nu)n^2 + \frac{3+2\nu}{K}\right] + \gamma^2 p^4\left[\frac{3-\nu}{1-\nu}\frac{1}{K} + \frac{4}{1-\nu}n^2\right]$	$-\gamma p^2\left(\frac{3-\nu}{1-\nu}n^6 + \frac{n^4}{K} + \frac{n^2}{K} - \frac{3-\nu}{1-\nu}n^2\right) + \gamma^2 p^4\left[\frac{3-\nu}{1-\nu}\frac{n^2}{K} + \frac{2}{1-\nu}n^4 + \frac{2}{(1-\nu)K} - \frac{4n^2}{1-\nu} + \frac{2}{1-\nu}\right] - \frac{2}{(1-\nu)K}\gamma^3 p^6$	Vlasov
$-\frac{3-\nu}{1-\nu}\gamma p^2$	$-\gamma p^2\left[\frac{3(3-\nu)}{1-\nu}n^2 + \frac{1}{K}\right] + \frac{2}{1-\nu}\gamma^2 p^4$	$\gamma p^2\left[\frac{3(3-\nu)}{1-\nu}n^4 + 2\frac{n^2}{K} - \frac{(4-\nu)(3-\nu)}{2(1-\nu)^2}n^2 + \frac{3+2\nu}{K} + \frac{(2+\nu)(3-\nu)}{2(1-\nu)^2}\right] + \gamma^2 p^4\left[\frac{3-\nu}{(1-\nu)K} + \frac{4n^2}{1-\nu}\right]$	$-\gamma p^2\left[\frac{3-\nu}{1-\nu}n^6 + \frac{n^4}{K} + \frac{n^2}{K} + \frac{(4+\nu)(3-\nu)}{2(1-\nu)^2}n^4 + \frac{(3-\nu)(2-\nu)}{2(1-\nu)^2}n^2\right] + \gamma^2 p^4\left[\frac{3-\nu}{1-\nu}\frac{n^2}{K} + \frac{2}{1-\nu}n^4 + \frac{2}{(1-\nu)}\frac{1}{K} + \frac{2+\nu}{(1-\nu)^2} - \frac{4-\nu}{(1-\nu)^2}n^2\right] - \frac{2}{(1-\nu)K}\gamma^3 p^6$	Kennard
$-\frac{3-\nu}{1-\nu}\gamma p^2$	$-\gamma p^2\left[\frac{3(3-\nu)}{1-\nu}n^2 + \frac{1}{K}\right] + \frac{2}{1-\nu}\gamma^2 p^4$	$-\gamma^2 p^2\left[\frac{3(3-\nu)}{1-\nu}n^4 + 2\frac{n^2}{K} + \frac{3+2\nu}{K}\right] + \gamma^2 p^4\left(\frac{3-\nu}{1-\nu}\frac{1}{K} + \frac{4}{1-\nu}n^2\right)$	$-\gamma p^2\left(\frac{3-\nu}{1-\nu}n^6 + \frac{n^4}{K} + \frac{n^2}{K}\right) + \gamma^2 p^4\left[\frac{3-\nu}{1-\nu}\frac{n^2}{K} + \frac{2}{1-\nu}n^4 + \frac{2}{(1-\nu)K}\right] - \frac{2}{(1-\nu)K}\gamma^3 p^6$	Naghdi and Berry

R = radius of cylindrical shell
n = number of circumferential waves
$K = h^2/(12R^2)$
h = shell thickness
λ = root of characteristic equation
ν = Poisson's ratio
$\gamma = \frac{1-\nu^2}{E}\rho R^2$
ρ = mass density
p = exponential index in expression for displacements u, v, w.

The flexural vibration of isotropic thin cylindrical shells has been studied analytically and experimentally by Arnold and Warburton (References 29 and 30). A similar problem was studied by Weigarten (Reference 31) with the results compared to those obtained by Arnold and Warburton. Employing a different approach, the study presented in this section investigates the vibration characteristics of mass-loaded shells as well as isotropic thin shells.

BASIC ASSUMPTIONS

1. The structure is a homogeneous, isotropic, thin shell mounted with a mass.

2. Hooke's Law applies in the stress-strain relationship.

3. The rotatory inertia is considered for the mass, but is negligible for the shell.

4. Transverse shear deformation is neglected.

5. The rigidity of the mass has negligible effect on that of the shell.

EQUATION OF MOTION

The partial differential equations describing the motion of the mass-loaded shell may be derived in terms of kinetic energy and strain energy using Lagrange's approach:

$$\frac{d}{dt}\left(\frac{\partial T}{\partial \dot{A}_{mn}}\right) - \frac{\partial T}{\partial A_{mn}} + \frac{\partial V}{\partial A_{mn}} = 0$$

$$\frac{d}{dt}\left(\frac{\partial T}{\partial \dot{B}_{mn}}\right) - \frac{\partial T}{\partial B_{mn}} + \frac{\partial V}{\partial B_{mn}} = 0 \qquad (4\text{-}1)$$

$$\frac{d}{dt}\left(\frac{\partial T}{\partial \dot{C}_{mn}}\right) - \frac{\partial T}{\partial C_{mn}} + \frac{\partial V}{\partial C_{mn}} = 0$$

KINETIC ENERGY

The kinetic energy of the mass-loaded shell, including the effect of the rotatory inertia of the mass, can be written as

$$T = \frac{ha\rho}{2g} \int_0^{2\pi} \int_0^{L} \left[\left(\frac{\partial u}{\partial t}\right)^2 + \left(\frac{\partial v}{\partial t}\right)^2 + \left(\frac{\partial w}{\partial t}\right)^2 \right] dx\, d\theta$$

$$+ \frac{h_o \rho}{2g} \int_0^{\theta_o} \int_0^{x_o} \left\{ \left(\frac{\partial w}{\partial t}\right)^2 + \left(\frac{\partial u}{\partial t} - e \frac{\partial^2 w}{\partial x \partial t} \right)^2 \right.$$

$$\left. + \left[\frac{\partial v}{\partial t} - e \left(\frac{\partial v}{a \partial t} + \frac{\partial^2 w}{\partial \theta \partial t} \right) \right]^2 \right\}_{x_a\, \theta_a} d\, x_o\, d\, \theta_o \qquad (4\text{-}2)$$

$$+ I_\theta \left(\frac{\partial w}{\partial x \partial t} \right)_{x_a \theta_a} + \frac{I_x}{a} \left(\frac{\partial v}{\partial t} + \frac{\partial^2 w}{\partial \theta \partial t} \right)_{x_a \theta_a}$$

STRAIN ENERGY

The strain energy of the mass-loaded shell with negligible rigidity introduced by the added mass can be described by the following partial differential equation:

$$V = \frac{E\, h}{2(1-\nu^2)} \int_0^{2\pi} \int_0^{L} \left\{ \left[\frac{\partial u}{\partial x} + \frac{1}{a} \left(\frac{\partial v}{\partial \theta} - w \right) \right]^2 - 2(1-\nu) \right.$$

$$\left. \times \left[\frac{1}{a} \left(\frac{\partial u}{\partial x} \frac{\partial v}{\partial \theta} - w \frac{\partial u}{x} \right) - \frac{1}{4} \left(\frac{1}{a} \frac{\partial u}{\partial \theta} + \frac{\partial v}{\partial x} \right)^2 \right] \right\} a\, dx\, d\theta \qquad (4\text{-}3)$$

$$+ \frac{E\, h^3}{24(1-\nu^2)} \int_0^{2\pi} \int_0^{L} \left[\left(\frac{\partial^2 w}{\partial x^2} + \frac{\partial v}{a^2 \partial \theta} + \frac{\partial^2 w}{a^2 \partial \theta^2} \right)^2 \right.$$

$$\left. - \frac{2(1-\nu)}{a^2} \left(\frac{\partial^2 w}{\partial x^2} \frac{\partial v}{\partial \theta} + \frac{\partial^4 w}{\partial x^2 \partial \theta^2} \right) - \frac{2(1-\nu)}{a^4} \left(\frac{\partial v}{\partial x} + \frac{\partial^2 w}{\partial x \partial \theta} \right)^2 \right] a\, dx\, d\theta$$

DISPLACEMENT FUNCTIONS

The displacement functions of the mass-loaded shell structure are assumed to be represented with sufficient accuracy by the following Fourier series:

A. Symmetrical Case

$$u(\theta,x,t) = \sum_{m=1}^{M} \sum_{n=0}^{N} A_{mn} \cos \alpha_m x \cos n\theta \, e^{-i\omega t}$$

$$v(\theta,x,t) = \sum_{m=1}^{M} \sum_{n=0}^{N} B_{mn} \sin \alpha_m x \sin n\theta \, e^{-i\omega t} \qquad (4\text{-}4)$$

$$w(\theta,x,t) = \sum_{m=1}^{M} \sum_{n=0}^{N} C_{mn} \sin \alpha_m x \cos n\theta \, e^{-i\omega t}$$

B. Antisymmetrical Case

$$u(\theta,x,t) = \sum_{m=1}^{M} \sum_{n=0}^{N} A_{mn} \cos \alpha_m x \sin n\theta \, e^{-i\omega t}$$

$$v(\theta,x,t) = \sum_{m=1}^{M} \sum_{n=1}^{N} B_{mn} \sin \alpha_m x \cos n\theta \, e^{-i\omega t} \qquad (4\text{-}5)$$

$$w(\theta,x,t) = \sum_{m=1}^{M} \sum_{n=1}^{N} C_{mn} \sin \alpha_m x \sin n\theta \, e^{-i\omega t}$$

SOLUTIONS

A set of linear algebraic equations can be obtained from the equations of motion by substitution of the kinetic energy Equation 4-2, the strain energy Equation 4-3, and the displacement functions Equations 4-4 and 4-5 into Equation 4-1:

$$- 0.3 D_A C_{mn} + 0.65 D_A B_{mn} - D\left(\alpha_m a + 0.35 \frac{n^2}{\alpha_m a^2}\right) A_{mn}$$

$$+ \omega^2 \left[0.5 M_S A_{mn} + m_a \cos \alpha_m x_a \cos \frac{n\pi}{2} \sum_{i=1}^{M} \sum_{j=0}^{N} \left(- e \alpha_i C_{ij} + A_{ij}\right) \cos \alpha_i x_a \cos \frac{j\pi}{2} \right] = 0 \quad .$$

$$0.65\, D_B\, n\, A_{mn} - \left[D_A \left(\frac{n}{\alpha_m\, a} + 0.35\, \alpha_m \right) + D_B \left(\frac{n^2}{\alpha_m\, a^3} + 1.4\, \frac{\alpha_m}{a} \right) \right] B_{mn}$$

$$+ \left[D_A\, \frac{n}{\alpha_m\, a} + D_B \left(1.7\, \alpha_m\, \frac{n}{a} + \frac{n^3}{\alpha_m\, a^3} \right) \right] C_{mn} + \omega^2 \left\{ 0.5\, M_S\, B_{mn} \right.$$

$$+ M_a \left(1 - \frac{e}{a} \right) \sin \alpha_m\, x_a \sin \frac{n\pi}{2} \sum_{i=1}^{M} \sum_{j=0}^{N} \left[\frac{ej}{a}\, C_{ij} \right.$$

$$\left. + \left(1 - \frac{e}{a} \right) B_{ij} \right] \sin \alpha_i\, x_a \sin \frac{j\pi}{2} + \frac{1}{a^2}\, I_x \sin \alpha_m\, x_a \sin \frac{n\pi}{2}$$

$$\left. \sum_{i=1}^{M} \sum_{j=0}^{N} \left(- j\, C_{ij} + B_{ij} \right) \sin \alpha_i\, x_a \sin \frac{j\pi}{2} \right\} = 0$$

$$\left[D_B \left(1.7\, \alpha_m\, \frac{n}{a} + \frac{n^3}{\alpha_m\, a^3} \right) + D_A\, \frac{n}{\alpha_m\, a} \right] B_{mn} - 0.3\, D_A\, A_{mn}$$

$$- \left[D_B\, \frac{a}{\alpha_m} \left(\alpha_m^{\,2} + \frac{n^2}{a^2} \right)^2 + D_A\, \frac{L}{m\pi a} \right] C_{mn} + \omega^2 \left\{ 0.5\, M_S\, C_{mn} \right.$$

$$+ m_a \left[\sin \alpha_m\, x_a \cos \frac{n\pi}{2} \sum_{i=1}^{M} \sum_{j=0}^{N} C_{ij} \sin \alpha_i\, x_a \cos \frac{j\pi}{2} \right.$$

$$- e\, \alpha_m \cos \alpha_m\, x_a \cos \frac{n\pi}{2} \sum_{i=1}^{M} \sum_{j=0}^{N} \left(A_{ij} - e\, \alpha_i\, C_{ij} \right) \cos \alpha_i\, x_a$$

$$\left. \times \cos \frac{j\pi}{2} + \frac{1}{a}\, e\, n \sin \alpha_m\, x_a \sin \frac{n\pi}{2} \sum_{i=1}^{M} \sum_{j=0}^{N} \left(\frac{e}{a}\, j\, C_{ij} \right. \right.$$

$$+ B_{ij} - \frac{e}{a} B_{ij}) \sin \alpha_i x_a \sin \frac{j\pi}{2} \Bigg] + I_\theta \Bigg(\alpha_m \cos \alpha_m x_a$$

$$\times \cos \frac{n\pi}{2} \sum_{i=1}^{M} \sum_{j=0}^{N} \alpha_i C_{ij} \cos \alpha_i x_a \cos \frac{j\pi}{2} \Bigg)$$

$$+ \frac{1}{a^2} I_x \Bigg[- n \sin \alpha_m x_a \sin \frac{n\pi}{2} \sum_{i=1}^{M} \sum_{j=0}^{N} (B_{ij} - j C_{ij})$$

$$\sin \alpha_i x_a \sin \frac{j\pi}{2} \Bigg] \Bigg\} = 0$$

Matrix iteration methods now can be applied, and computer programs can be conveniently written for solving the natural frequencies and modes. The Jacobian subroutine used in this study resulted in solution of 33 natural frequencies. Although only a few terms (M = N = 3) were used, and extremely short computer time was consumed, the analytical results appear to be surprisingly accurate in comparison with the experimental data and results obtained by Arnold and Warburton (References 29 and 30) and by Weigarten (Reference 31). Part of the analytical results are presented in Table 3 and will be compared in a later section with the experimental data for the lower frequencies, which are generally most important in engineering applications. Unfortunately, the experiment could not provide more corresponding frequencies for comparisons because of the limitation of the structural response characteristics of a thin shell to a point excitation at the circumference.

The solutions presented are for the symmetric case. Similar frequency equations and solutions with only a few different terms and sign changes can be found for the antisymmetric case resulting from the substitution of the corresponding displacement function, Equation 4-5.

Through a similar procedure, the solution for forced vibration response can be directly obtained by solving the equations of motion, which include

the forcing function terms. Adding the generalized forces Q_x, Q_θ, and Q_w to Equation 4-1, the equations of motion for forced vibration are

$$\frac{d}{dt}\left(\frac{\partial T}{\partial \dot{A}_{mn}}\right) - \frac{\partial T}{\partial A_{mn}} + \frac{\partial V}{\partial A_{mn}} = Q_x$$

$$\frac{d}{dt}\left(\frac{\partial T}{\partial \dot{B}_{mn}}\right) - \frac{\partial T}{\partial B_{mn}} + \frac{\partial V}{\partial B_{mn}} = Q_\theta$$

$$\frac{d}{dt}\left(\frac{\partial T}{\partial \dot{C}_{mn}}\right) - \frac{\partial T}{\partial C_{mn}} + \frac{\partial V}{\partial C_{mn}} = Q_w$$

Table 3. Computed Natural Frequencies (CPS) of Shell

Case Number	0	1	2	3	4	5	6
M_2/M_1 / Mode No.	0	0.16	0.32	0.60	0.82	1.40	1.90
1	75.8	75.7	75.6	75.2	75.0	74.7	73.7
2	121.3	117.9	114.1	105.7	102.7	94.6	83.7
3	221.2	220.6	219.8	217.7	216.9	214.7	209.5
4	322.6	321.5	320.4	318.5	317.2	313.8	255.7
5	416.0	411.6	407.4	399.3	388.0	324.2	309.7
6	446.1	445.5	444.7	426.0	401.7	385.1	369.8
7	798.7	664.5	564.5	442.7	442.1	440.3	436.5
8	939.4	933.1	927.3	917.3	917.3	893.7	874.8
9	1355.4	1344.4	1332.2	1306.6	1291.4	1232.7	973.3
10	1560.6	1556.0	1551.8	1544.7	1526.1	1281.9	1209
11	2521.8	2521.8	2234.2	1648.3	1540.0	1529.7	1518.4
12	2591.5	2584.2	2521.7	2521.6	2521.6	2521.4	2376.1
13	3240.3	2675.4	2579.1	2567.1	2557.9	2528.8	2521.2
14	3243.8	3239.5	3238.8	3089.6	2992.5	2760.1	2549.7
15	3675.3	3545.0	3401.9	3237.4	3236.4	3233.3	3229.6
16	3844.5	3807.5	3776.9	3722.8	3689.3	3614.3	3519.3
17	3944.5	3941.0	3937.9	3932.7	3928.1	3915.1	3900.8

For systems including damping, the strain energy is described in terms of complex Modulus of Elasticity ($\bar{E}$) instead of the Young's modulus of elasticity (E) which is all that is required for undamped structures. Since the free-vibration characteristics have been solved, the laborious computations given herein may be substituted with simple textbook methods for solving forced vibrations of simple systems. The empirical information provided in later sections may be used for estimating the transmissibility characteristics of mass-loaded ring and shell structures.

PRECEDING PAGE BLANK NOT FILMED

5.0 EXPERIMENTAL INVESTIGATION

DESIGN AND FABRICATION

Two test specimens were designed and fabricated for the experimental investigation: (1) an aluminum ring of 18-in. OD, 0.050-in. thickness, and 3-in. length and (2) an aluminum cylindrical shell of 18-inch OD, 0.050-inch thickness, and 72-inch length with a 1/4-inch-thick flange welded to the upper end and a 1/2-inch-thick flange welded to the lower end. This is one of the three shell models previously fabricated for the Axial Transmissibility Contract, NAS8-18124.

Thirteen aluminum or steel blocks of various sizes also were fabricated; their properties are given in Table 4. By mounting one or more of these solid blocks on the ring or shell, the mass-loaded test speciments were obtained.

TEST SET-UP AND INSTRUMENTATION

Ring Test Set-up

The vibration test set-up is shown in Figure 10. The ring specimen was suspended by five nylon strings on a test fixture on load from the California Institute of Technology. An electroinduction shaker, built for the mass-loaded beam vibration test in the Phase I program of the contract, was installed beside the ring to produce a constant force excitation. An optical micrometer, which was set up to observe the gap between the ring and the shaker. A constant gap of 0.057 inch was maintained during all test runs.

The attached mass, cemented on the outer surface of the ring, also was suspended on the fixture by strings to prevent twisting of the ring.

The vibration responses were measured by a proximity gage and 16 miniature accelerometers. The proximity gage, a Photocon Model PT-3, was mounted on the test fixture. The probe of the gage was kept close to the inner surface of the ring with a gap of about 0.125 inch. A small d-c motor was used to drive the proximity gage around the ring so that the radial displacement response could be measured and plotted continuously against the circumferential distance of the ring. Each of the accelerometers, except the one at the mass location, was attached to a lightweight fiberglass block, which in turn, was cemented on the outer surface of the ring. At the mass location, the accelerometer was mounted directly on the ring and under the mass.

Table 4. Properties of Attached Masses

Mass No.	Material	Thickness (Inches)	Weight (Grams)	Length of 1/4-Inch Bolt (Inches)	Weight of 4 Bolts (Grams)
K	Alum.	1/4	64.5	--	--
J	Alum.	3/8	94	--	--
b_1	Alum.	1/2	127	--	--
b_2	Alum.	1/2	127	--	--
H_1	Steel	1/4	181	1/2	19
G_1	Steel	3/8	280	3/4	25
G_2	Steel	3/8	283	3/4	25
F_1	Steel	1/2	365	3/4	25
E_2	Steel	5/8	480	1	29
C_1	Steel	1	740	1-1/2	40.5
B_2	Steel	1-1/4	890	1-1/2	40.5
A_1	Steel	1-1/2	1110	2	63
A_2	Steel	1-1/2	1110	2	63

Note: All masses are rectangular blocks 2 inches wide and 3 inches long.

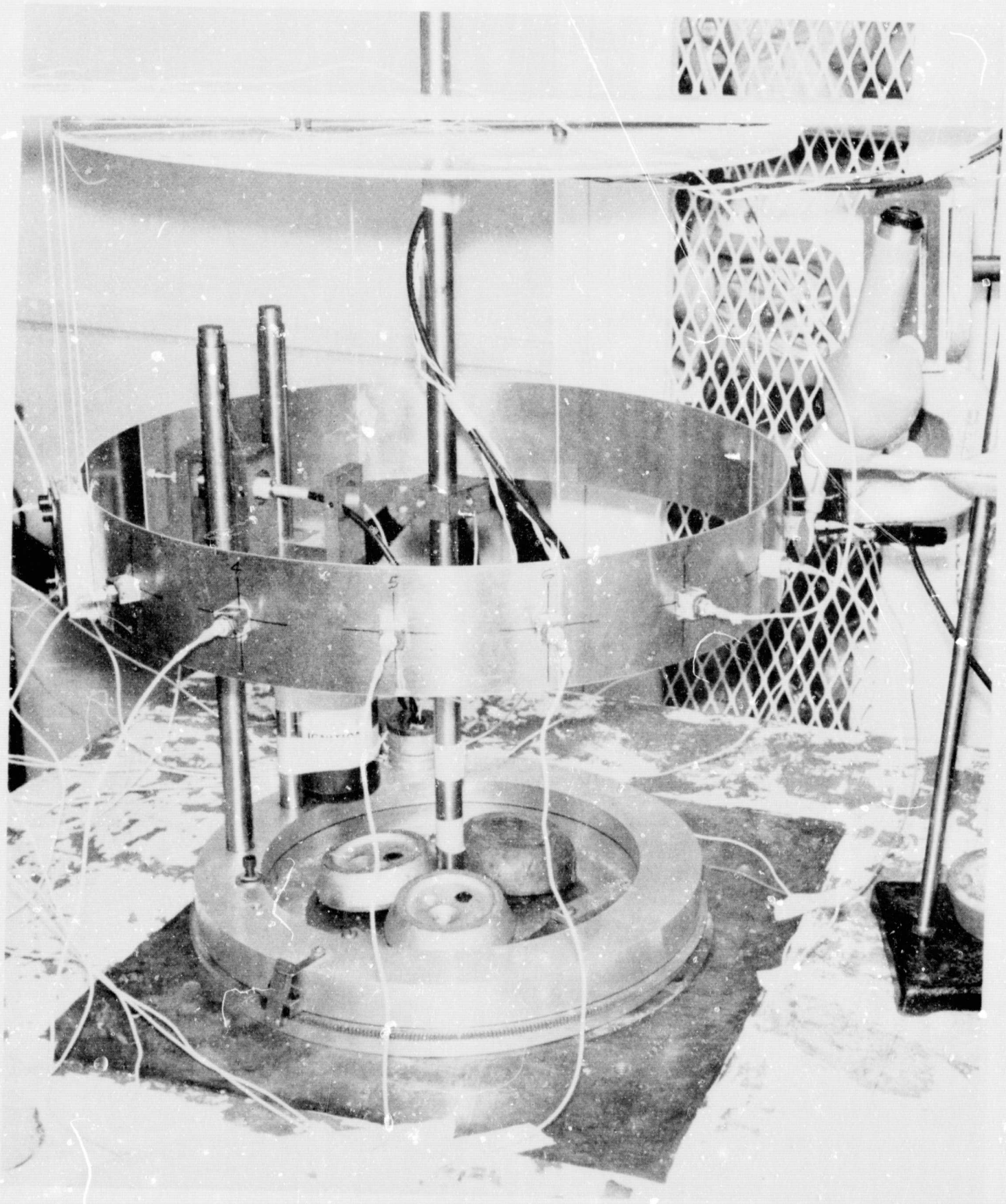


Figure 10. Vibration Test Set-up for Ring

Shell Test Set-up

The general arrangement of the vibration test of the shell is shown in Figure 11. The shell was placed upright on a rigid floor with its lower flange fastened by bolts. The electroinduction shaker was set up at a Level F, 54 inches above the lower end. The proximity gage set-up used in the ring test was suspended above the cylinder with the gage extended downward inside the shell to survey the mode shape as shown in Figure 12. The acceleration responses were measured by 20 miniature accelerometers of which 16 were equally spaced around the circumference at Level F and the rest placed at Column 2 as shown in Figure 13.

Other test equipments used in both ring and shell test included the following:

1. Driving amplifier
2. Band spread oscillator
3. Electronic counter
4. Dual beam oscilloscope
5. Voltmeter
6. 100-channel switch box
7. Visicorder
8. X-Y plotter

Some of the equipments listed are shown in Figures 14 and 15.

TEST OPERATION OF UNLOADED AND MASS-LOADED RINGS

Two sets of vibration tests were performed for the mass-loaded and unloaded rings. One set of tests was for the cases with only one accelerometer on the ring (the one at the mass location). In these cases, the ring was called Ring I. The other set of tests was for the cases with 16 accelerometers equally spaced on the ring circumference; the ring was called Ring II. All test runs are listed in Table 5. Test started from the unloaded ring, then went on to the mass-loaded cases. Both of the masses b_1 and K have concave contours on one side to match the outer surface of the ring. They were cemented to the ring at Location 2, opposite the shaker. The other solid masses were bolted to mass b_1 at various combinations to give different mass ratios.

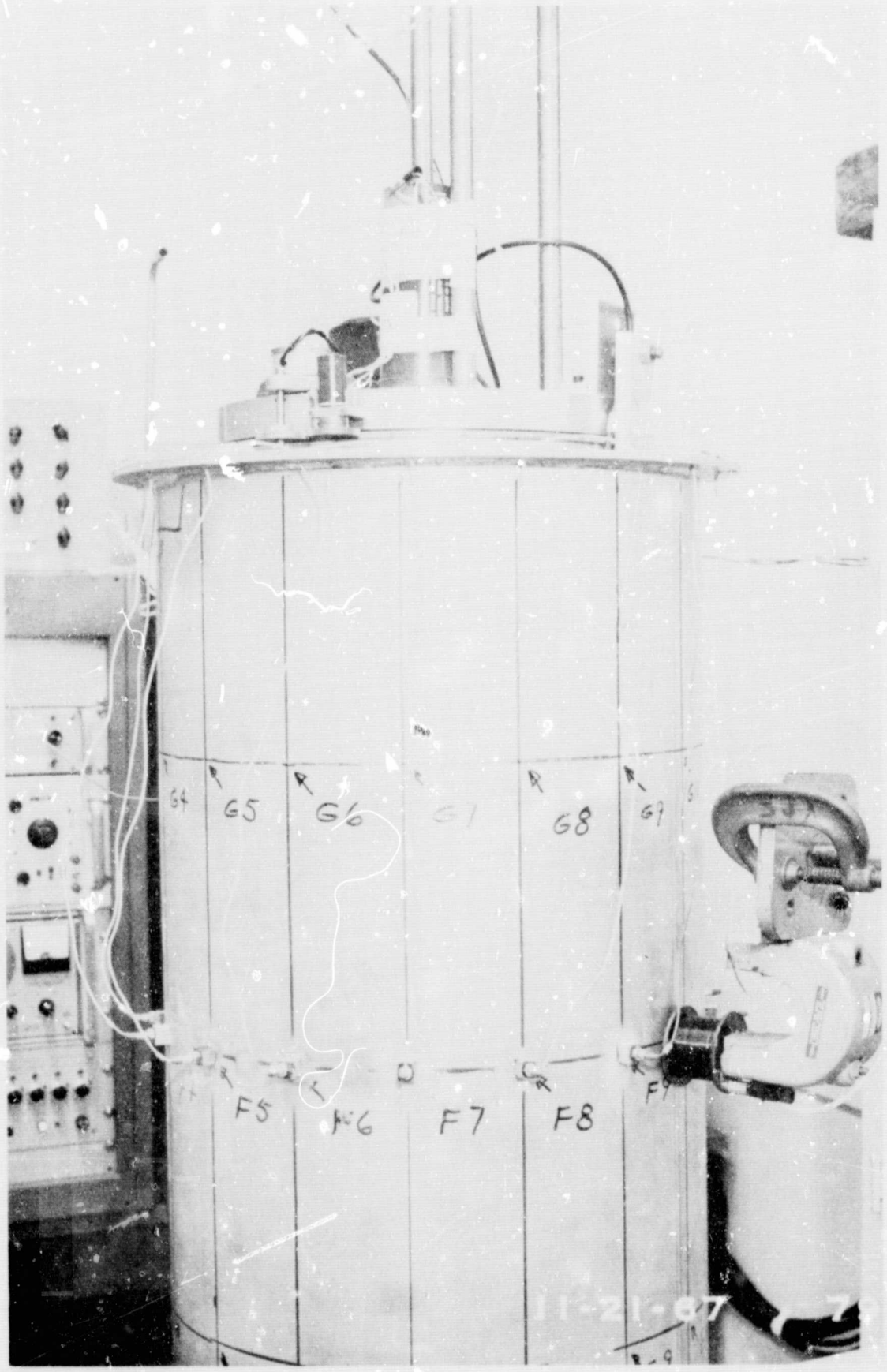


Figure 11. Vibration Test Set-up for Shell

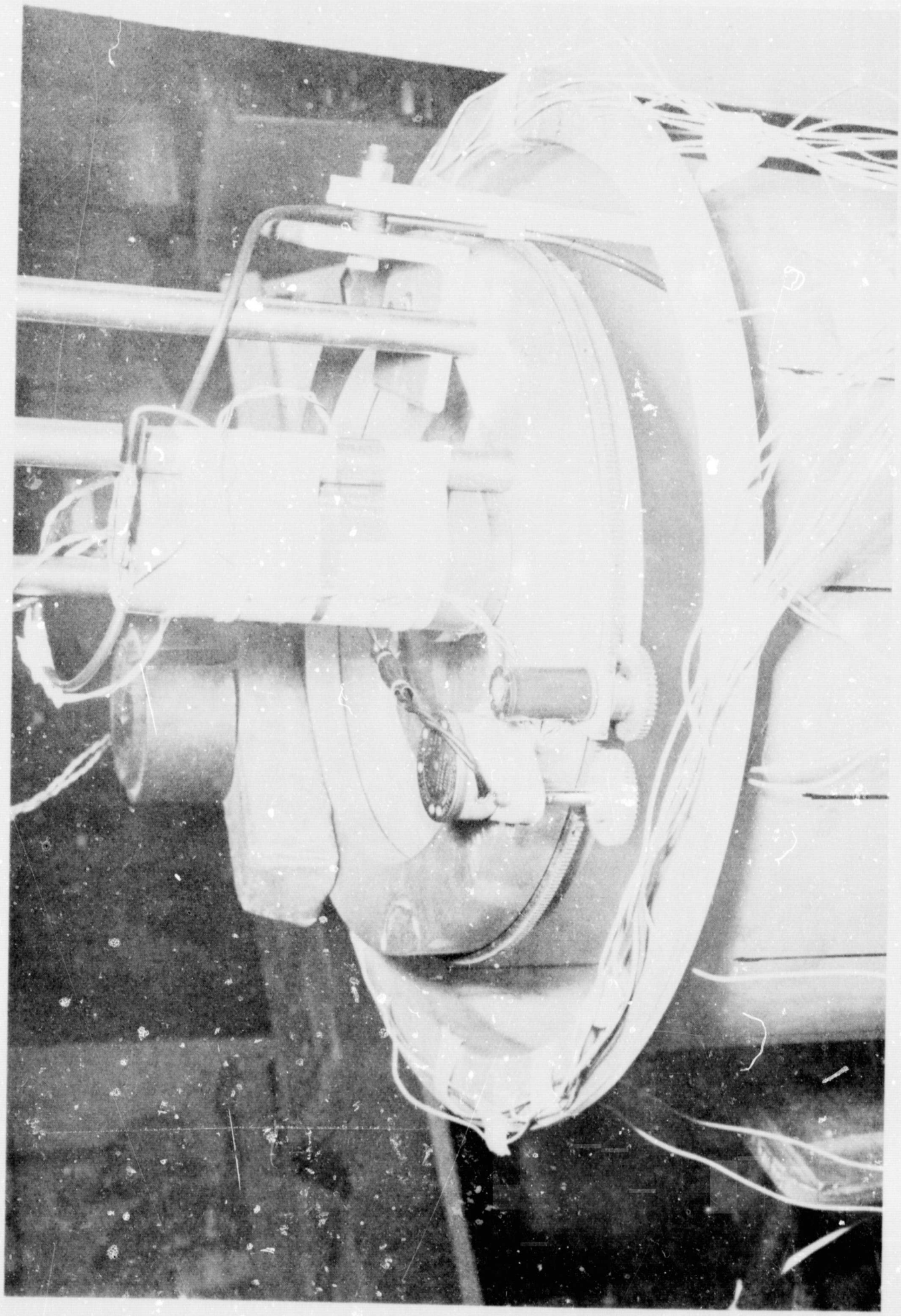


Figure 12. Proximity Gage Set-up for Plotting Radial Mode Shapes of Shell

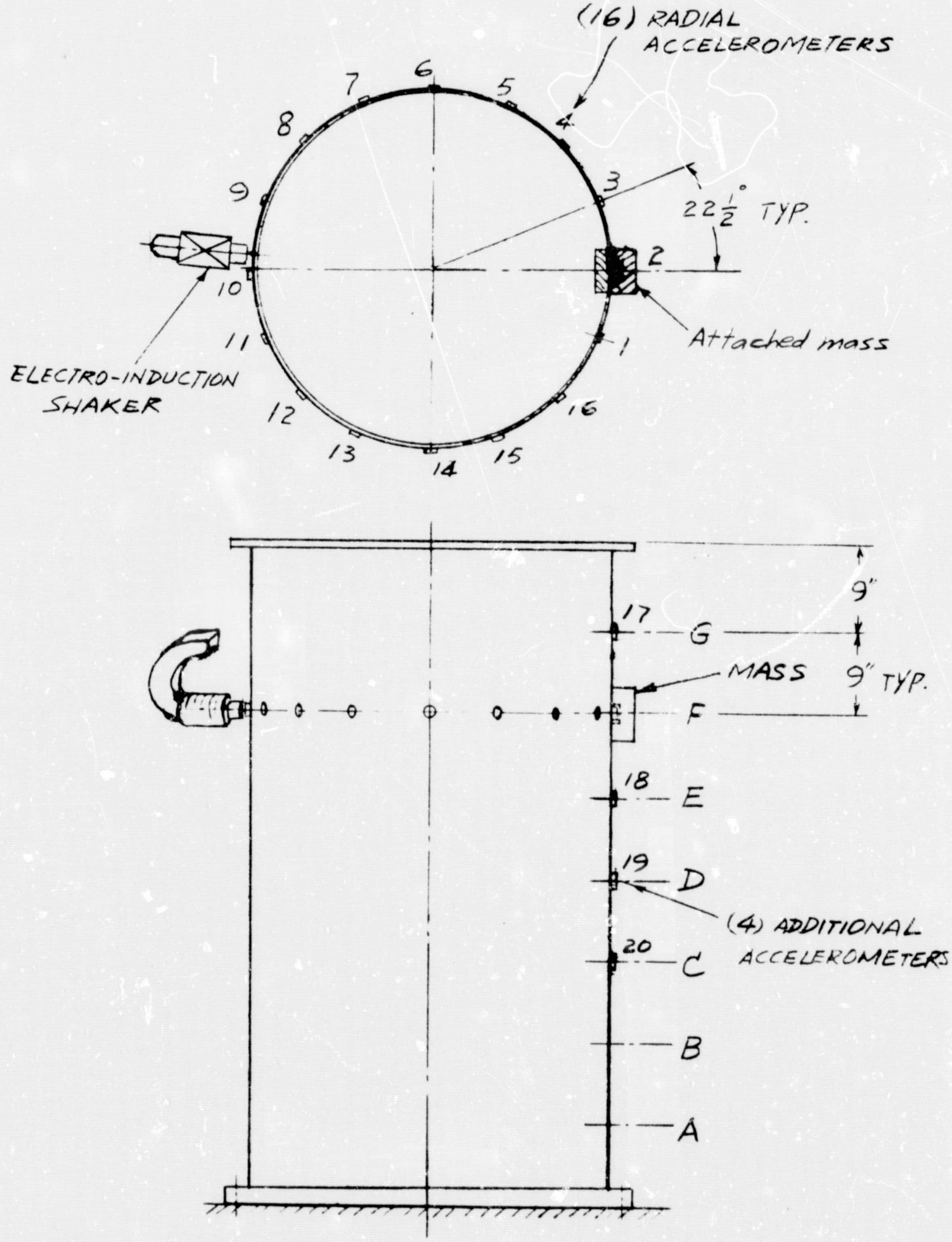


Figure 13. Accelerometers Set-up for Vibration Test of Mass-Loaded Shell

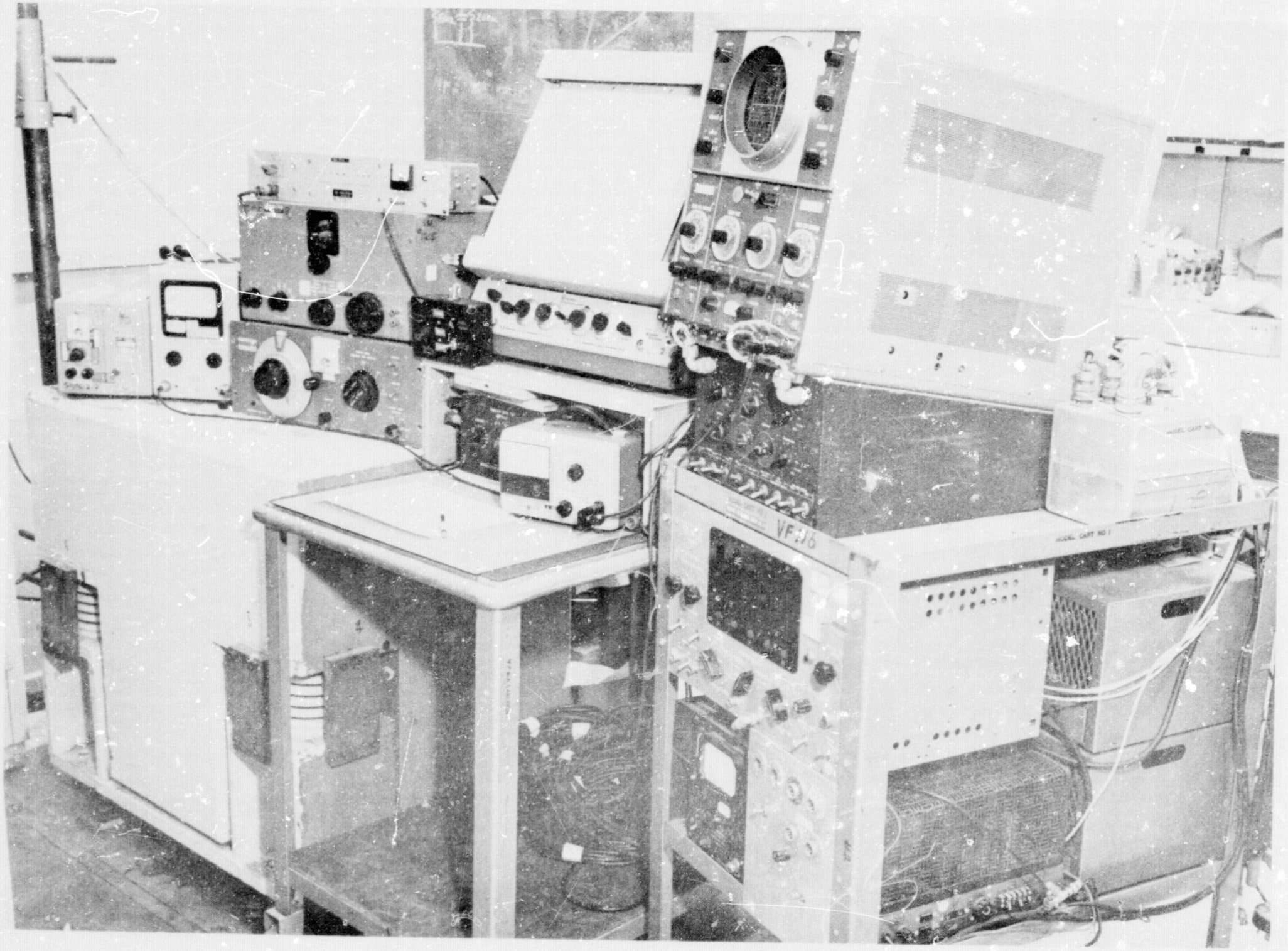


Figure 14. Instrumentation Set-up for Vibration Tests of Ring and Shell, Part I

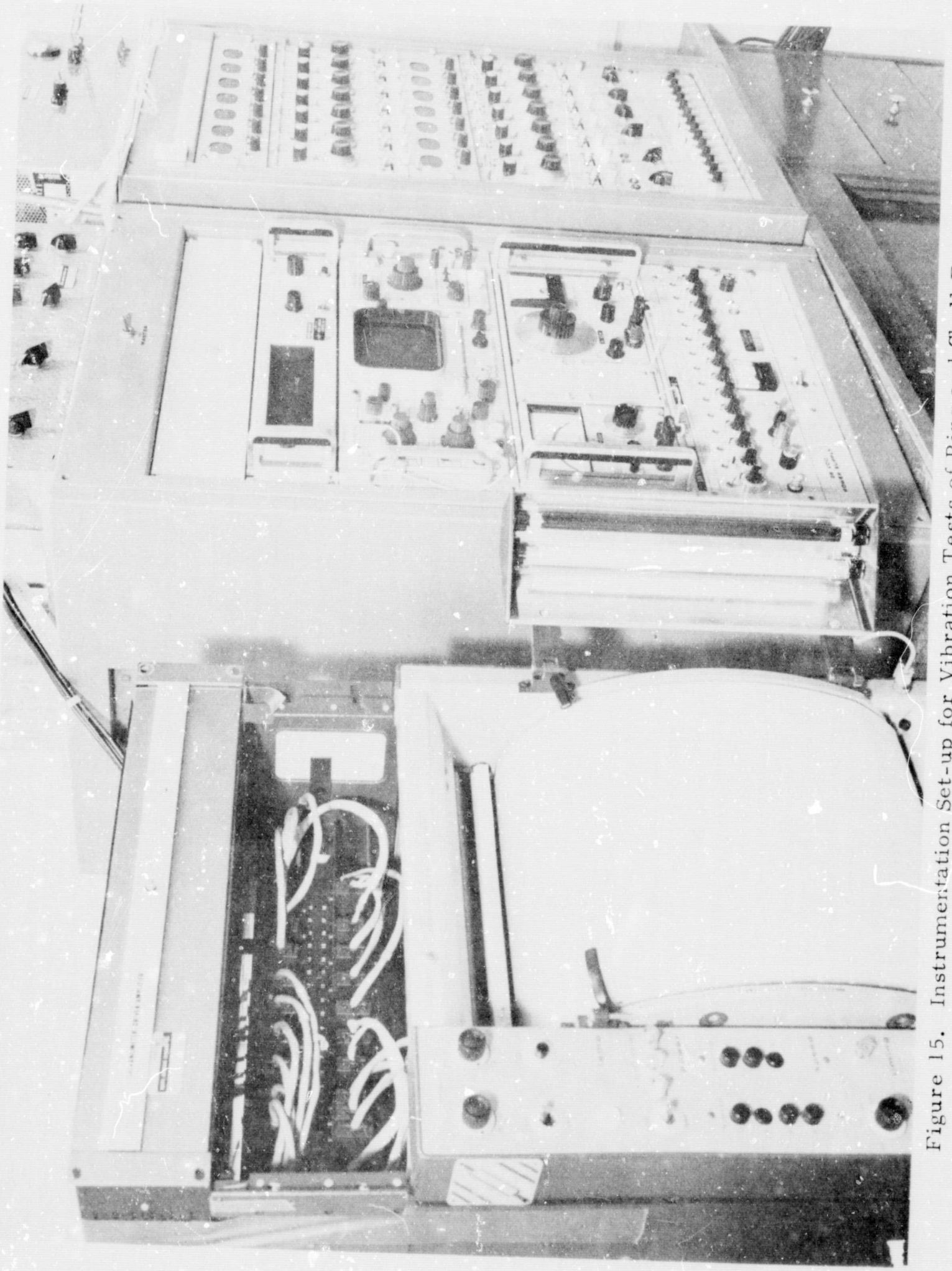


Figure 15. Instrumentation Set-up for Vibration Tests of Ring and Shell, Part II

Table 5. Vibration Test Runs for Unloaded and Mass-Loaded Rings

Run Number (1)	Mass Number	Weight of Mass (Grams)	Weight of 4 Bolts (Grams)	Total Weight M_2 (Grams)	Mass Ratio M_2/M_1 (2)
0, 0-1	0	0	0	0	0
1.1	K	64.5	0	64.5	0.16
1, 1-1	b_1	127	0	127	0.32
1.2, 1.2-1	$b_1 + J$	221	19	240	0.60
2, 2-1	$b_1 + H_1$	308	19	327	0.82
4, 4-1	$b_1 + G_1$	407	25	432	1.08
5, 5-1	$b_1 + H_1 + G_2$	591	40.5	631.5	1.58
7, 7-1	$b_1 + E_2 + F_1$	972	40.5	1012.5	2.54
8, 8-1	$b_1 + C_1 + E_2$	1347	63	1410	3.52

NOTES: (1) The Run Numbers from 0 to 8 are for the cases with only one accelerometer on the ring. Those numbers followed by -1 are for the cases with 16 accelerometers on the ring.

(2) M_1 = 400 gm. = weight of the unloaded ring.

The test operation was as follows:

1. Unloaded Ring

   a. Performed a resonance survey using a sinusoidal sweep at one minute per octave from 5 to 3800 cps. Maintained a constant voltage of 6 volts input to the shaker for all test runs. Repeated the sweep from 5 to 760 cps.
   b. Obtained X-Y plots for the accelerometer output at the mass location during the above sweeps to determine the natural frequencies and maximum responses.
   c. At the first five natural frequencies obtained the following data:

      (1) Mode shape plots from the proximity gage.
      (2) Oscillograph records for all accelerometer responses.
      (3) Meter readings for all accelerometer outputs.

2. Mass-Loaded Ring

   a. Mounted the solid mass (or masses) on the ring according to Table 5.
   b. Performed sinusoidal test as in Steps A-1 to A-3.

TEST OPERATION OF UNLOADED AND MASS-LOADED SHELLS

Three sets of vibration tests using the electroinduction shaker were performed for the mass-loaded and unloaded shells. The first set of tests was for the cases with only one accelerometer on the shell at the mass location F2 (Figure 13). The shell was called Shell I in these cases. The second set of tests was for the cases with 20 accelerometers on the shell, of which 16 were equally spaced on the shell circumference at level F and 4 were placed in the same column, No. 2, as the mass but at different levels, C, D, E and G, as shown in Figure 13. In these cases, the test specimen was called Shell II. The third set of tests was for the cases with 15 accelerometers attached to the shell in a single column, No. 2, and equally spaced at 15 levels, plus 5 accelerometers at 5 levels in Column 14, 90 degrees apart from Column 2. In these cases the test model was called Shell 3. All test runs are listed in Table 6. The method of mounting the various masses on the shell was the same as described previously for the mass-loaded ring except that the mass b_2 was cemented on the inner surface of the shell at the mass location to reduce rocking motion of the heavy masses attached outside the cylinder. In Table 6, the test run numbers are also identified by mass ratios M_2/M_1. The quantity M_1 is defined as the mass of the unloaded shell section whose length is the same as the attached mass, 3 inches in the present cases. This shell section under the attached mass is

Table 6. Vibration Test Runs for Unloaded and Mass-Loaded Shells Excited by Electroinduction Shaker

Run Number	Mass Number	Weight of Mass (Grams)	Weight of 4 Bolts (Grams)	Total Weight M_2 (Grams)	Mass Ratio M_2/M_1
0, 0-2, 0-3	0	0	0	0	0
1a-2	K	64.5	0	64.5	0.16
1, 1-2, 1-3	b_1	127	0	127	0.32
1.2-2	$b_1 + J$	221	19	240	0.60
2-2	$b_1 + H_1$	308	19	327	0.82
3, 3-2, 3-3	$b_1 + b_2$	245	0	245	0.61
4, 4-2, 4-3	$b_1 + b_2 + G_1$	525	25	550	1.40
5, 5-2, 5-3	$b_1 + b_2 + H_1 + G_2$	709	44	753	1.90
7, 7-2, 7-3	$b_1 + b_2 + E_2 + F_1$	1090	54	1144	2.86
8, 8-2, 8-3	$b_1 + b_2 + C_1 + E_2$	1465	69.5	1534.5	3.84
9, 9-2, 9-3	$b_1 + b_2 + B_2 + C_1$	1875	81	1956	4.9

Notes: (1) Runs 0, 1, 3, 4, 5, 7, 8, and 9 are the cases with 16 accelerometers around the shell at the same Level F. Run numbers with -2 are the cases with only one accelerometer at the mass location. Run numbers with -3 are the cases with 15 accelerometers in one Column No. 2 along the shell

(2) All solid masses except b_2 are mounted on the outer surface of the shell.

(3) M_1 = 400 gm = weight of unloaded shell section of 3 inches long.

then identical to the ring test model. Therefore, M_1 is taken to be 400 gm or 0.883 lb.

The test operations for the unloaded and mass-loaded Shells I and II were the same as those for the ring tests. On Shell III the radial accelerometers were placed in two columns to measure lateral bending modes. Only oscillographs and meter readings were taken during each resonance. No X-Y plots were made.

PRECEDING PAGE BLANK NOT FILMED

6.0 COMPARISON OF ANALYTICAL AND EXPERIMENTAL RESULTS

For verification of the results, the experimental data obtained from various tests in the program are compared with the analytical solutions. Two groups of data are presented: (1) natural frequencies and modes of free vibration, and (2) acceleration response or transmissibility in forced vibration.

Notations used in the tables and diagrams of this section are the following:

f = natural frequency in cps

G = maximum acceleration response in g's measured at the discrete mass mounting location

M = mass

m = number of axial half-waves in shell

n = number of circumferential waves in ring or shell

Subscripts:

1 = unloaded ring or shell

2 = mass-loaded ring or shell

MASS-LOADED AND UNLOADED RINGS

Vibration test data of the mass-loaded and unloaded rings are presented in Tables 7 and 8. Listed in these tables are the natural frequencies and acceleration responses (at the mass location) for the first five modes of the ring. Frequency ratios f_2/f_1 and acceleration ratios (G_2/G_1) are also given. For Ring I, there is one unloaded case $(M_2/M_1 = 0)$ and 8 mass-loaded cases with mass ratio M_2/M_1 ranging from 0.16 to 3.52. For Ring II, there are seven mass-loaded cases with M_2/M_1 ranging from 0.32 to 3.52 in addition to one unloaded case.

A comparison of the natural frequencies of Ring I between the analytical and experimental results are presented in Tables 9 and 10. Plots of the first five natural frequencies versus mass ratios are shown in Figures 16 and 17. Comparisons of the frequency ratios are given in Figures 18 through 23.

Table 7. Vibration Test Data of Ring I With One Accelerometer on Ring

Run No.		0	1.1	1	1.2	2	4	5	7	8
M_2/M_1		0	0.16	0.32	0.60	0.82	1.08	1.58	2.54	3.52
Mode 1, n = 2	Freq. (cps)	16.6	15.8	15.0	13.95	13.62	13.21	12.63	12.1	11.9
	f_2/f_1	1.0	0.951	0.902	0.840	0.821	0.796	0.761	0.729	0.717
	Accel. (g's)	6.5	4.6	3.54	2.2	2.0	1.6	1.28	0.94	0.76
	G_2/G_1	1.0	0.708	0.545	0.348	0.308	0.246	0.197	0.145	0.117
Mode 2, n = 3	Freq. (cps)	46.7	45.2	43.8	42.3	41.6	40.5	40.0	39.4	39.7
	f_2/f_1	1.0	0.967	0.937	0.905	0.890	0.866	0.855	0.841	0.848
	Accel. (g's)	14.5	10.6	6.0	4.65	3.9	2.84	2.2	1.48	0.95
	G_2/G_1	1.0	0.73	0.414	0.321	0.269	0.196	0.152	0.102	0.066
Mode 3, n = 4	Freq. (cps)	89.6	88.3	86.2	84.4	84.1	83.5	82.9	82.0	82.1
	f_2/f_1	1.0	0.985	0.962	0.941	0.939	0.931	0.925	0.915	0.915
	Accel. (g's)	23.5	12.5	7.9	5.2	4.1	2.97	1.8	1.42	1.15
	G_2/G_1	1.0	0.531	0.336	0.221	0.174	0.126	0.077	0.060	0.049
Mode 4, n = 5	Freq. (cps)	145.0	144.3	143.2	142.0	140.4	139.0	138.0	138.2	138.5
	f_2/f_1	1.0	0.995	0.988	0.979	0.968	0.959	0.952	0.953	0.955
	Accel. (g's)	31.0	8.5	6.7	4.5	3.8	2.75	1.82	1.32	1.00
	G_2/G_1	1.0	0.274	0.216	0.145	0.123	0.089	0.059	0.043	0.032
Mode 5, n = 6	Freq. (cps)	213.2	213.0	212.0	211.1	210.8	208.9	208.3	208.0	208.8
	f_2/f_1	1.0	1.0	1.0	0.996	0.989	0.980	0.977	0.976	0.980
	Accel. (g's)	41.3	13.8	8.0	5.2	4.2	3.1	2.62	1.25	1.00
	G_2/G_1	1.0	0.334	0.194	0.126	0.102	0.075	0.063	0.030	0.024

Table 8. Vibration Test Data of Ring II With 16 Accelerometers on Ring

Run No.		0-1	1-1	1.2-1	2-1	4-1	5-1	7-1	8-1
M_2/M_1		0	0.32	0.60	0.82	1.08	1.58	2.54	3.52
Mode 1, n = 2	Freq (cps)	15.0	13.72	12.78	12.46	12.10	11.50	11.0	10.6
	f_2/f_1	1.0	0.916	0.851	0.830	0.806	0.766	0.733	0.706
	Accel (g's)	4.2	2.65	1.92	1.35	0.93	0.70	0.51	0.39
	G_2/G_1	1.0	0.630	0.457	0.322	0.222	0.167	0.121	0.093
Mode 2, n = 3	Freq (cps)	42.2	39.4	37.7	37.2	36.6	36.1	35.4	35.1
	f_2/f_1	1.0	0.933	0.894	0.881	0.867	0.855	0.839	0.831
	Accel (g's)	6.1	3.3	2.8	2.3	2.0	1.5	0.99	0.76
	G_2/G_1	1.0	0.541	0.459	0.377	0.328	0.246	0.162	0.125
Mode 3, n = 4	Freq (cps)	80.7	77.4	75.5	74.8	74.3	73.6	73.1	72.8
	f_2/f_1	1.0	0.960	0.935	0.926	0.920	0.913	0.906	0.901
	Accel (g's)	8.3	3.0	2.05	1.8	1.45	0.94	0.75	0.48
	G_2/G_1	1.0	0.362	0.247	0.217	0.175	0.113	0.090	0.058
Mode 4, n = 5	Freq (cps)	130.9	127.7	125.1	124.3	123.8	123.4	122.5	122.5
	f_2/f_1	1.0	0.975	0.955	0.950	0.945	0.943	0.935	0.935
	Accel (g's)	5.2	2.45	1.57	1.0	0.77	0.53	0.37	0.27
	G_2/G_1	1.0	0.471	0.302	0.192	0.148	0.102	0.071	0.052
Mode 5, n = 6	Freq (cps)	190.9	188.3	186.7	186.6	186.2	185.5	185.0	184.5
	f_2/f_1	1.0	0.987	0.978	0.977	0.976	0.971	0.969	0.966
	Accel (g's)	7.4	2.08	1.52	1.03	0.81	0.65	0.46	0.33
	G_2/G_1	1.0	0.281	0.207	0.139	0.109	0.088	0.062	0.044

Table 9. Comparison of Natural Frequencies of Rings, Cases 0 to 4

Case Number	0		1		2		3		4	
Test Run Number	0		1.1		1		1.2		2	
$M_2 M_1$	0		0.16		0.32		0.60		0.82	
Mode \ Freq. cps	Comp.	Test	Comp.	Test	Comp.	Test	Comp.	Test	Comp.	Test
1	15.6	16.6	14.7	15.8	13.8	15.0	12.7	14.0	12.2	13.6
2	44.2	46.7	42.0	45.2	40.0	43.8	38.3	42.3	37.6	41.6
3	84.9	89.6	81.5	88.3	79.0	86.2	77.0	84.4	76.5	84.1
4	137.5	145.0	133.3	144.3	130.4	143.2	128.7	142.0	128.1	140.4
5	202.3	213.2	198.0	213.0	195.2	212.0	193.2	211.1	192.8	210.8
6	281.0	293.9	276.5	289.0	273.5	284.6	271.5	294.0	271.0	282.1
7	375.0	387.0	371.0	384.5	367.5	382.1	365.5	383.0	365.0	375.9
8	489.0	492.5	484.0	494.0	480.0	489.8	477.5	494.0	477.5	481.4
9	624.5	609.9	616.0	616.0	612.5	609.4	611.0	616.0	609.0	600.1
10	761.0	744.7	757.0	742.0	754.0	740.0	752.0	740.0	751.5	---

Table 10. Comparison of Natural Frequencies of Rings

Cases 5 to 8

Case Number	5		6		7		8	
Test Run Number	4		5		7		8	
M_2/M_1	1.08		1.58		2.54		3.52	
Mode \ Freq. (cps)	Comp.	Test	Comp.	Test	Comp.	Test	Comp.	Test
1	11.8	13.2	11.2	12.6	10.8	12.1	10.6	11.9
2	37.2	40.5	36.6	40.0	36.1	39.4	35.9	39.7
3	76.0	83.5	75.5	82.9	75.0	82.0	74.7	82.1
4	127.5	139.0	127.0	138.0	126.8	138.2	126.4	138.5
5	192.2	208.9	192.0	208.3	191.5	208.0	191.0	208.8
6	271.0	297.0	270.0	292.1	269.7	290.9	269.5	292.5
7	364.5	371.3	364.0	389.1	363.5	387.4	363.5	389.5
8	477.0	476.2	476.5	499.5	476.0	497.2	475.5	500.5
9	609.0	593.4	609.0	622.5	609.0	619.9	609.0	623.8
10	751.0	723.0	751.0	759.0	751.0	---	751.0	---

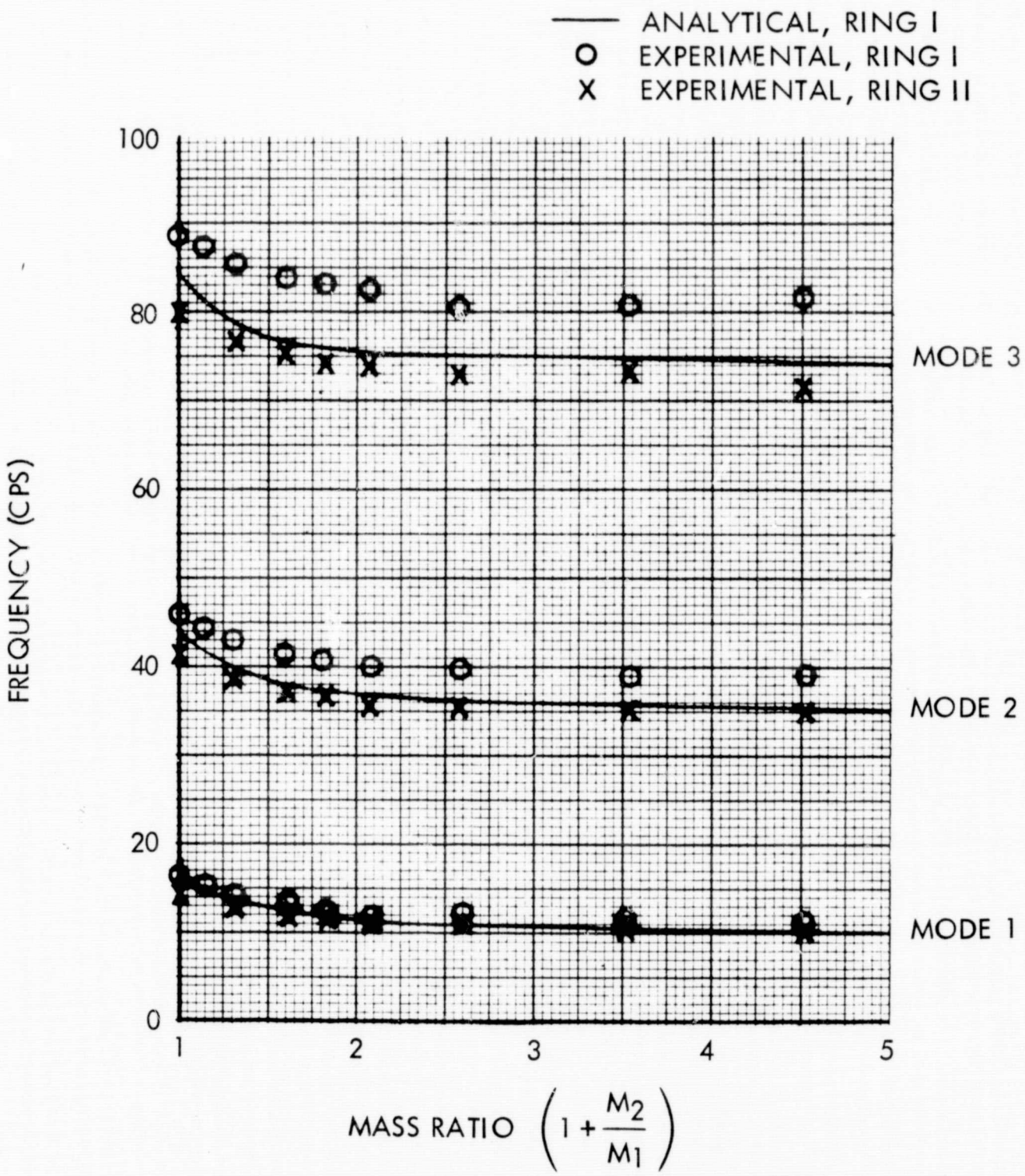


Figure 16. Comparison of Natural Frequencies of Rings, Modes 1, 2, and 3

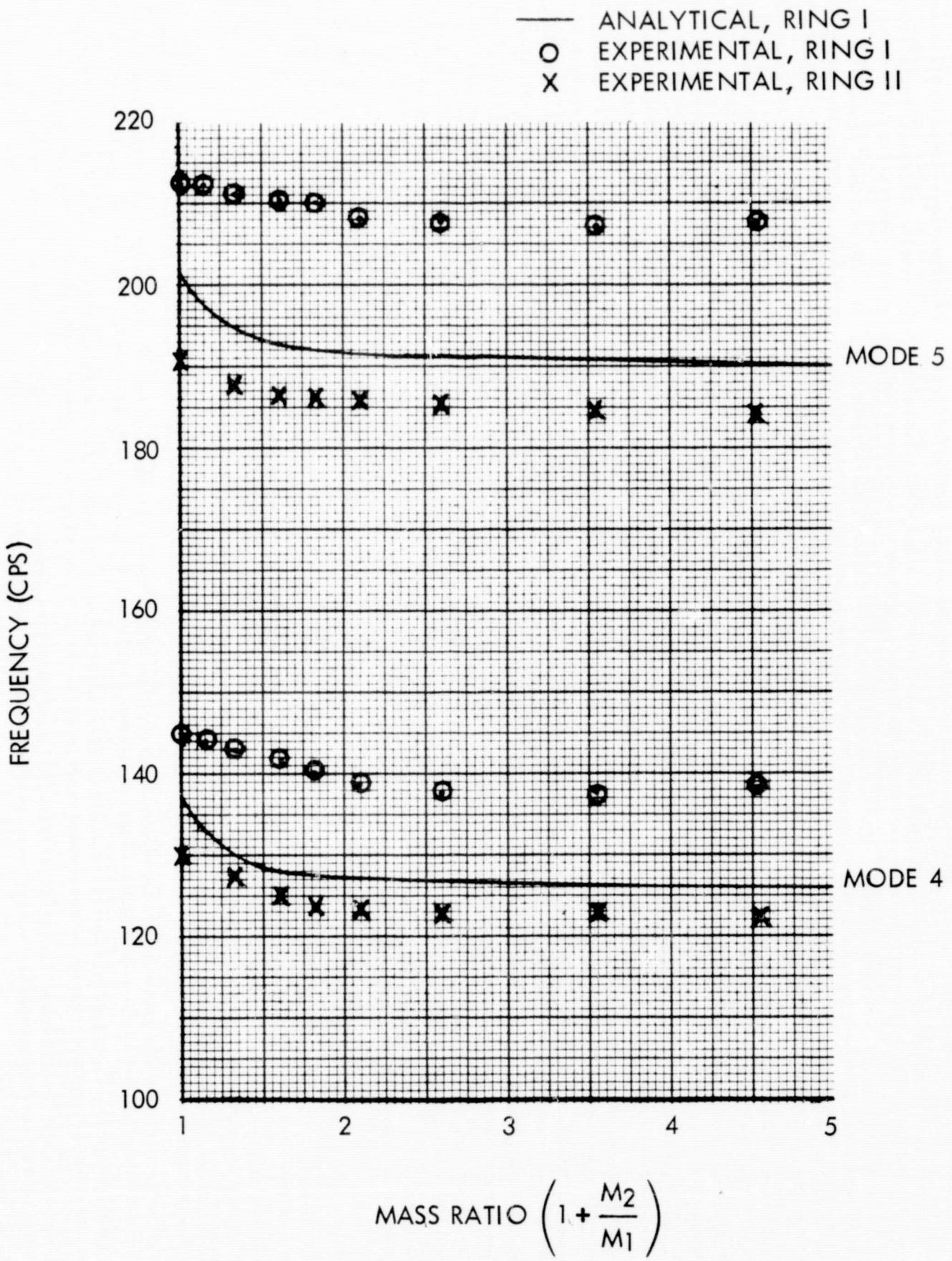


Figure 17. Comparison of Natural Frequencies of Rings, Modes 4 and 5

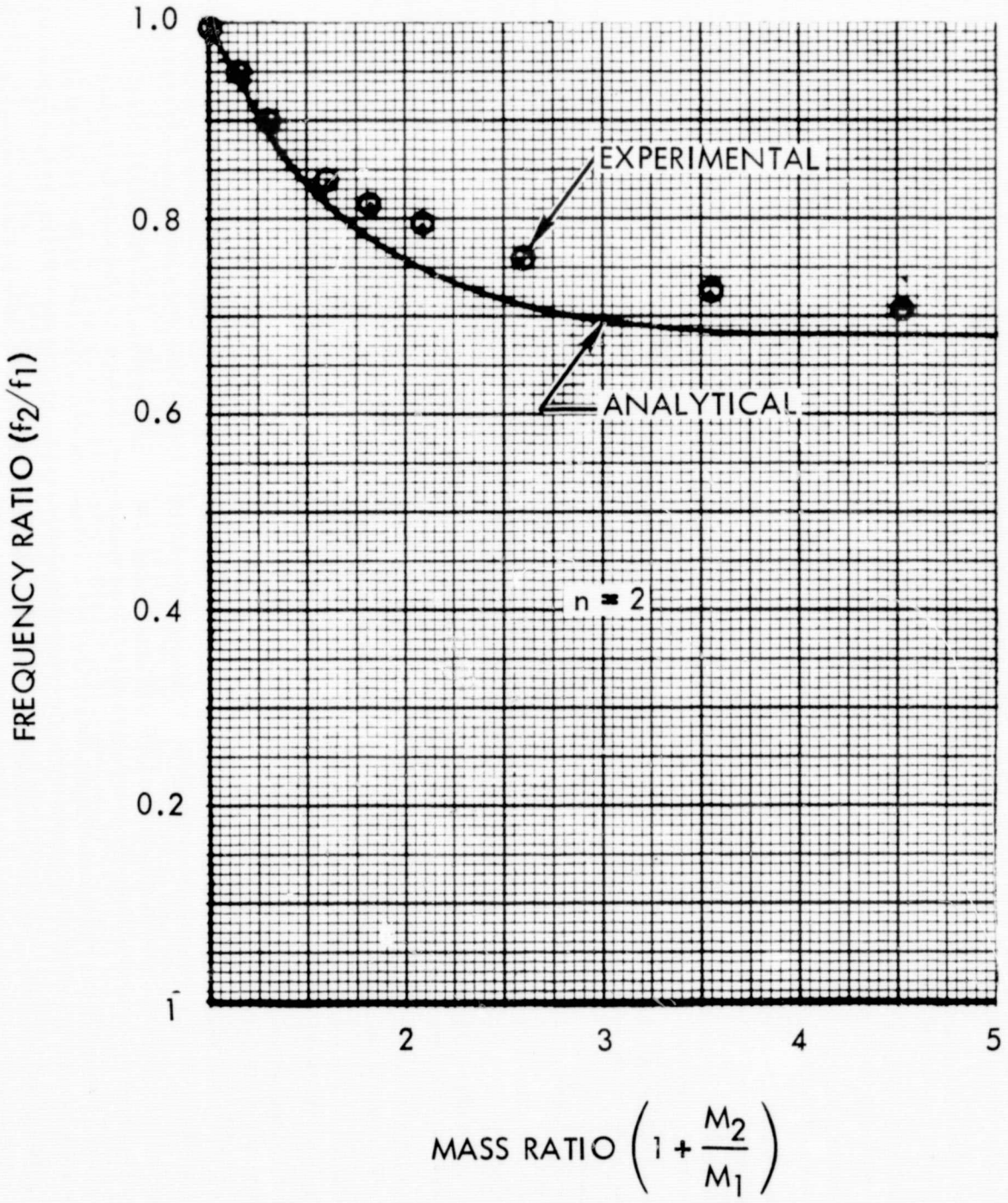


Figure 18. Comparison of Frequency Ratio of Ring I, Mode 1

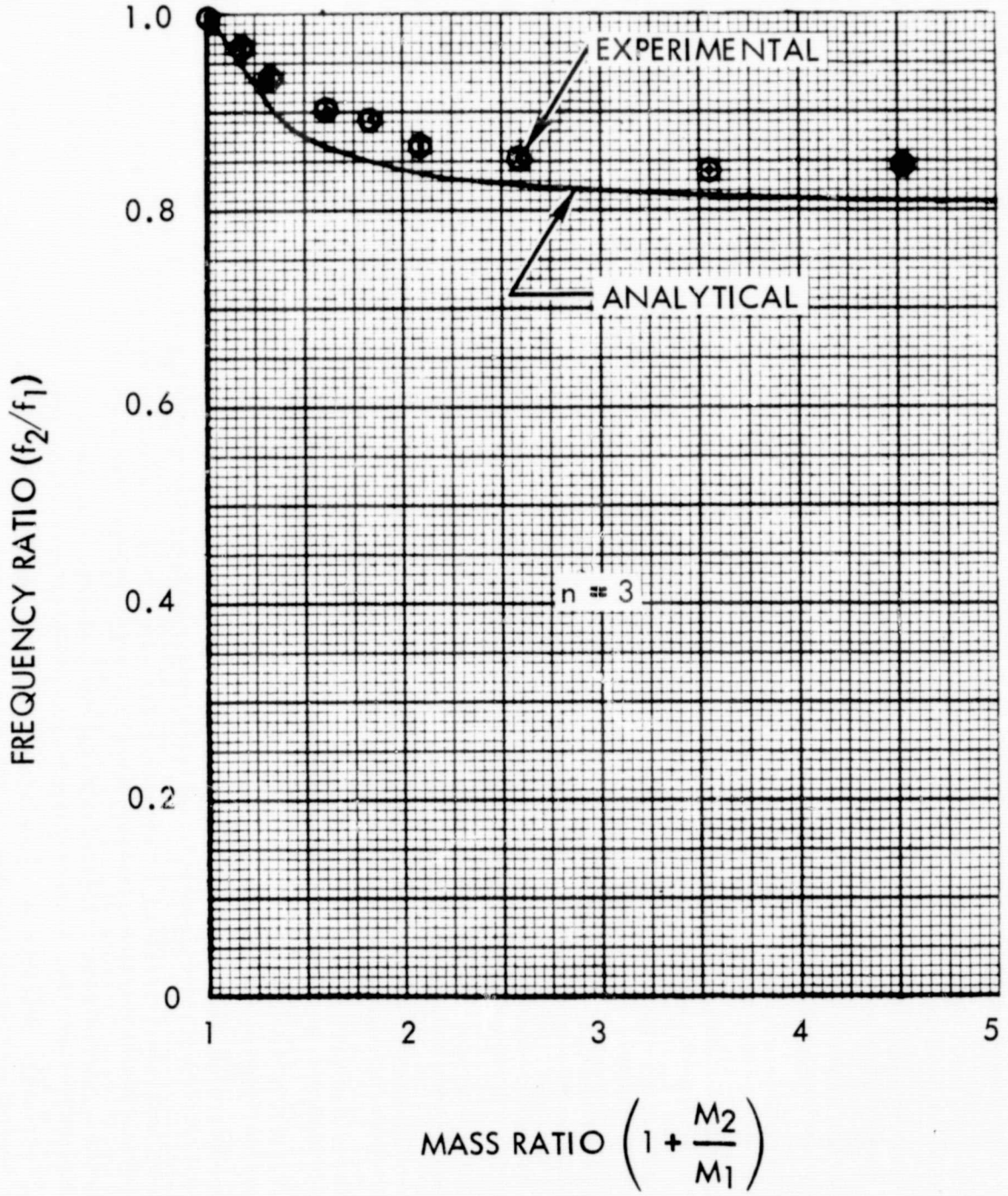


Figure 19. Comparison of Frequency Ratio of Ring I, Mode 2

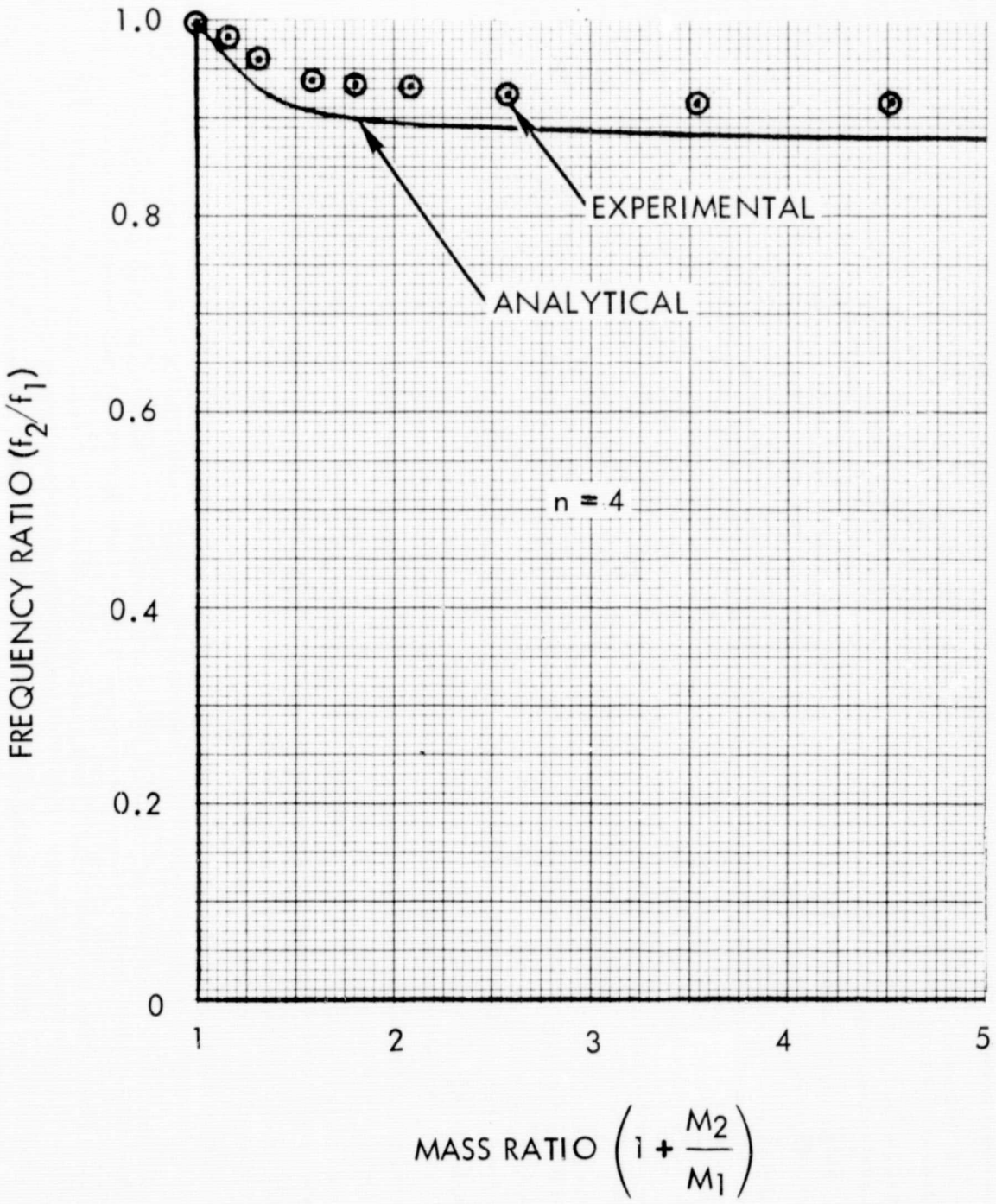


Figure 20. Comparison of Frequency Ratio of Ring I, Mode 3

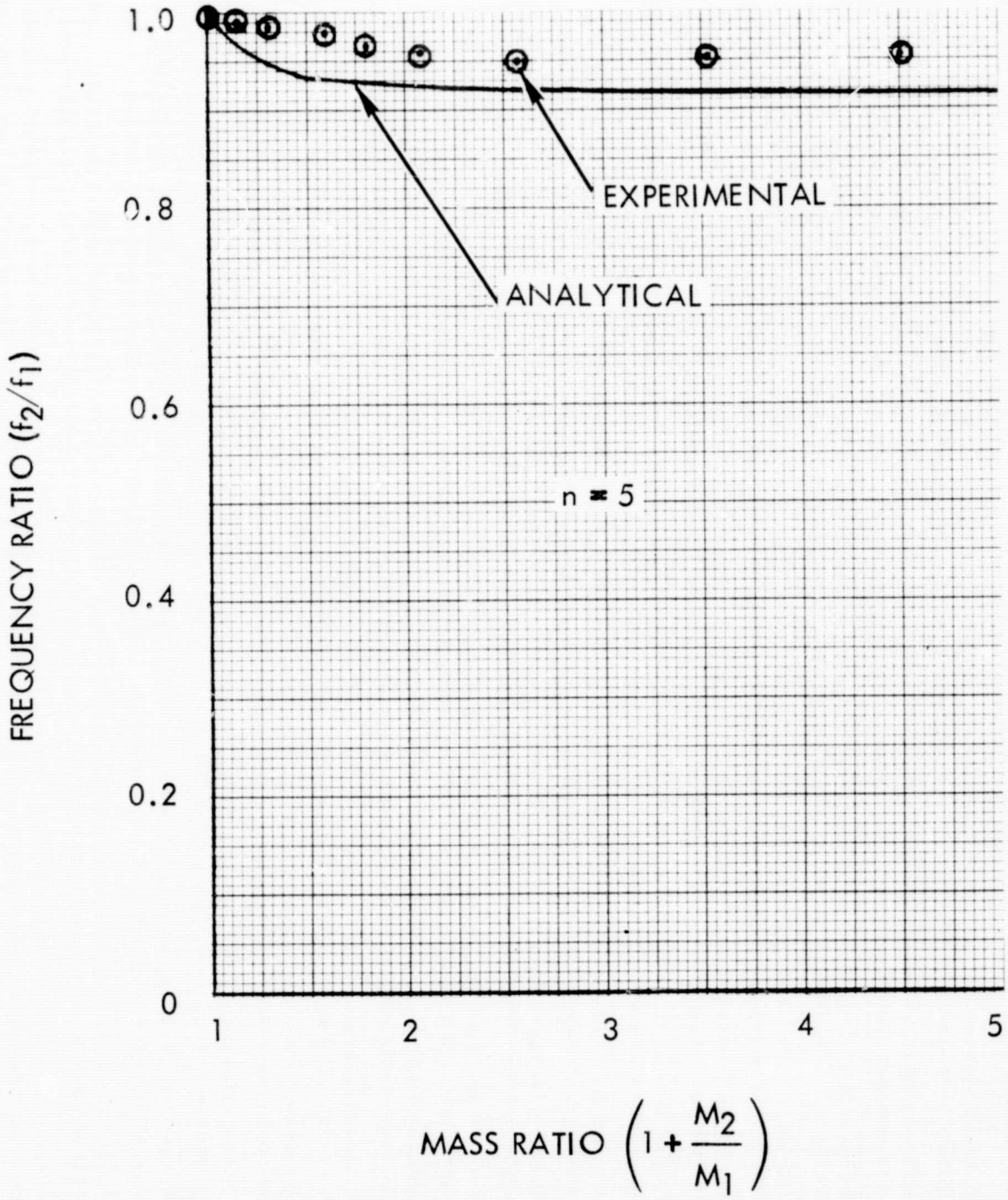


Figure 21. Comparison of Frequency Ratio of Ring I, Mode 4

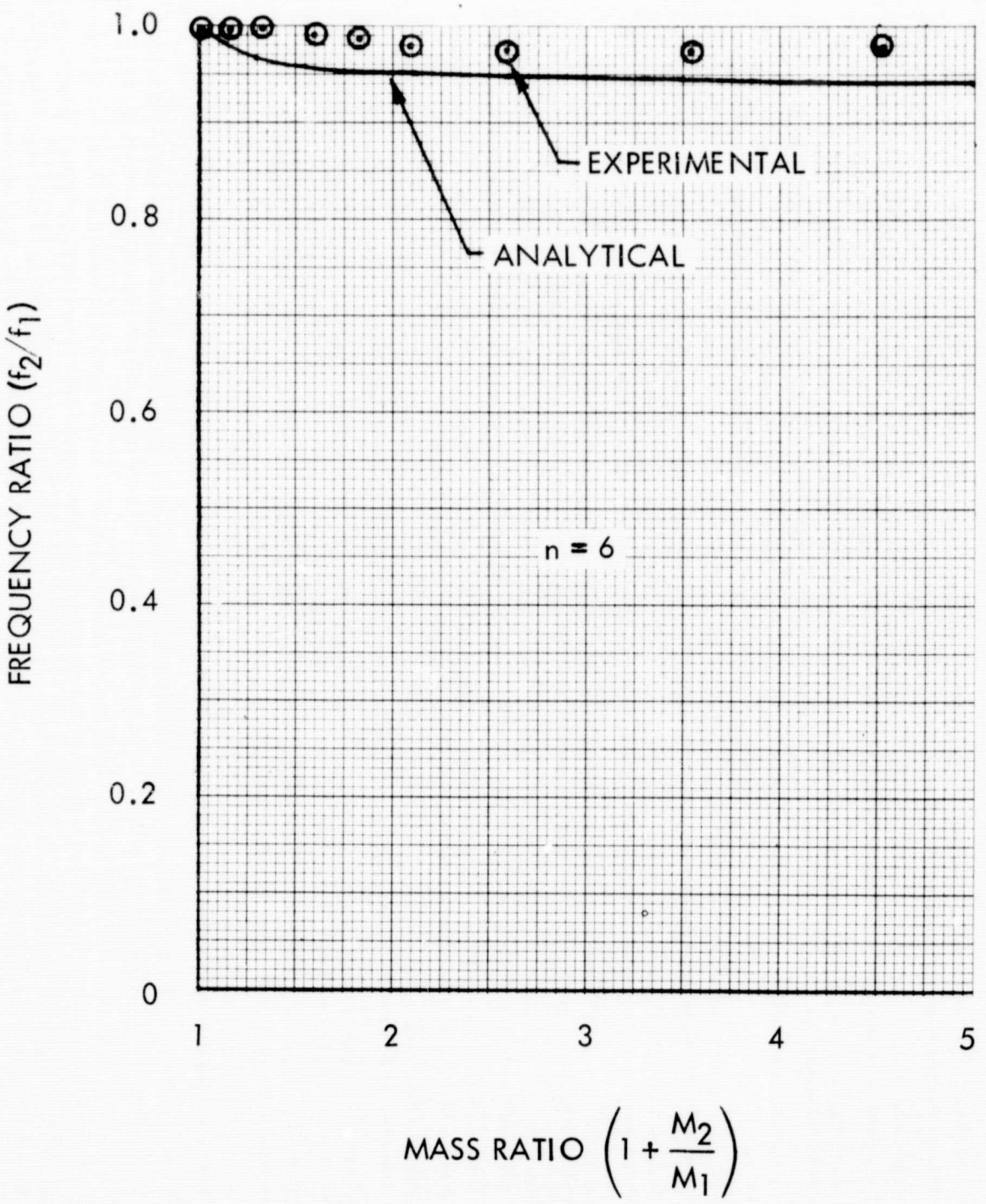


Figure 22. Comparison of Frequency Ratio of Ring I, Mode 5

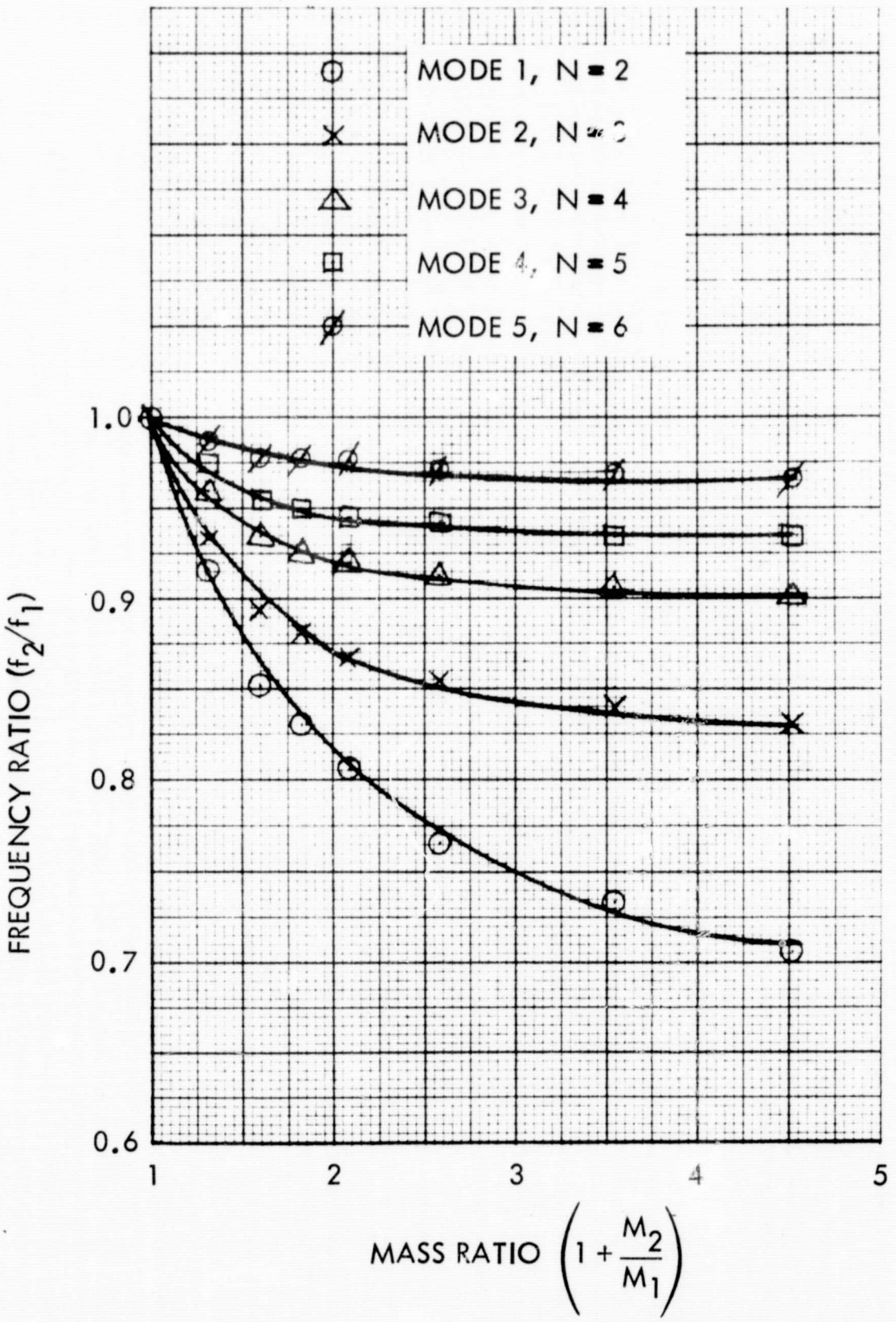


Figure 23. Test Data of Mass-Loading Effect on Natural Frequencies of Ring II

By observing these frequency data, the following conclusions can be made:

1. The analytical prediction of natural frequencies agrees well with the experimental results. However, the computer values are generally somewhat lower (under 10 percent) than the test data.

2. The frequency attenuation, one of the important phenomena of mass-loading effects, is clearly seen in the frequency ratio plots, Figures 18 through 23. The analytical values are very close to the experimental data for all modes.

3. For the cases with a mass ratio, M_2/M_1, larger than 2, the frequency shifts due to increasing mass loading become less significant. This is especially true for the higher modes.

4. The mass loading effect on frequencies from the additional 15 miniature accelerometers can be seen also in Figures 16 and 17. The No. 1 ring with 16 accelerometers has lower frequencies than the No. 2 ring, which has only one accelerometer. The trends of frequency attenuation for both rings are nearly identical.

Mass-loading effects on vibration transmissibility of rings are shown by the X-Y plots in Figure 24. These plots are the acceleration responses at the mass location. It is seen that the response amplitudes are rapidly decreased and many higher modes disappear as the attached M_2 increases. This effect constitutes another important phenomenon of mass loading effects.

The acceleration ratio data given in Tables 7 and 8 are plotted in Figures 25 through 29 for Ring I, and in Figures 30 through 34 for Ring II. The response attenuation phenomenon due to increasing mass loading is obviously seen throughout these figures.

Radial vibration mode shapes of the mass-loaded and unloaded rings were obtained from the proximity gage output. A typical mode shape plot is shown in Figure 35. The numbers 1 to 16 are station numbers around the circumference of Ring I. At Station 2, where the mass (M_2 = 0.95 lb) is attached, it can be visualized that the relative displacement gradually decreases as the frequency increases, then finally reduces to a nodal point. This fact gives another proof that higher modes disappear because of mass loading.

More comparisons of the radial acceleration response are illustrated in Figures 36 through 40 for Ring II, in which the nodal points were determined from the proximity gage plots and the amplitudes were obtained from

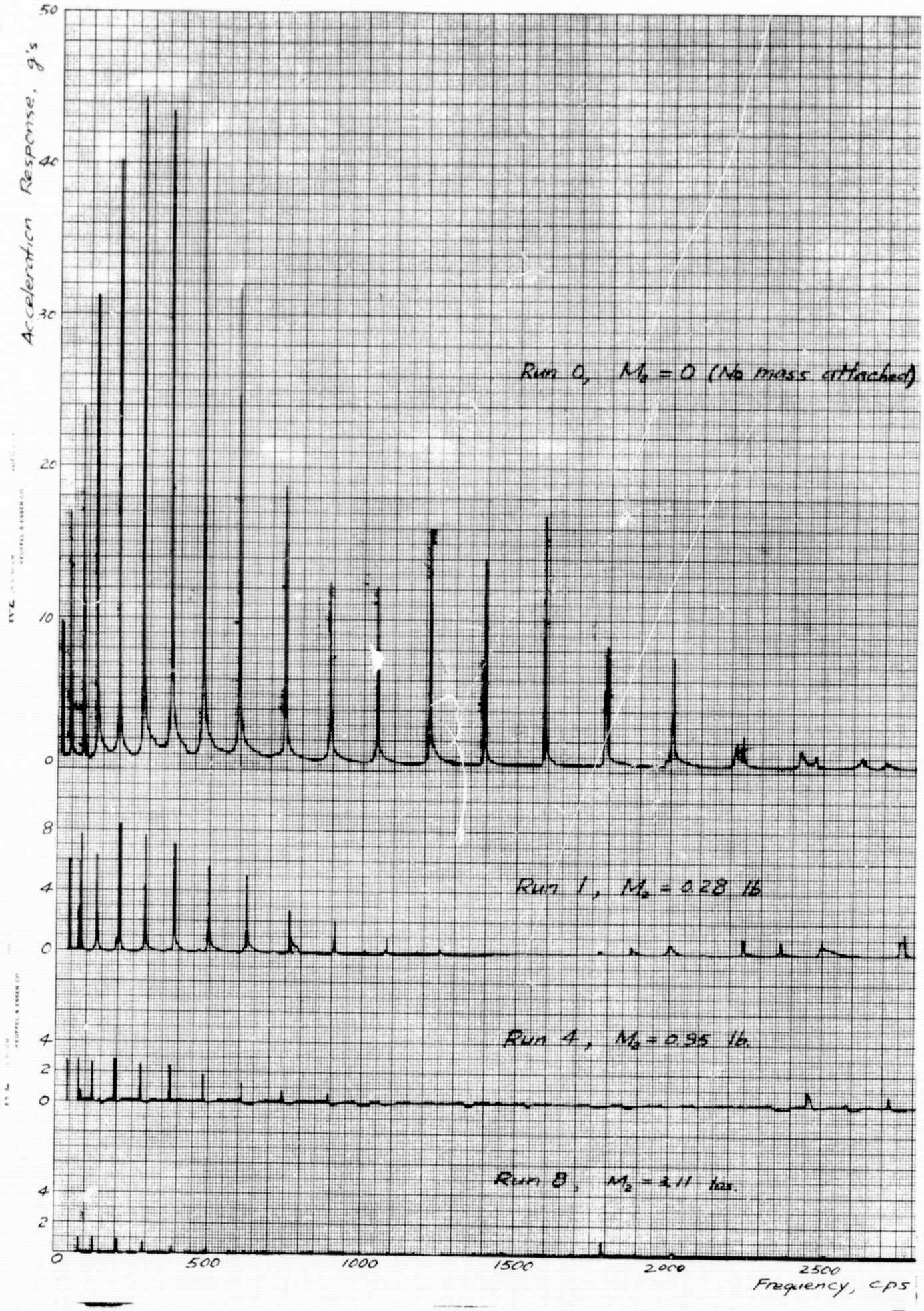


Figure 24. Mass-Loading Effect on Vibration Transmissibility of Ring

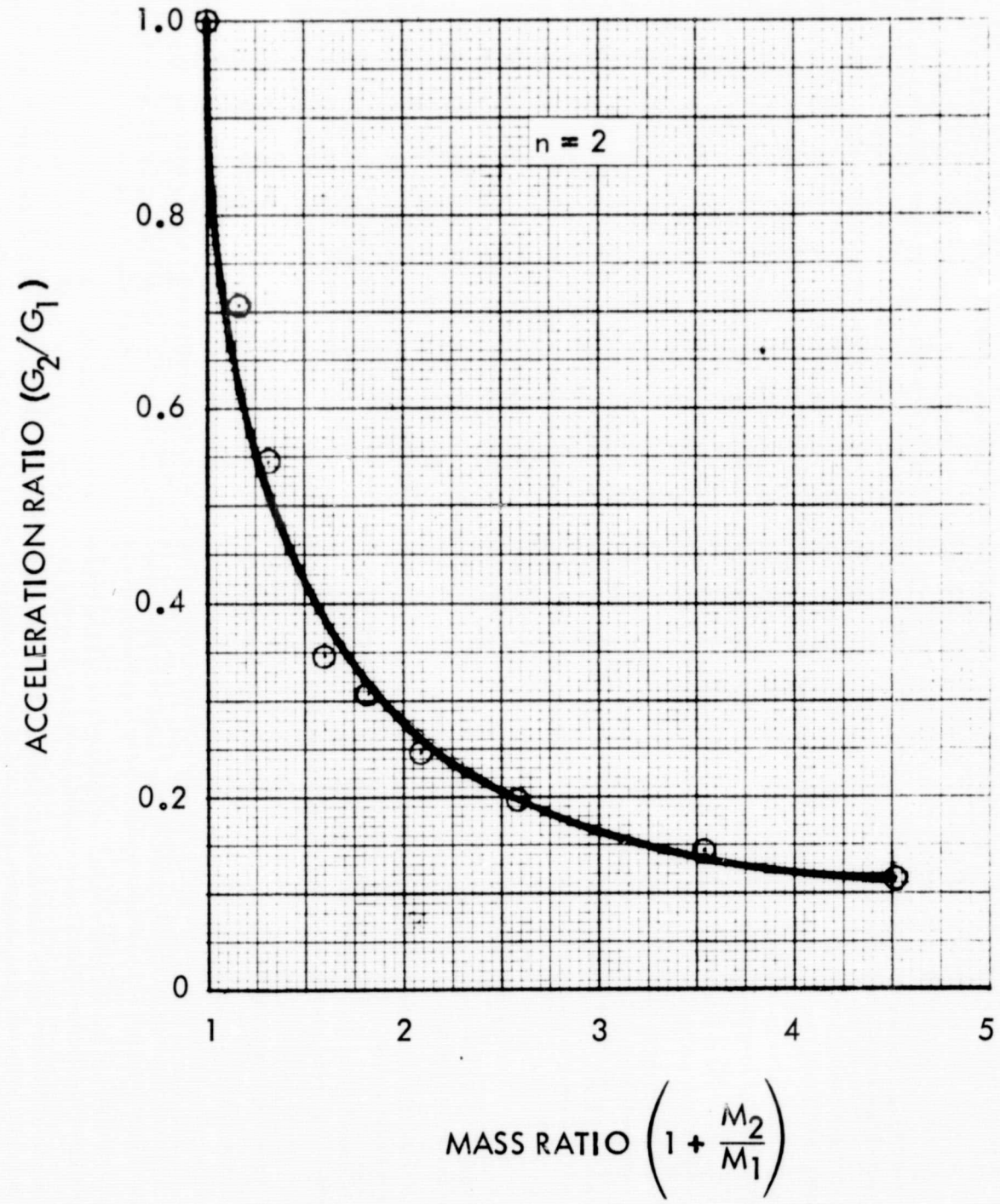


Figure 25. Mass-Loading Effect on Acceleration Response of Ring I, Mode 1

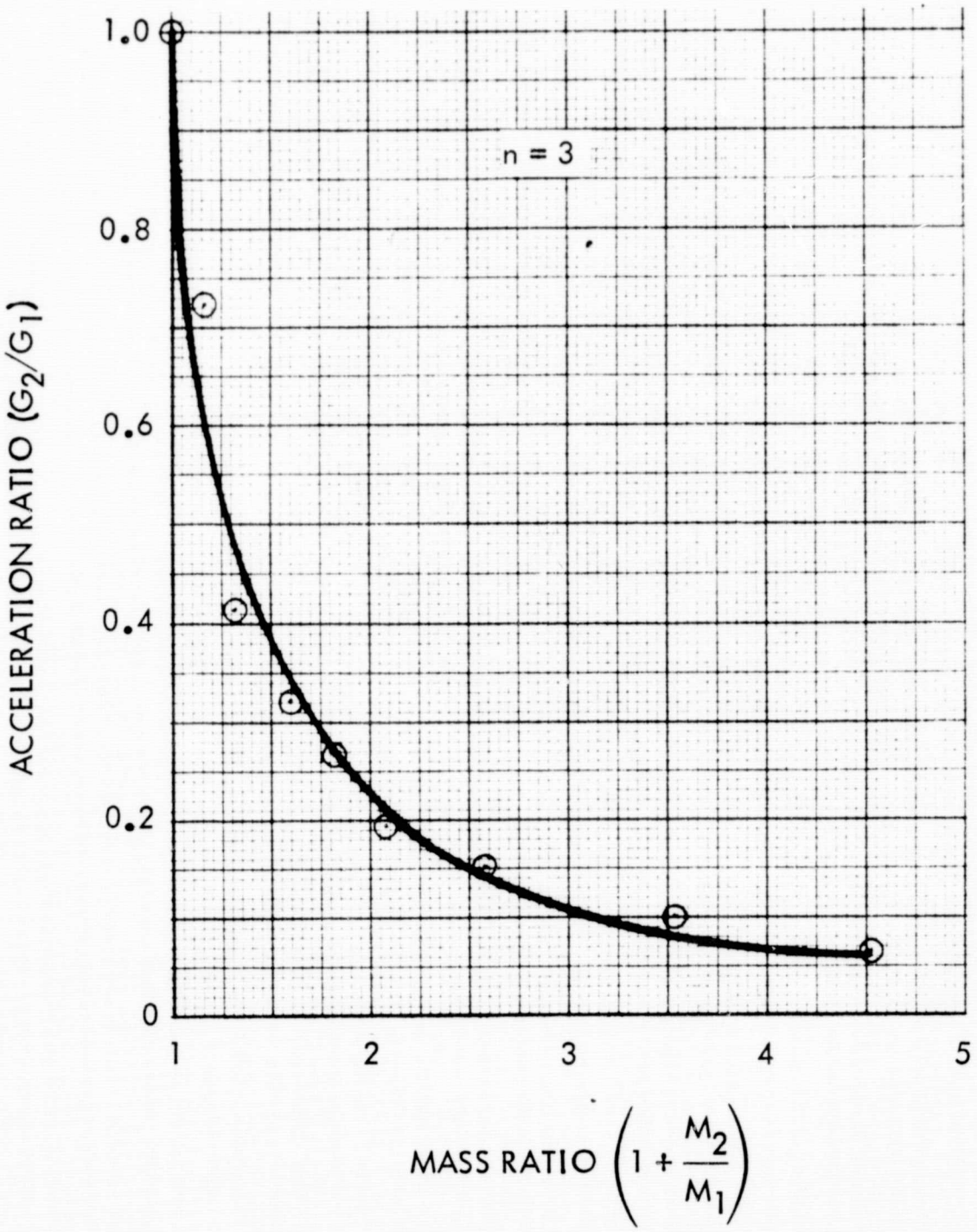


Figure 26. Mass-Loading Effect on Acceleration Response of Ring I, Mode 2

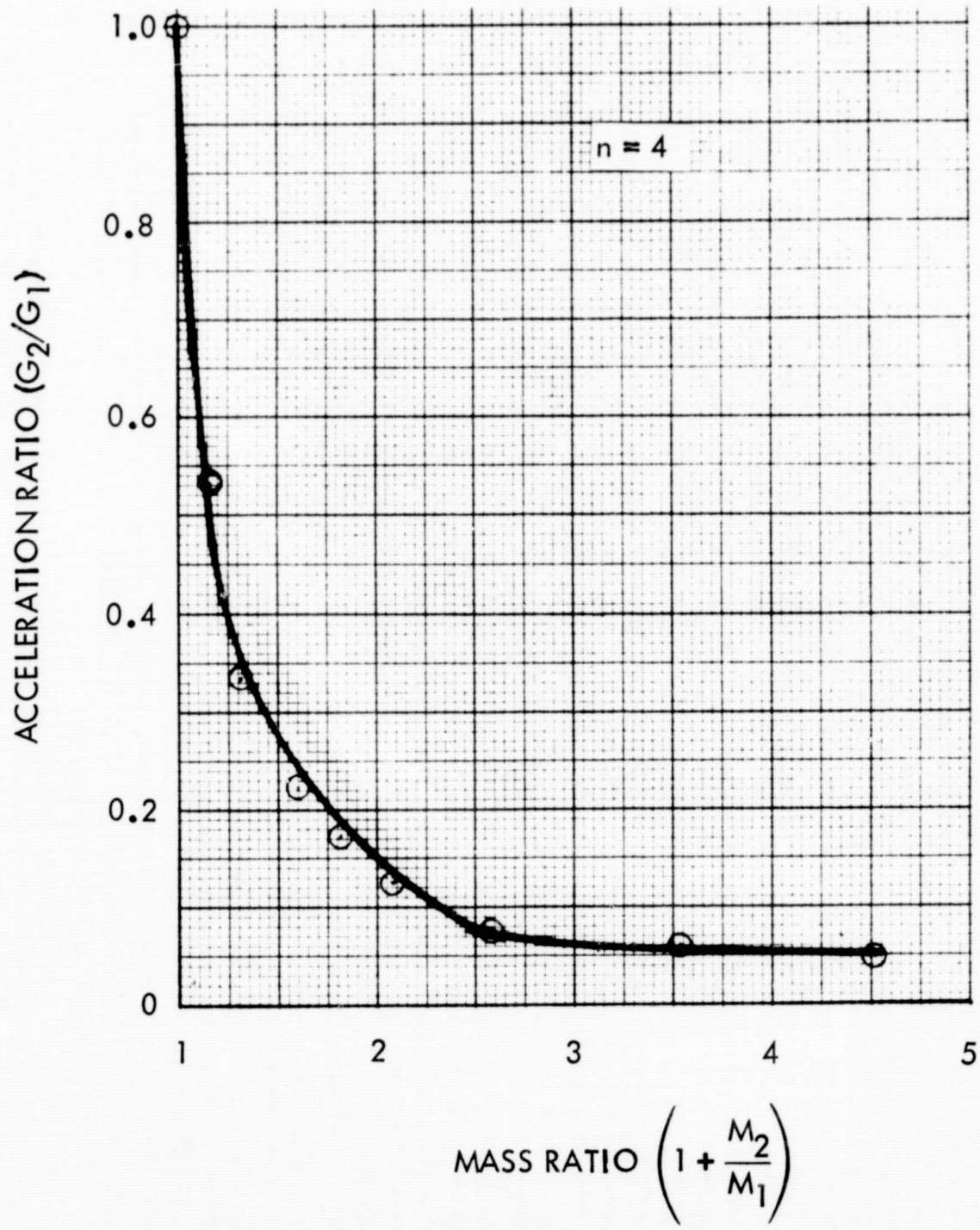


Figure 27. Mass-Loading Effect on Acceleration Response of Ring I, Mode 3

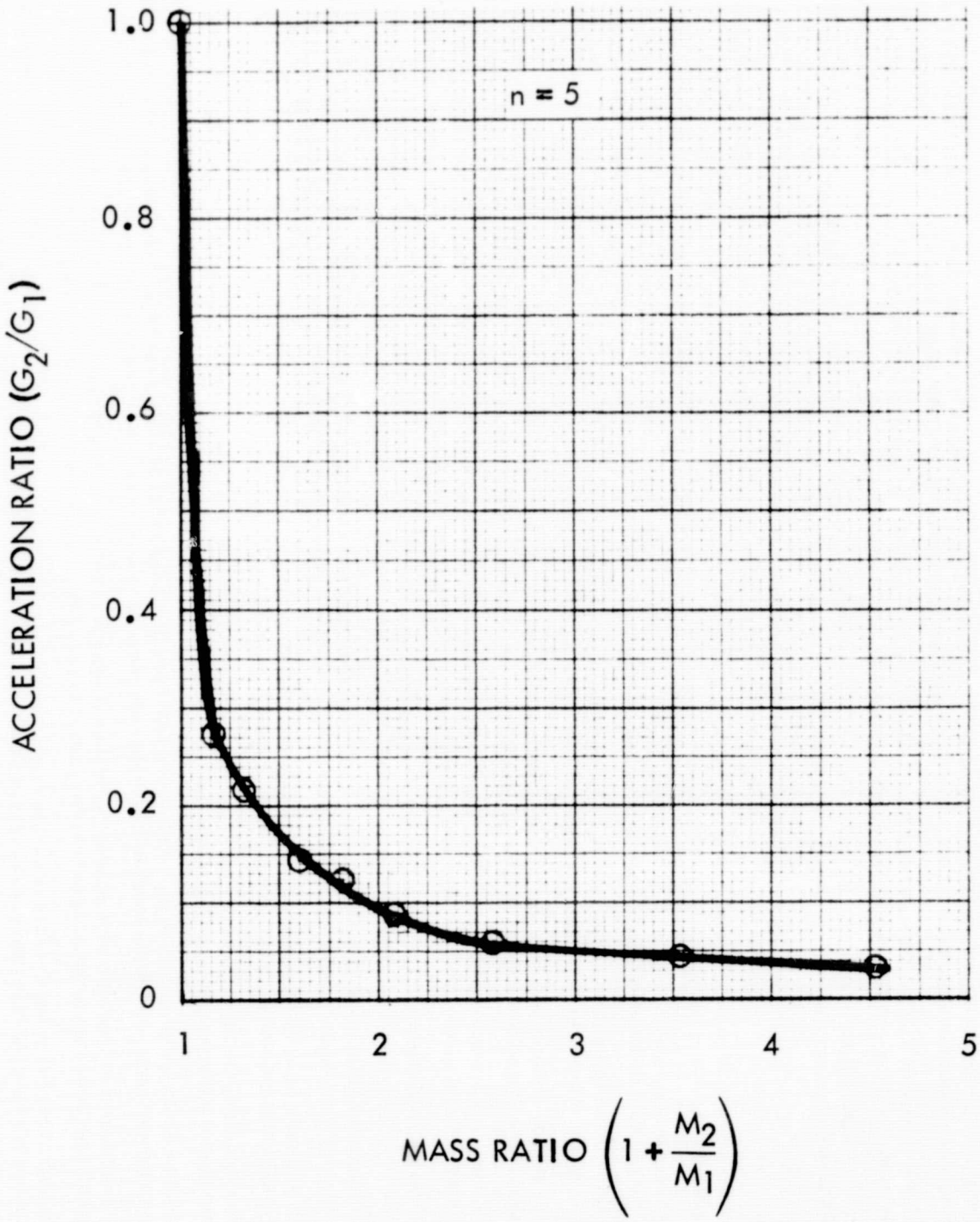


Figure 28. Mass-Loading Effect on Acceleration Response of Ring I, Mode 4

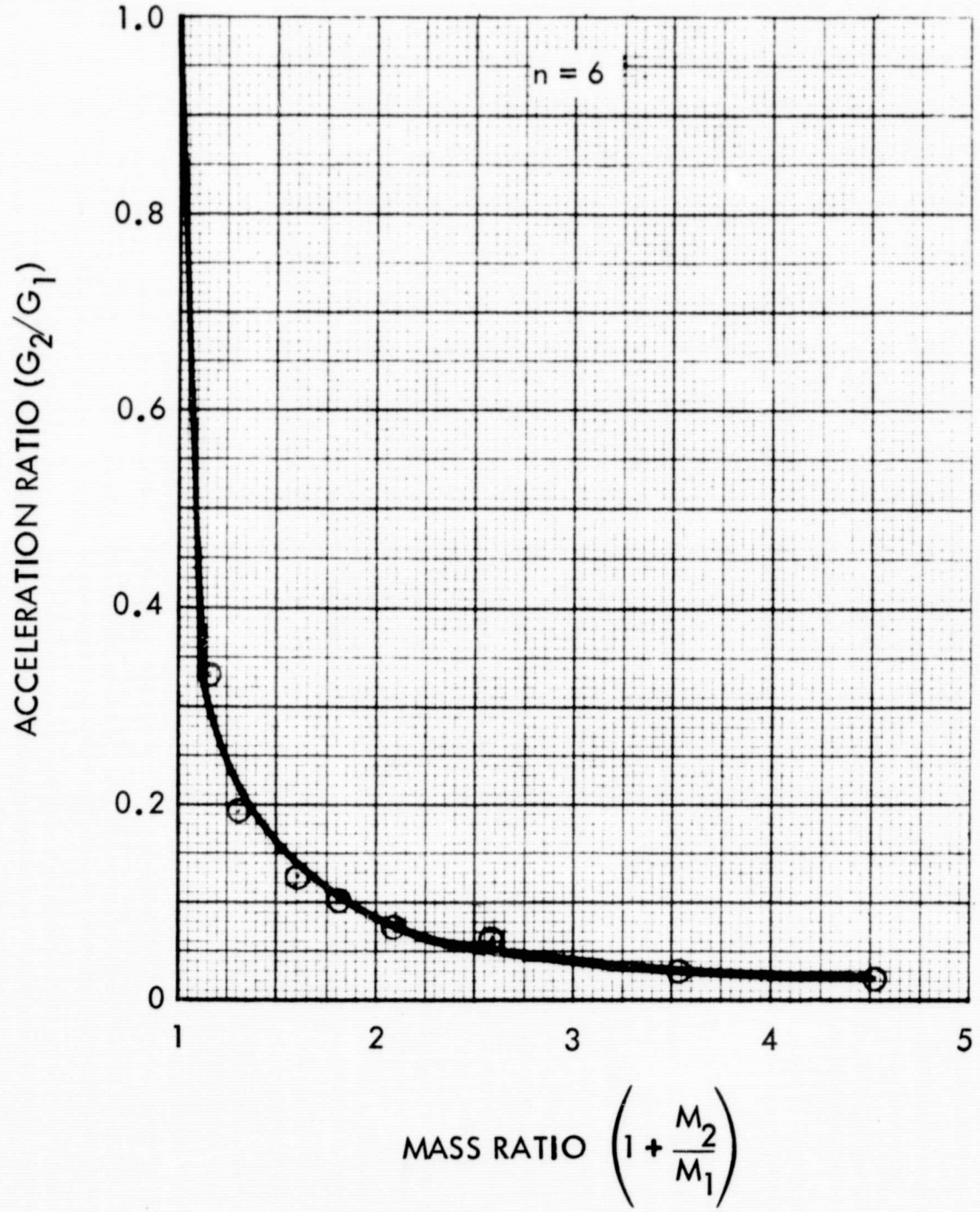


Figure 29. Mass-Loading Effect on Acceleration Response of Ring I, Mode 5

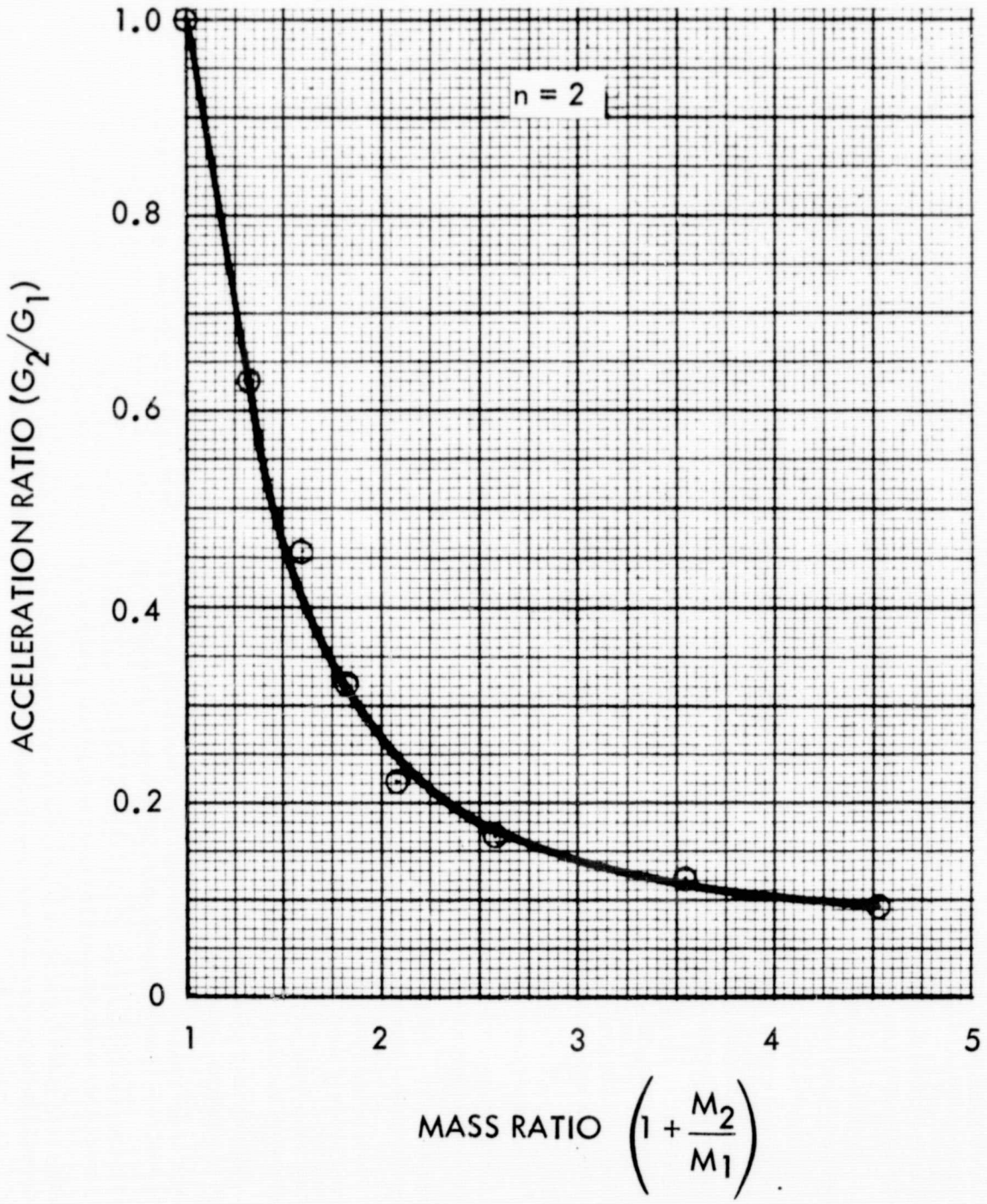


Figure 30. Mass-Loading Effect on Acceleration Response of Ring II, Mode 1

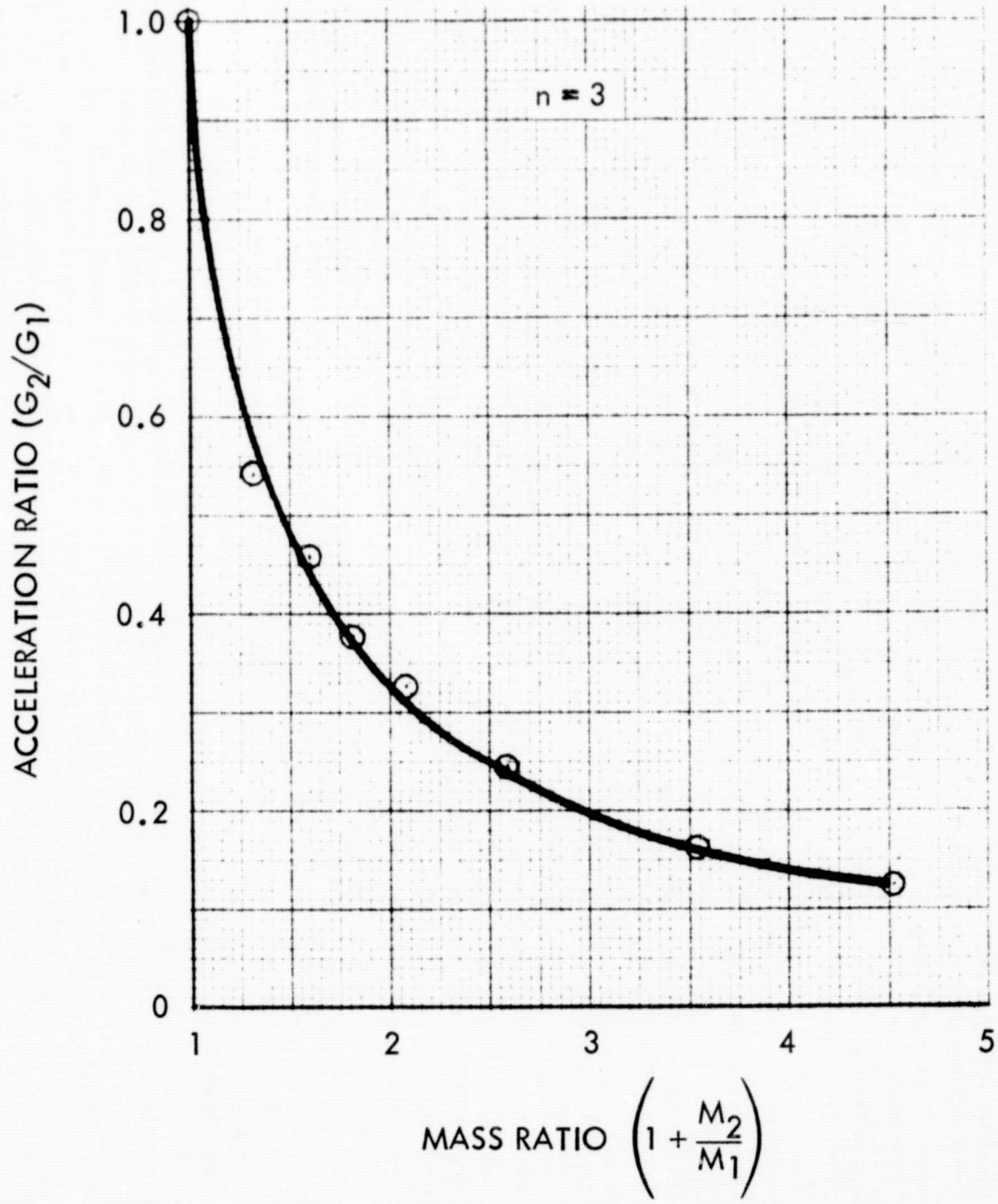


Figure 31. Mass-Loading Effect on Acceleration Response of Ring II, Mode 2

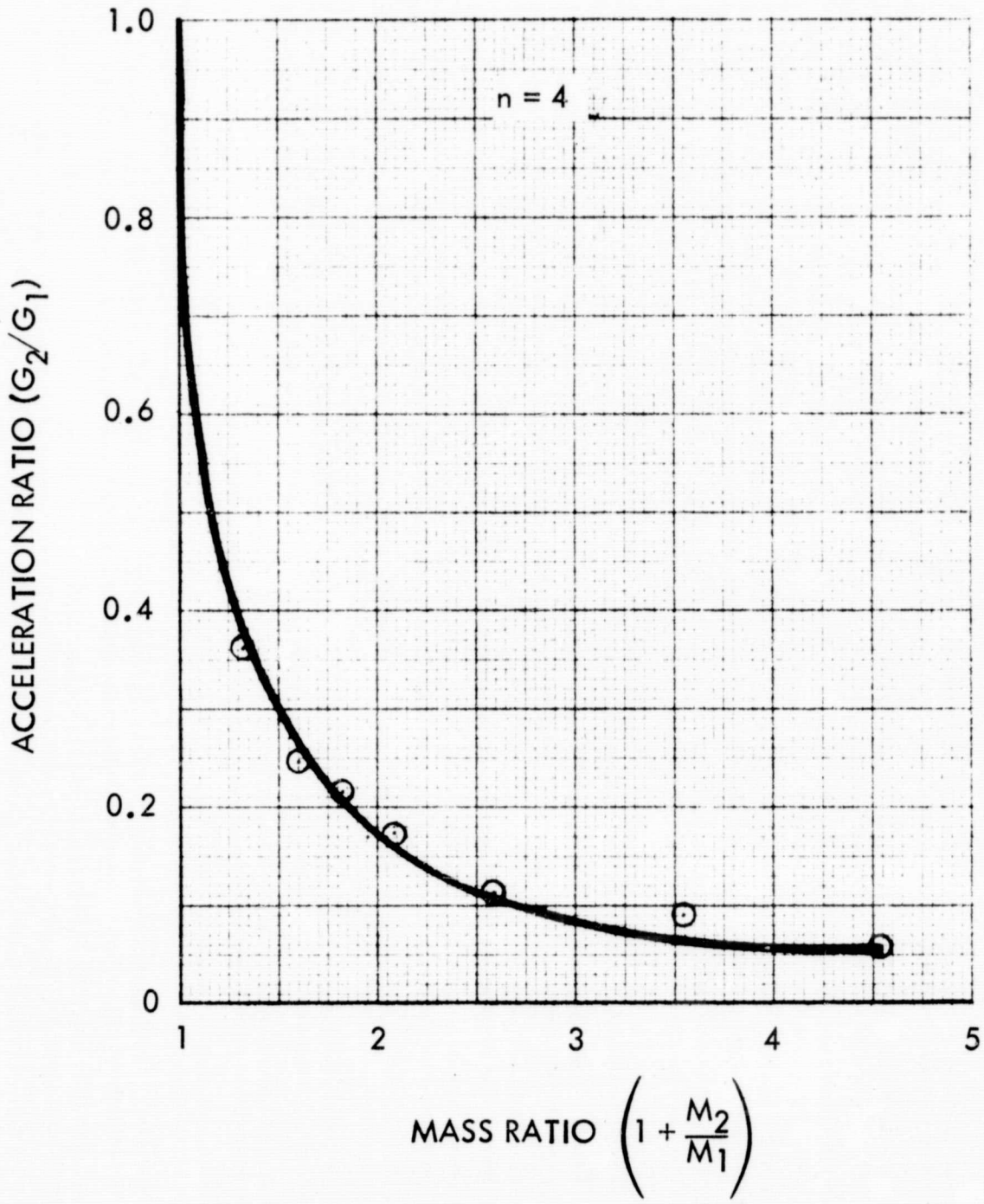


Figure 32. Mass-Loading Effect on Acceleration Response of Ring II, Mode 3

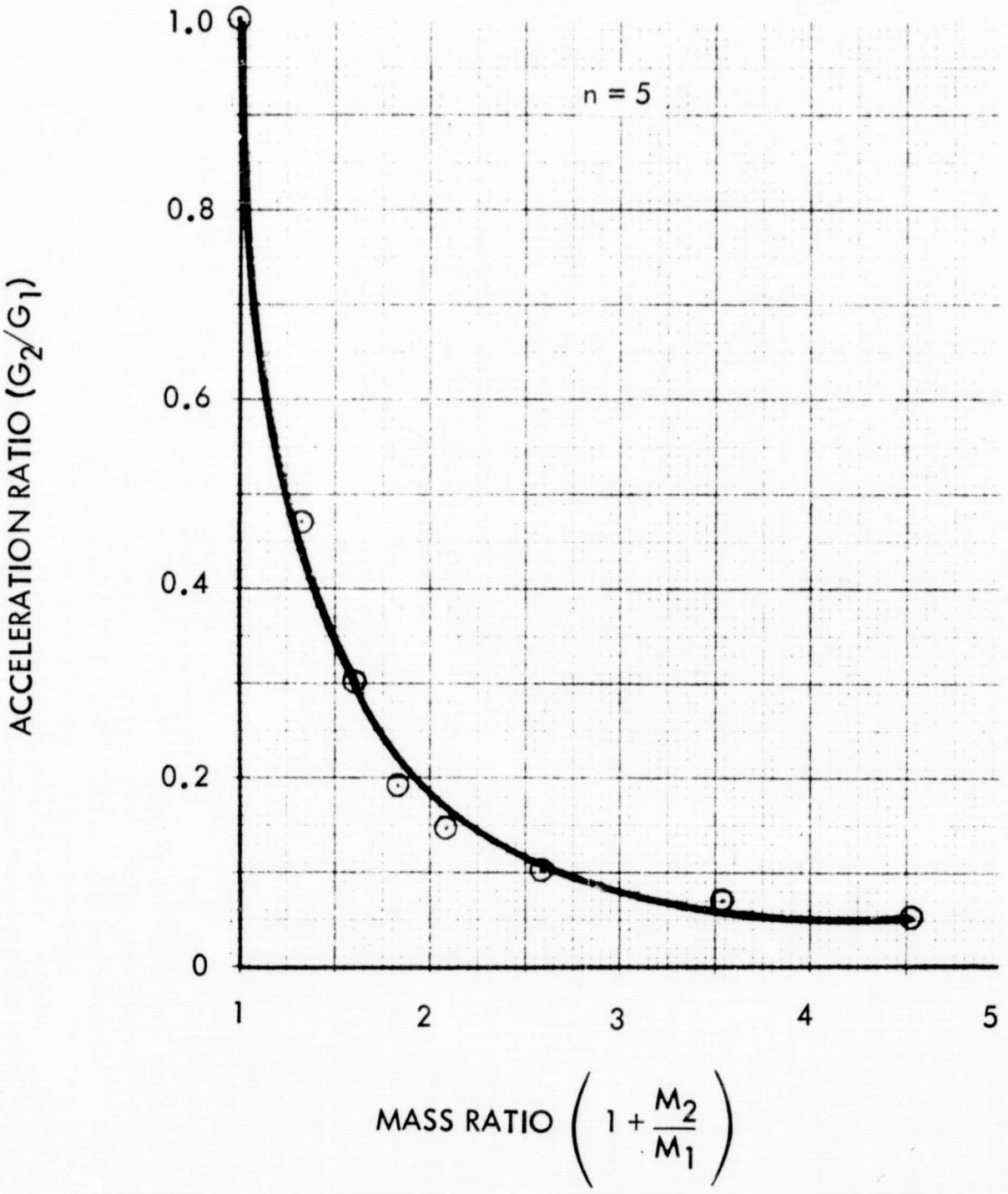


Figure 33. Mass-Loading Effect on Acceleration Response of Ring II, Mode 4

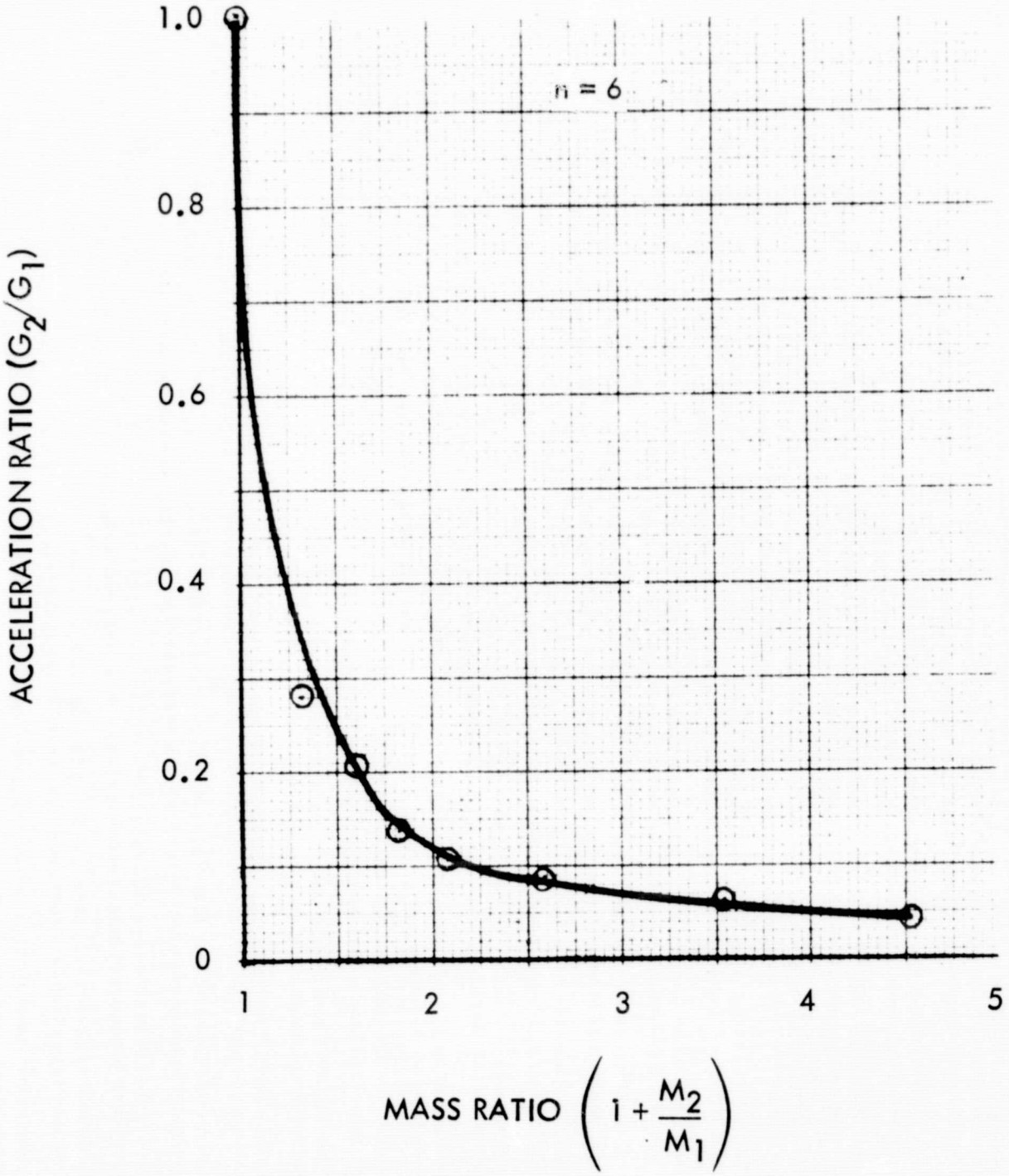


Figure 34. Mass-Loading Effect on Acceleration Response of Ring II, Mode 5

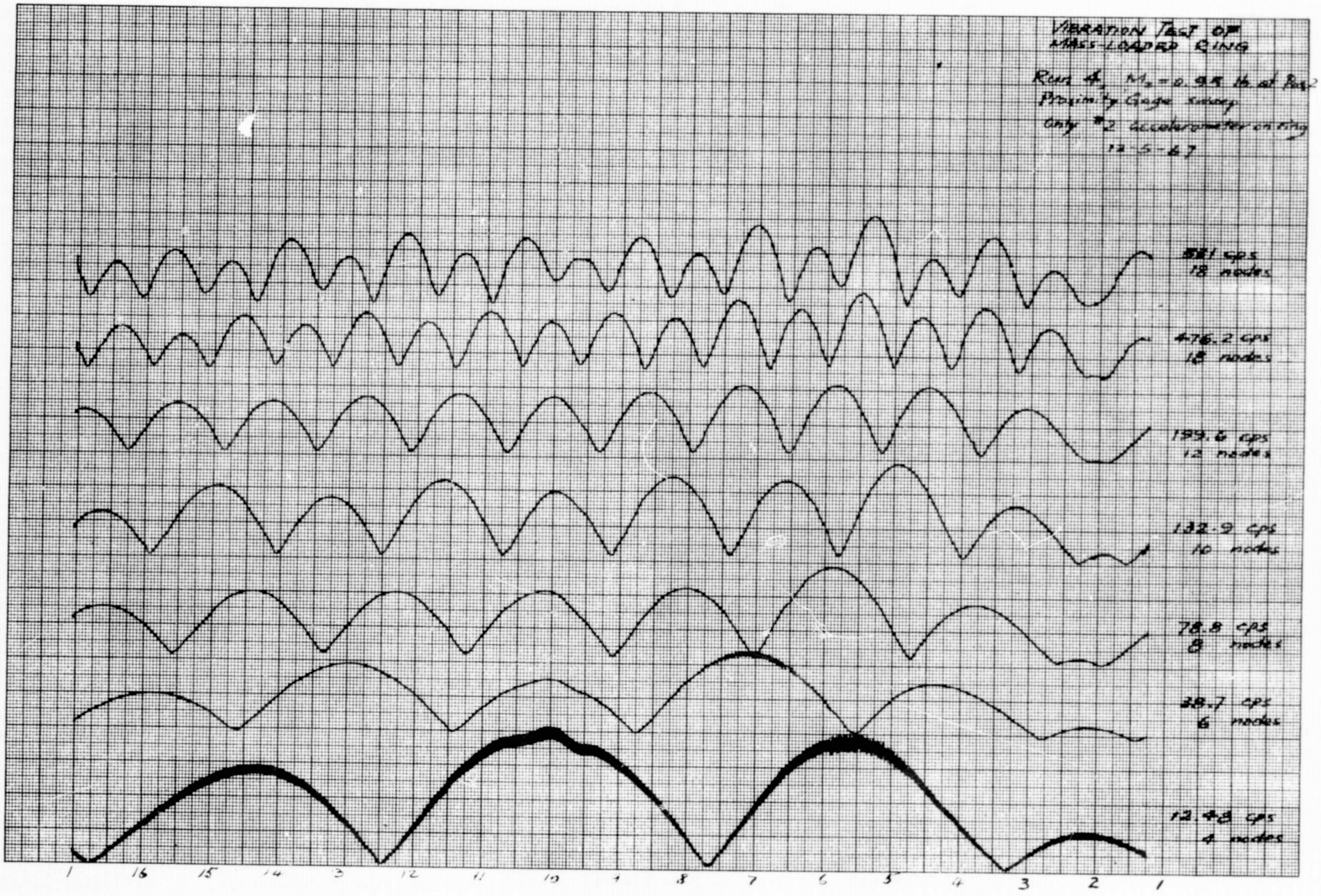
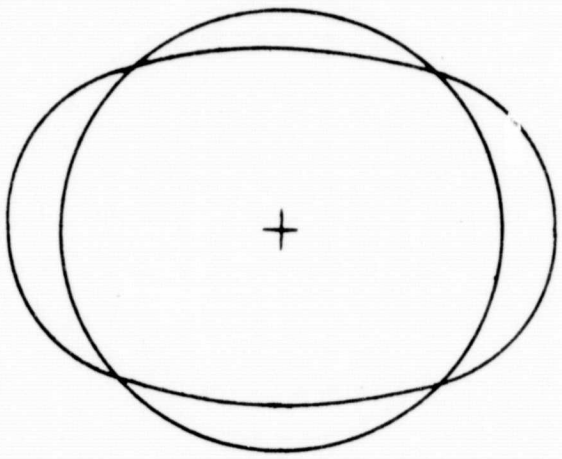
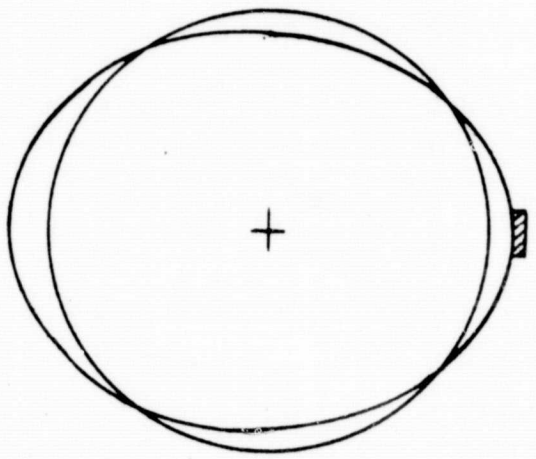


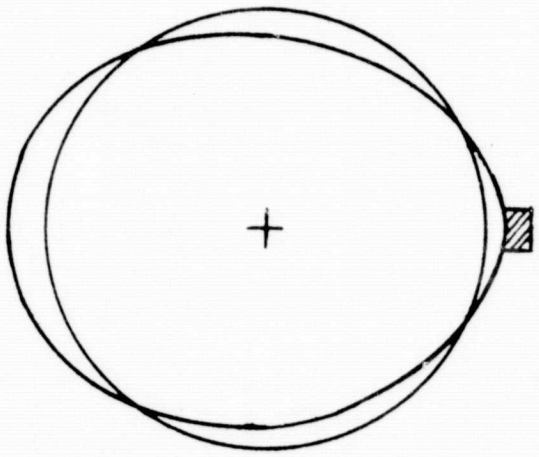
Figure 35. Typical Mode Shapes of Mass-Loaded Ring



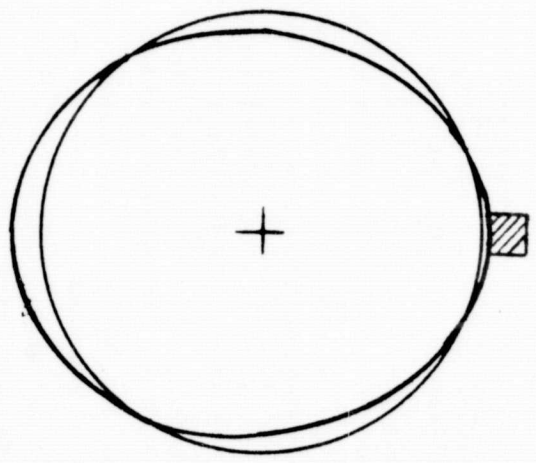
$M_2/M_1 = 0$, f = 15.0 cps



$M_2/M_1 = 0.82$, f = 12.46 cps

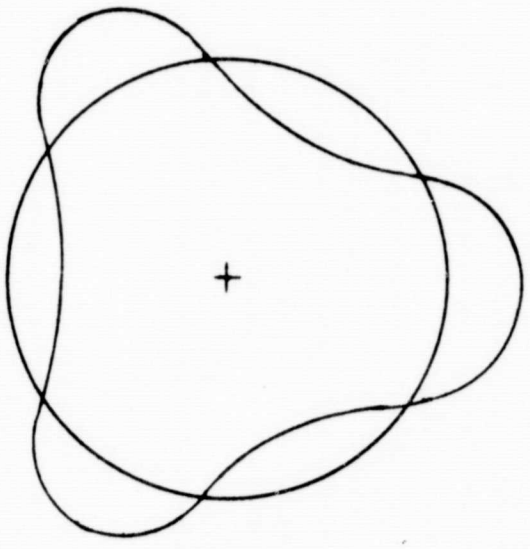


$M_2/M_1 = 1.58$, f = 11.5 cps

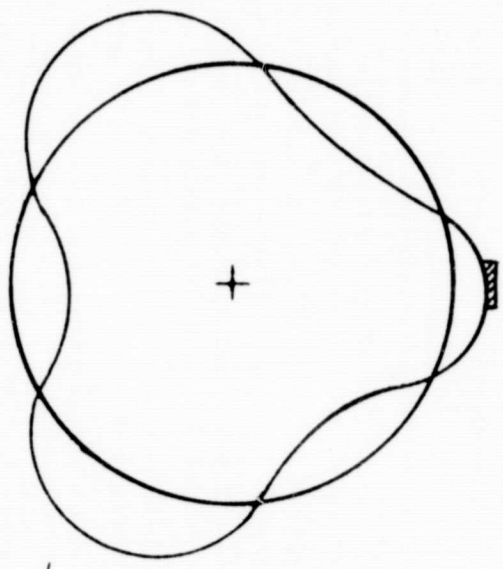


$M_2/M_1 = 3.52$, f = 10.6 cps

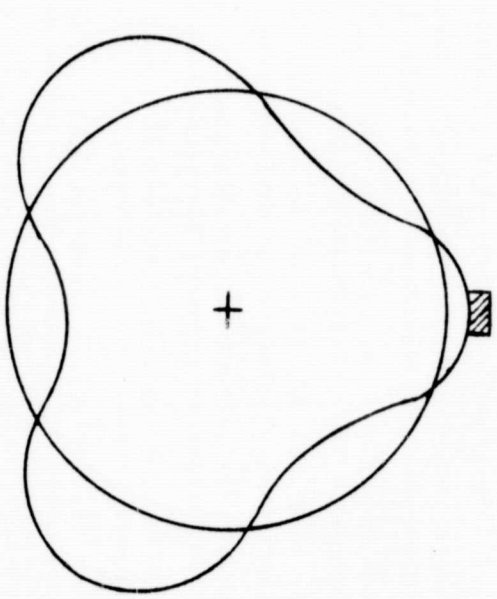
Figure 36. Mass-Loading Effect on Radial Acceleration Response of Ring II, Mode 1, n = 2



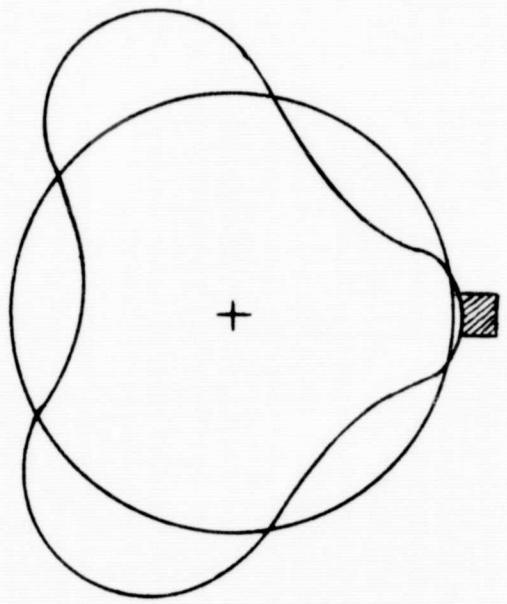
$M_2/M_1 = 0$, f = 42.2 cps



$M_2/M_1 = 0.82$, f = 37.2 cps

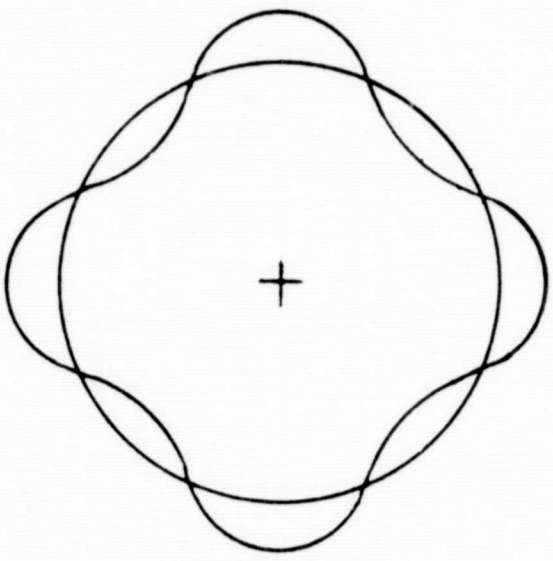


$M_2/M_1 = 1.58$, f = 36.1 cps

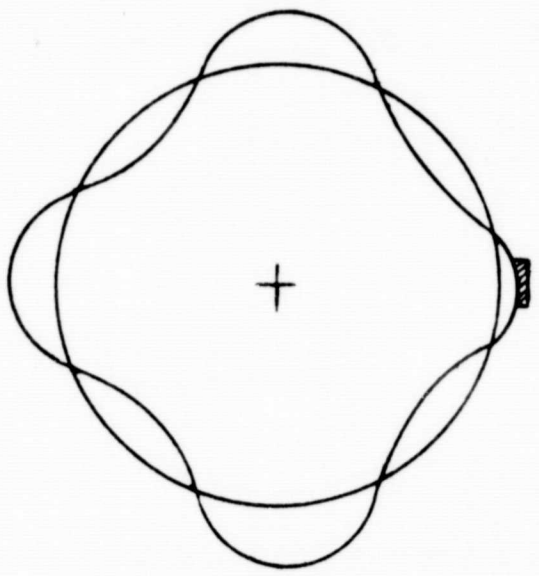


$M_2/M_1 = 3.52$, f = 35.1 cps

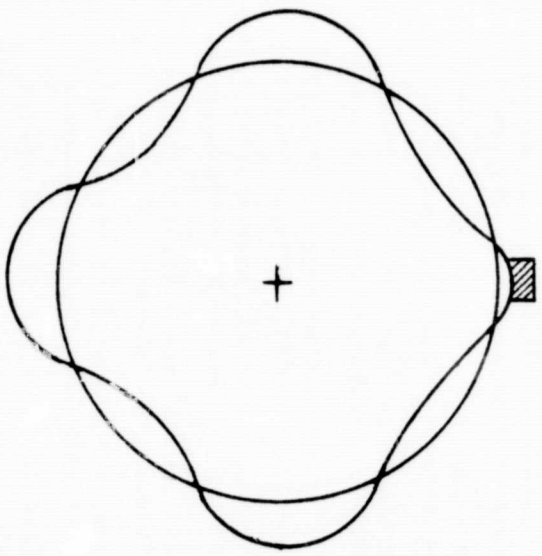
Figure 37. Mass-Loading Effect on Radial Acceleration Response of Ring II, Mode 2, n = 3



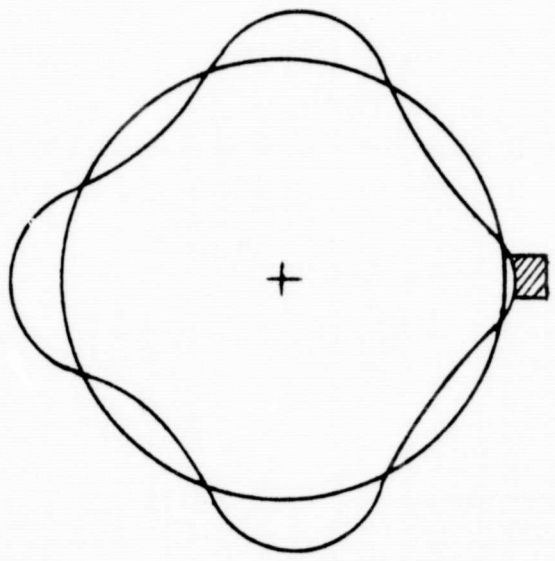
$M_2/M_1 = 0$, f = 80.7 cps



$M_2/M_1 = 0.82$, f = 74.8 cps

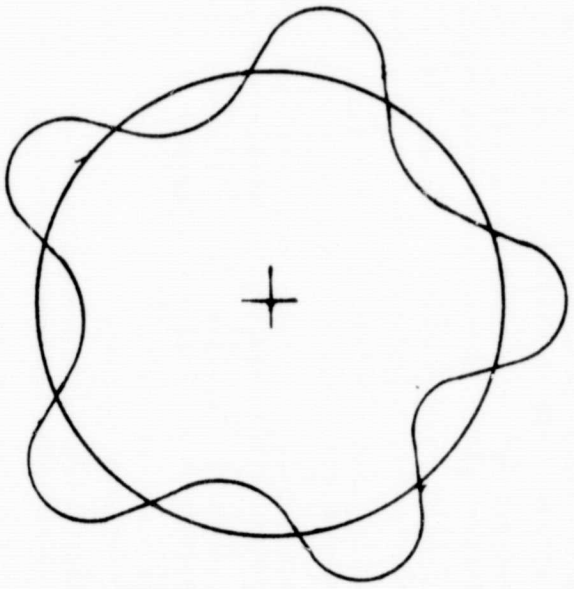


$M_2/M_1 = 1.58$, f = 73.6 cps

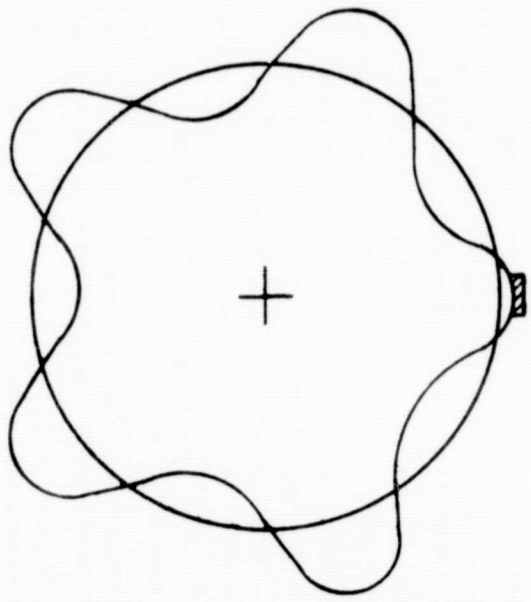


$M_2/M_1 = 3.52$, f = 72.8 cps

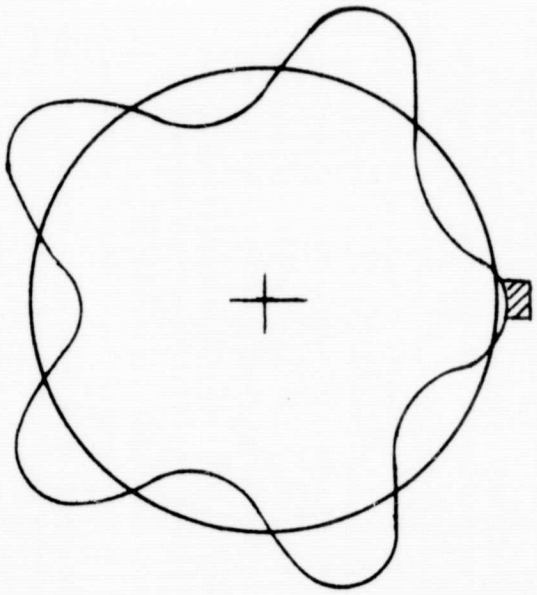
Figure 38. Mass-Loading Effect on Radial Acceleration Response of Ring II, Mode 3, n = 4



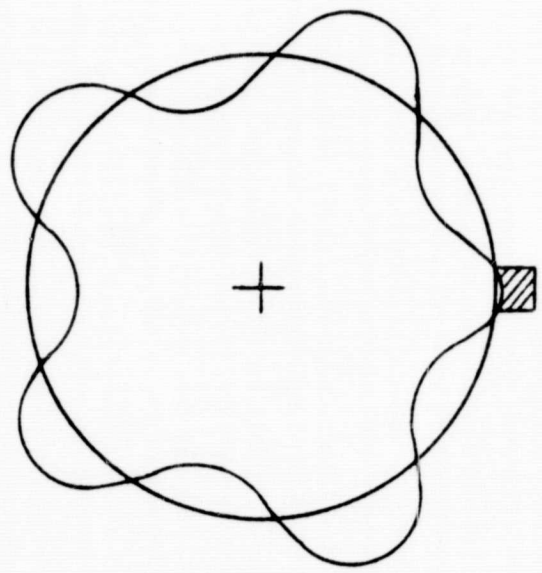
$M_2/M_1 = 0$, f = 130.9 cps



$M_2/M_1 = 0.82$, f = 124.3 cps

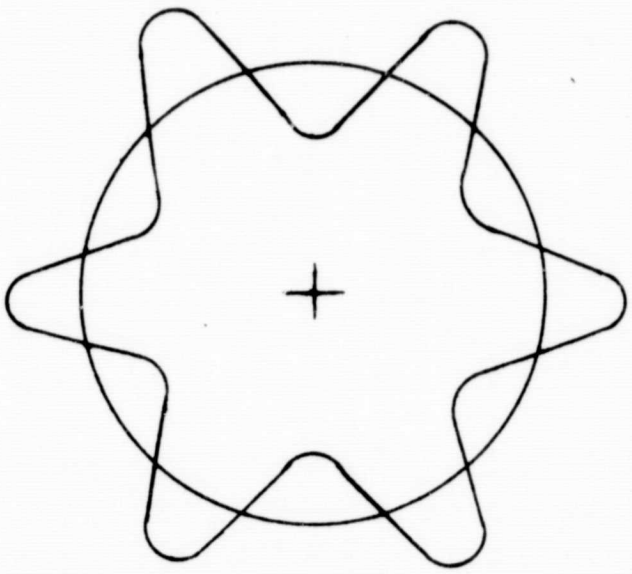


$M_2/M_1 = 1.58$, f = 123.4 cps

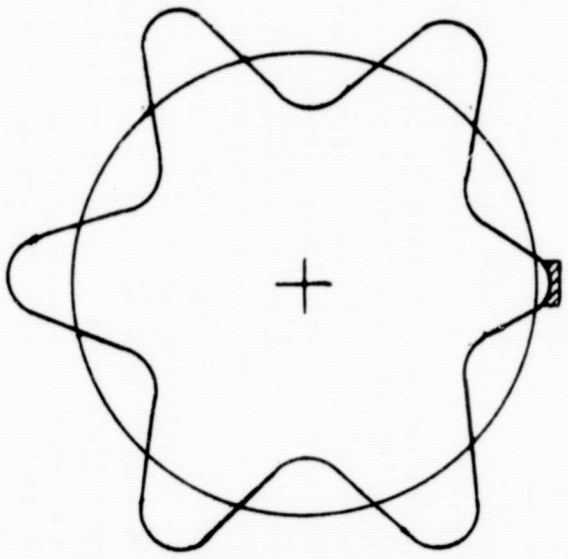


$M_2/M_1 = 3.52$, f = 122.5 cps

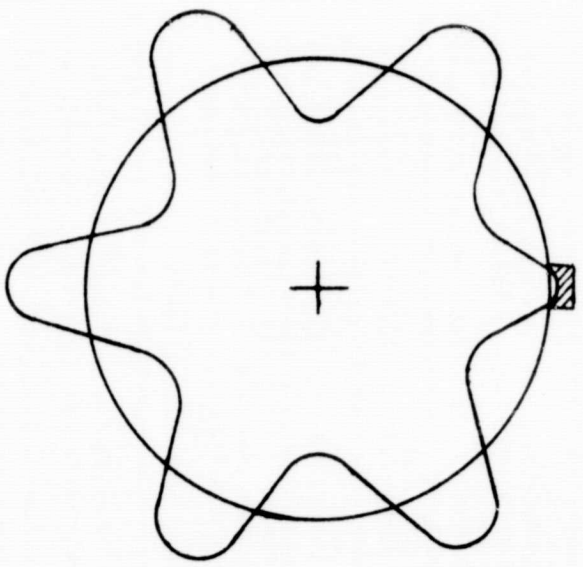
Figure 39. Mass-Loading Effect on Radial Acceleration Response of Ring II, Mode 4, n = 5



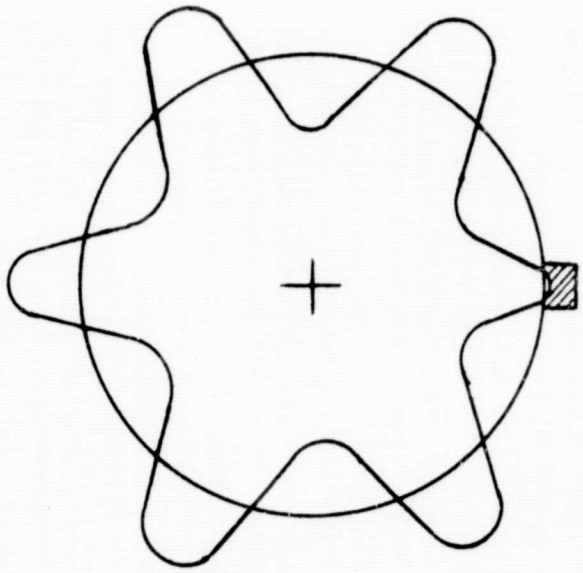
$M_2/M_1 = 0$, f = 190.9 cps



$M_2/M_1 = 0.82$, f = 186.6 cps



$M_2/M_1 = 1.58$, f = 185.5 cps



$M_2/M_1 = 3.52$, f = 184.5 cps

Figure 40. Mass-Loading Effect on Radial Acceleration Response of Ring II, Mode 5, n = 6

meter readings of the 16 accelerometer outputs. These illustrations show once more the mass-loading phenomenon of response attenuation. It is also noted that these response curves follow the analytical mode shapes presented previously in Figures 5 through 8.

MASS-LOADED AND UNLOADED SHELLS

Vibration test data of the mass-loaded and unloaded shells are presented in Tables 11 through 14. For shell I with only one accelerometer, there are nine mass-loaded cases with mass ratio M_2/M_1 ranging from 0.16 to 4.9 in addition to one unloaded case. For shell II with 20 accelerometers, there are eight mass loaded cases with M_2/M_2 ranging from 0.32 to 4.9 in addition to one unloaded case.

The mass-loading effect on radial acceleration response at the mass location of Shell I can be seen from two typical X-Y plots in Figure 41, where the upper curve is for the unloaded case while the lower one is for the heaviest mass-loaded case. The frequency shift and response attenuation between the two cases are apparent. On these X-Y plots, there are numerous resonance frequencies. For the purposes of systematic analysis and comparison, the frequencies are so chosen that they are for the corresponding mode. For example, in Tables 11 and 13, Mode 1 has been chosen to have $m = 1$ and $n = 3$. For the other modes, however, the values of m or n are not identical throughout all cases because the effect of mass loading causes a change in modal response, which had been observed through careful survey during the tests.

A comparison of the analytical and experimental frequencies of Shell I is given in Table 12, which indicates the very close agreement between the two sets of frequencies. In this table, three lower frequencies for each case are presented, since these are the most important ones and the few modes correspond to each other in the analytical and experimental results. Due to the local excitation on thin shells in the experiments, a large number of radial modes ($n = 2$ to 7) were obtained with only a few lateral bending modes corresponding to the analytical results. The data presented in Table 15 are also shown in Figure 42 for better comparison.

The data of frequency ratios, f_2/f_1, are plotted in Figures 43 through 48, and those of acceleration response ratio, G_2/G_1, in Figures 49 through 58.

By observing these data, similar conclusions, as for the mass-loaded ring, can be made as follows:

1. The analytical prediction of natural frequencies of mass-loaded and unloaded shells closely agrees with the experimental data.

2. The frequency shifts due to mass-loading effects are significant only in the lower modes, such as Modes 1 and 2, in Figures 43, 44 and 48. For the higher modes the changes are within 5 percent difference from the unloaded case.

3. The addition of 19 miniature accelerometers on the shell has lowered the natural frequencies for all modes. This effect can be seen by comparing the test data between Shell I and Shell II given in Tables 11 through 14.

4. The response-attenuation phenomenon is observed in all modes as the mass ratio increases. For mass ratios M_2/M_1 larger than 2.5, the reduction in response is nearly constant except for Mode 1. For higher Modes 4 and 5, these responses are so low (within 10 percent of the unloaded case) as to be negligible.

Table 11. Vibration Test Data of Shell I Excited by Electroinduction Shaker, One Meter on Shell

	Run Number	0-2	1a-2	1-2	2-2	3-2	4-2	5-2	6-2	7-2	8-2
	M_2/M_1	0	0.16	0.32	0.60	0.82	1.40	1.90	2.86	3.84	4.90
Mode 1	m	1	1	1	1	1	1	1	1	1	1
	n	3	3	3	3	3	3	3	3	3	3
	Freq. cps	87.5	87.1	86.4	84.2	82.6	76.5	71.5	63.7	57.4	52.1
	f_2/f_1	1.0	0.995	0.987	0.962	0.944	0.875	0.817	0.728	0.655	0.596
	Accel. g's	2.50	2.40	2.25	2.10	1.98	1.52	1.28	0.87	0.57	0.43
	G_2/G_1	1.0	0.96	0.90	0.84	0.791	0.608	0.512	0.348	0.228	0.172
Mode 2	m	1	1	1	1	1	2	2	2	2	2
	n	2	2	2	2	2	4	4	4	4	4
	Freq. cps	128.6	128.0	127.0	124.5	123.1	119.6	118.0	115.4	114.4	113.8
	f_2/f_1	1.0	0.995	0.986	0.968	0.958	0.930	0.918	0.897	0.890	0.885
	Accel. g's	4.62	3.7	3.4	3.05	2.86	1.58	1.28	0.57	0.44	0.34
	G_2/G_1	1.0	0.800	0.735	0.660	0.619	0.342	0.277	0.123	0.095	0.074
Mode 3	m	1	1	1	1	1	3	3	3	3	3
	n	5	5	5	5	5	5	5	5	5	5
	Freq. cps	141.5	141.0	140.3	139.4	138.7	137.7	136.1	136.8	136.5	136.2
	f_2/f_1	1.0	0.995	0.991	0.985	0.980	0.972	0.962	0.966	0.965	0.963
	Accel. g's	1.75	1.64	1.55	1.35	1.23	0.99	0.47	0.46	0.34	0.27
	G_2/G_1	1.0	0.936	0.885	0.772	0.702	0.565	0.268	0.263	0.194	0.154

Table 12. Vibration Test Data of Shell I Excited by Electroinduction Shaker (Continued)

	Run Number	0-2	1a-2	1-2	2-2	3-2	4-2	5-2	6-2	7-2	8-2
	M_2/M_1	0	0.16	0.32	0.60	0.82	1.40	1.90	2.86	3.84	4.90
Mode 4	m	2	2	3	3	3	3	3	3	3	3
	n	3	3	3	3	3	6	6	6	6	6
	Freq. cps	233.9	232.2	230.7	228.5	228.1	226.7	226.1	223.2	226.7	226.3
	f_2/f_1	1.0	0.993	0.987	0.977	0.975	0.970	0.967	0.954	0.970	0.968
	Accel. (g's)	7.0	6.1	4.95	3.93	3.3	1.72	1.24	0.46	0.46	0.54
	G_2/G_1	1.0	0.870	0.707	0.561	0.471	0.246	0.177	0.066	0.066	0.077
Mode 5	m	1	1	1	1	1	2	2	3	3	3
	n	7	7	7	7	7	7	7	7	7	7
	Freq. cps	279.0	278.6	278.2	277.3	276.1	274.9	274.3	275.1	274.9	273.0
	f_2/f_1	1.0	0.998	0.997	0.993	0.990	0.985	0.983	0.986	0.985	0.978
	Accel. (g's)	2.51	1.51	1.42	1.0	0.97	0.52	0.40	0.20	0.20	0.14
	G_2/G_1	1.0	0.601	0.561	0.398	0.386	0.207	0.160	0.080	0.080	0.056

Table 13. Vibration Test Data of Shell II Excited by Electroinduction Shaker, 20 Accelerometers on Shell

Run Number		0	1	2	3	4	5	6	7	8
M_2/M_1		0	0.32	0.60	0.82	1.40	1.90	2.86	3.84	4.90
Mode 1	m	1	1	1	1	1	1	1	1	1
	n	3	3	3	3	3	3	3	3	3
	Freq. (cps)	86.7	85.5	82.7	81.1	74.2	70.1	62.0	55.8	49.5
	f_2/f_1	1.0	0.986	0.955	0.935	0.856	0.809	0.715	0.644	0.571
	Accel. (g's)	2.34	1.96	1.67	1.52	1.10	0.94	0.77	0.51	0.34
	G_2/G_1	1.0	0.837	0.714	0.65	0.47	0.401	0.329	0.218	0.145
Mode 2	m	1	1	1	1	2	2	2	2	2
	n	2	2	2	2	4	4	4	4	4
	Freq. (cps)	126.7	125.5	123.7	122.0	118.3	116.8	114.9	113.4	112.5
	f_2/f_1	1.0	0.990	0.976	0.963	0.935	0.922	0.907	0.895	0.888
	Accel. (g's)	2.84	2.68	2.36	2.00	1.27	1.00	0.48	0.34	0.29
	G_2/G_1	1.0	0.865	0.75	0.675	0.526	0.432	0.365	0.29	0.27
Mode 3	m	1	1	1	1	3	3	3	3	3
	n	5	5	5	5	5	5	5	5	5
	Freq. (cps)	140.9	132.9	137.6	137.4	135.8	136.0	134.9	134.7	134.5
	f_2/f_1	1.0	0.989	0.976	0.975	0.963	0.965	0.957	0.955	0.954
	Accel. (g's)	1.48	1.28	1.11	1.00	0.78	0.64	0.54	0.43	0.40
	G_2/G_1	1.0	0.865	0.75	0.675	0.526	0.432	0.365	0.29	0.27

Table 14. Vibration Test Data of Shell II Excited by Electroinduction Shaker (Continued)

Run Number		0	1	2	3	4	5	6	7	8
M_2/M_1		0	0.32	0.60	0.82	1.40	1.90	2.86	3.84	4.90
Mode 4	m	2	3	3	3	3	3	3	3	3
	n	3	3	3	3	6	6	6	6	6
	Freq. (cps)	230.9	228.1	225.6	225.0	223.8	222.9	225.9	225.5	224.1
	f_2/f_1	1.0	0.988	0.975	0.974	0.968	0.965	0.977	0.975	0.970
	Accel. (g's)	5.45	4.25	2.25	1.85	1.04	0.94	0.53	0.55	0.47
	G_2/G_1	1.0	0.78	0.413	0.34	0.191	0.172	0.097	0.101	0.086
Mode 5	m	1	1	1	1	2	2	3	3	3
	n	7	7	7	7	7	7	7	7	7
	Freq. (cps)	275.9	274.1	271.6	271.0	268.7	267.6	269.4	268.6	268.2
	f_2/f_1	1.0	0.993	0.983	0.982	0.974	0.969	0.976	0.973	0.972
	Accel. (g's)	2.78	1.48	1.02	0.62	0.28	0.16	0.11	0.08	0.07
	G_2/G_1	1.0	0.532	0.367	0.223	0.101	0.058	0.040	0.029	0.025

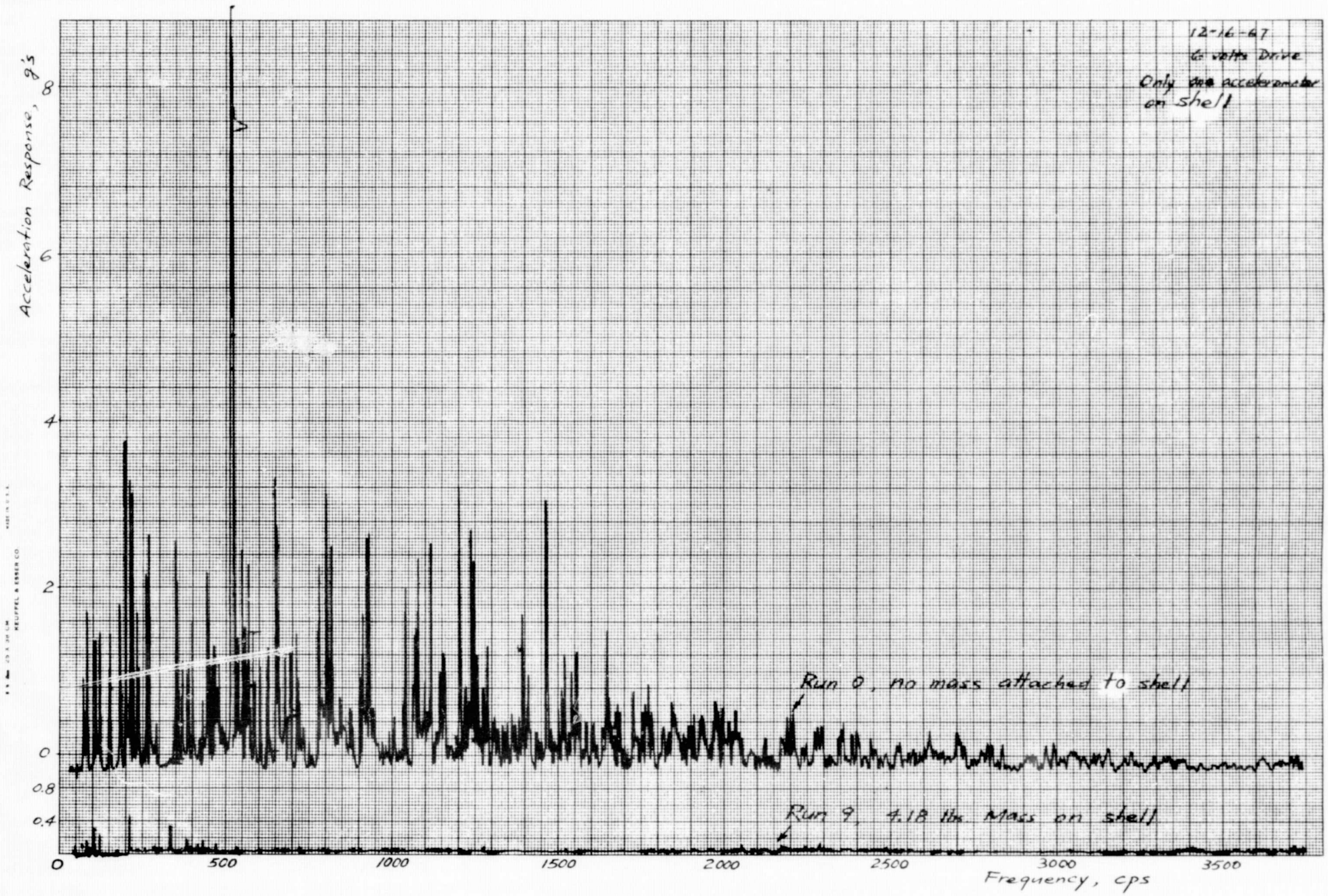


Figure 41. Mass-Loading Effect on Radial Acceleration of Shell

Table 15. Comparison of Natural Frequencies of Shell I

Case Number	Test Run No.	M_2/M_1	Mode / Freq. (cps)	1	2	3
0	0-2	0	Comp.	75.8	121.3	221.2
			Test	87.5	128.6	233.9
1	1a-2	0.16	Comp.	75.7	117.9	220.6
			Test	87.1	128.0	232.2
2	1-2	0.32	Comp.	75.6	114.1	219.8
			Test	86.4	127.0	230.7
3	2-2	0.60	Comp.	75.2	105.7	217.7
			Test	84.2	124.5	228.5
4	3-2	0.82	Comp.	75.0	102.7	216.9
			Test	82.6	123.1	228.1
5	4-2	1.40	Comp.	74.7	94.6	214.7
			Test	76.5	119.6	226.7
6	5-2	1.90	Comp.	73.7	83.7	209.5
			Test	71.5	118.0	226.1

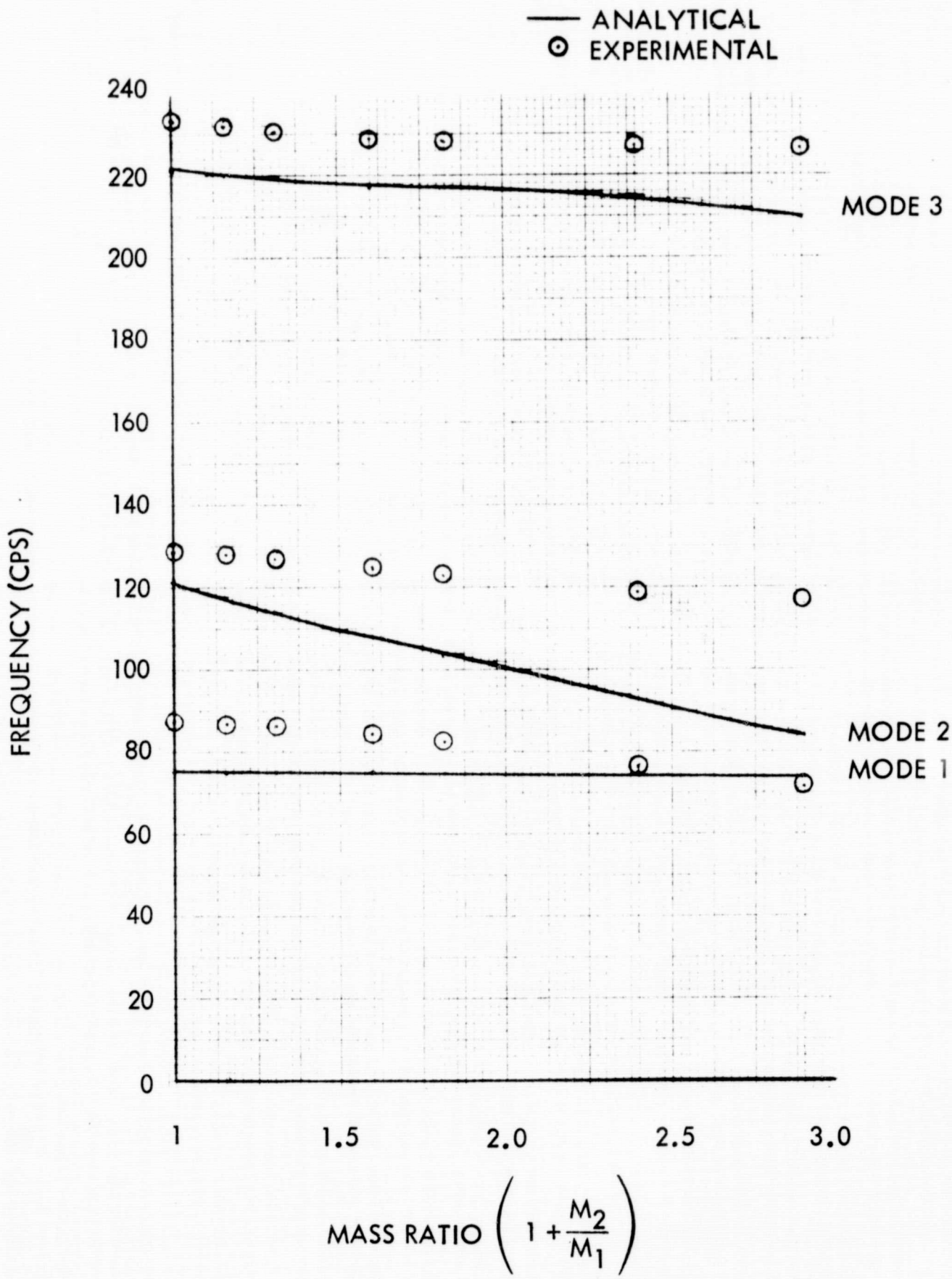


Figure 42. Comparison of Natural Frequencies of Shell I

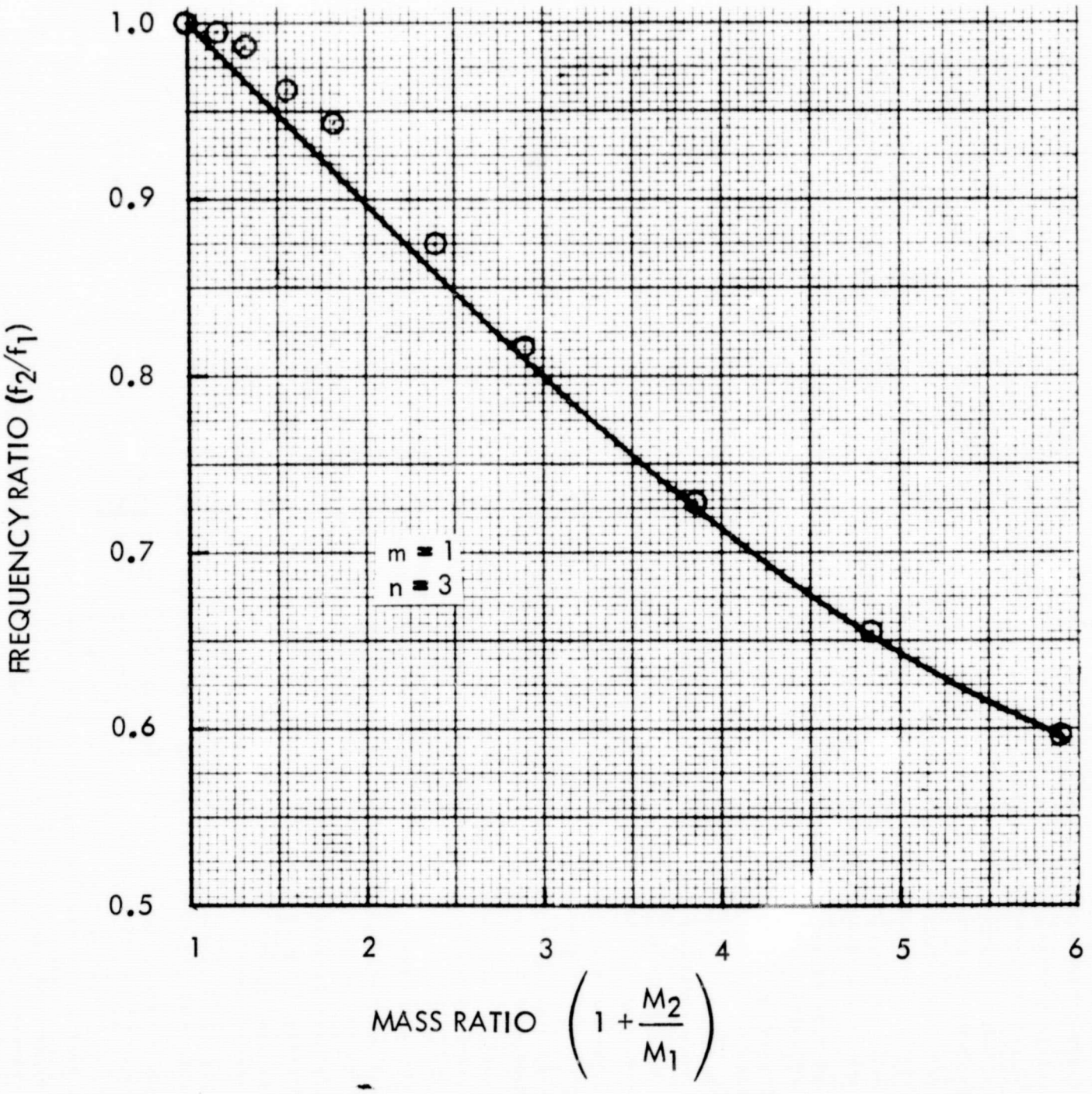


Figure 43. Mass-Loading Effect on Natural Frequencies of Shell I, Mode 1

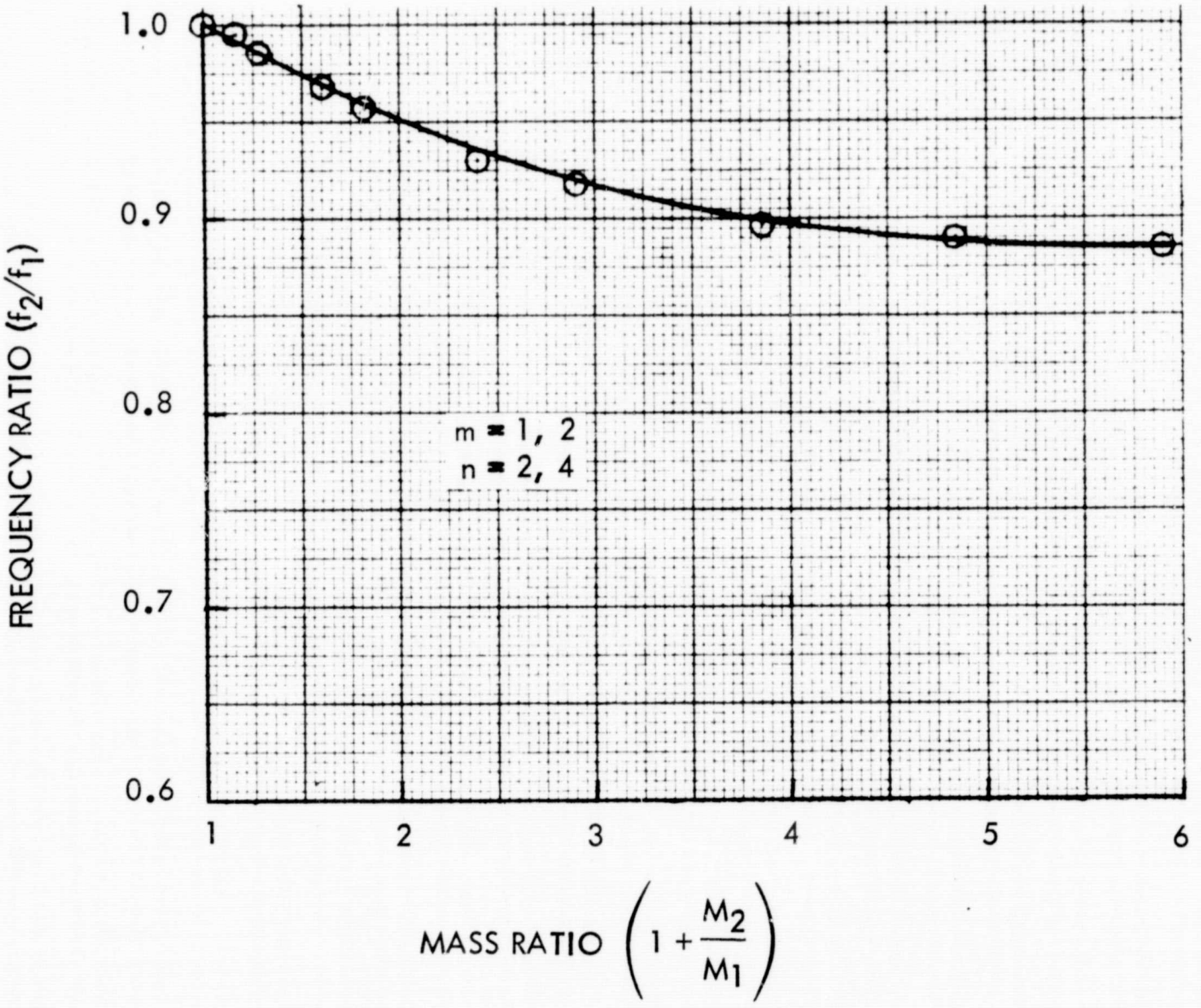


Figure 44. Mass-Loading Effect on Natural Frequencies of Shell I, Mode 2

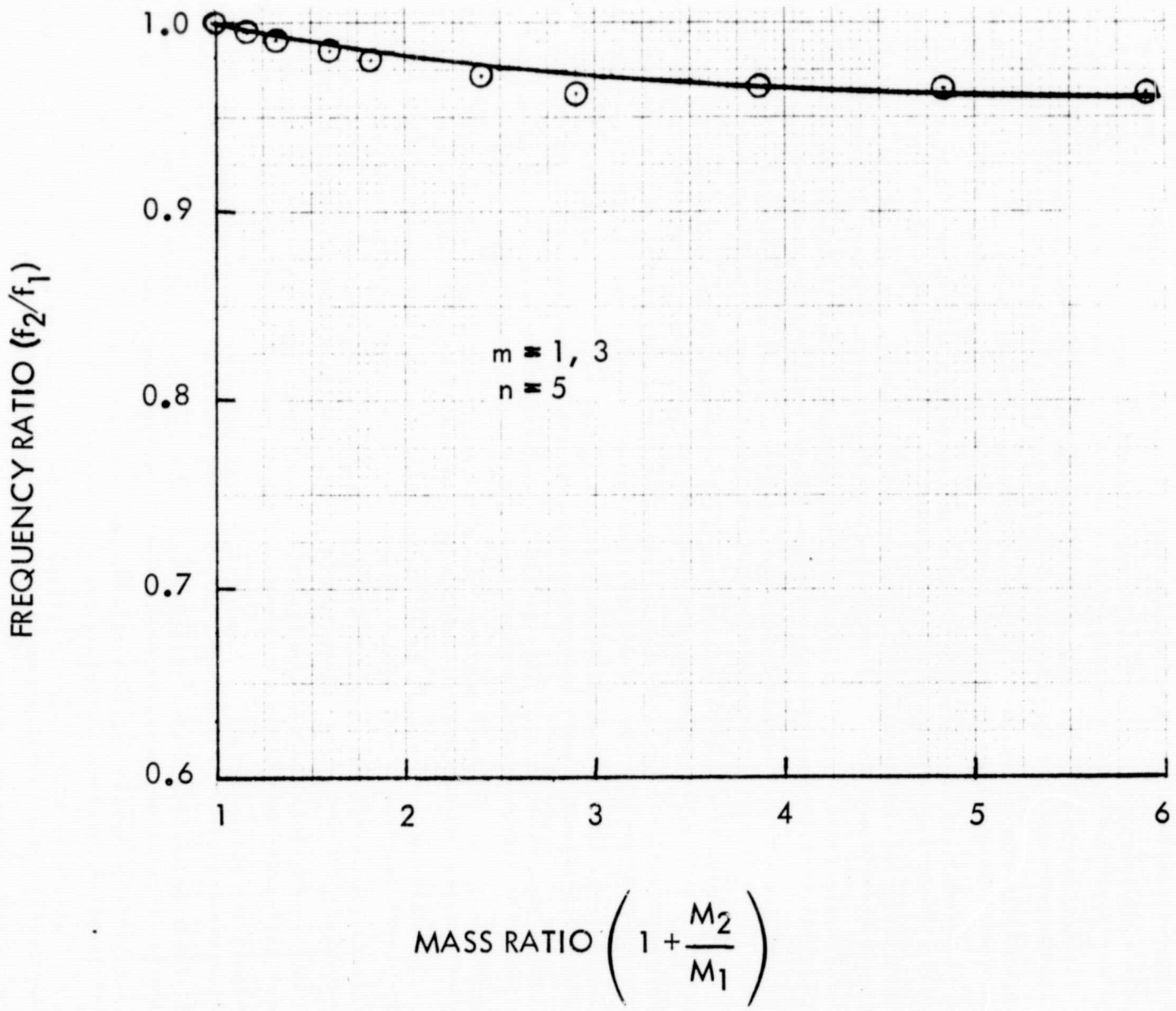


Figure 45. Mass-Loading Effect on Natural Frequencies of Shell I, Mode 3

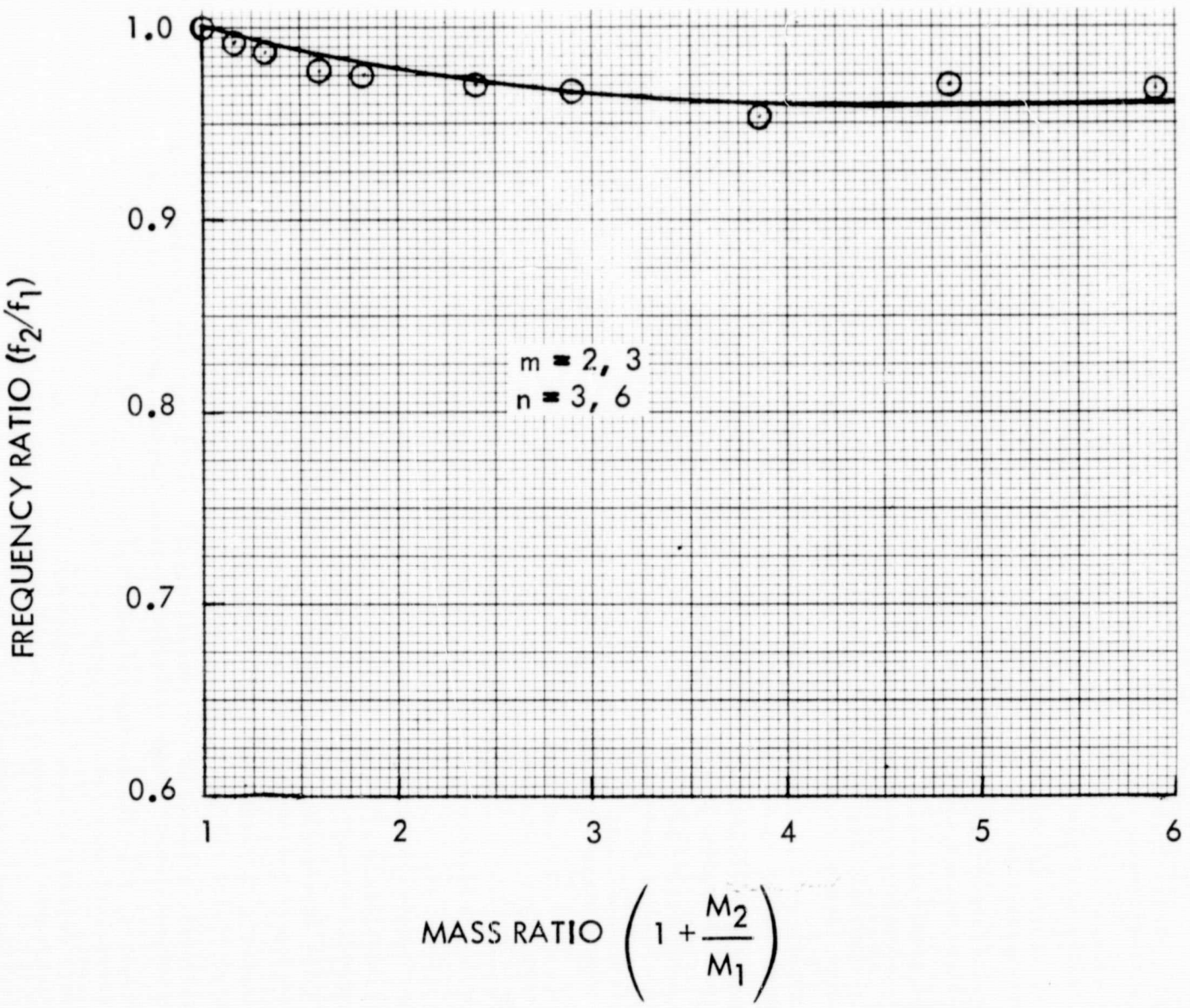


Figure 46. Mass-Loading Effect on Natural Frequencies of Shell I, Mode 4

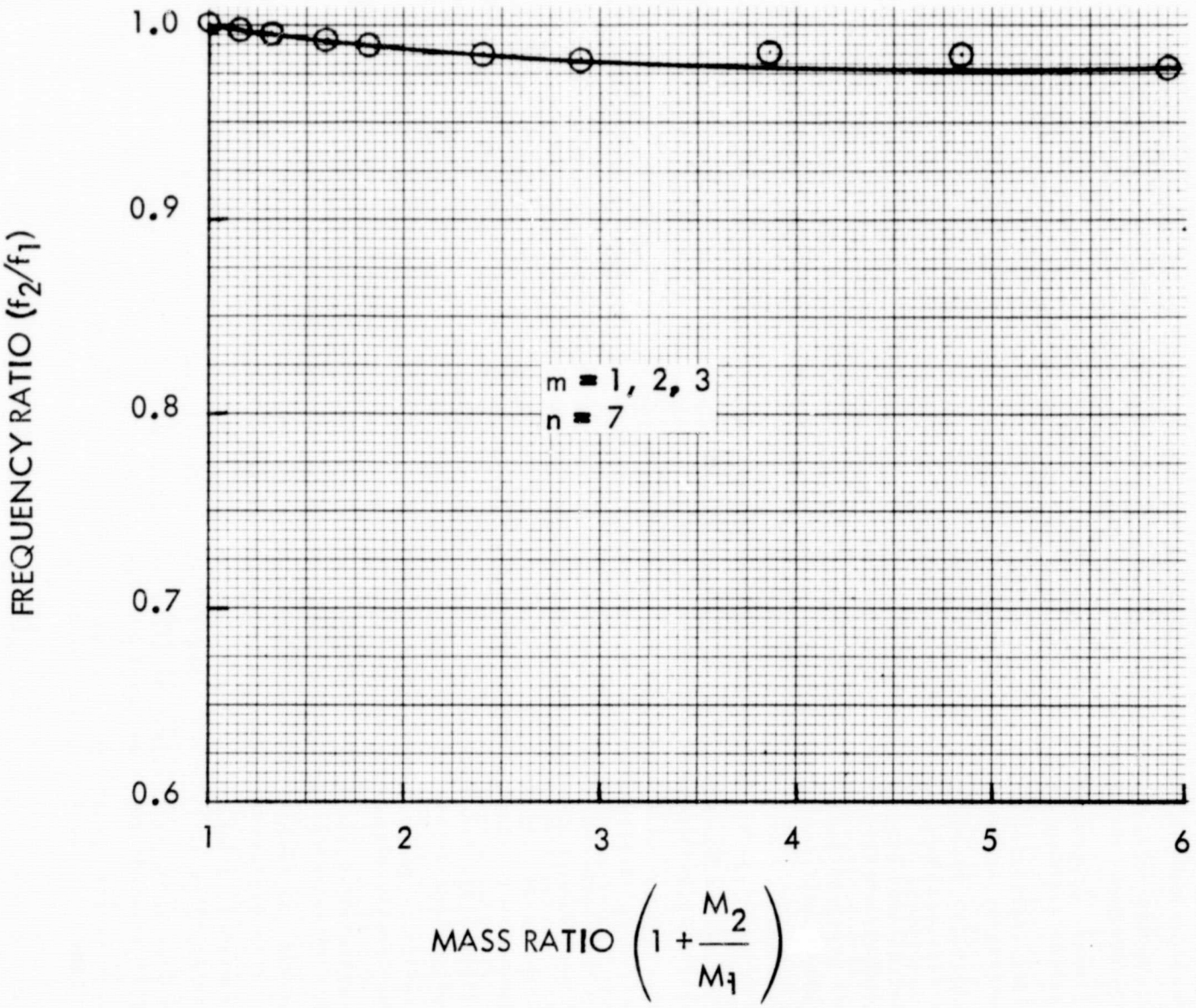


Figure 47. Mass-Loading Effect on Natural Frequencies of Shell I, Mode 5

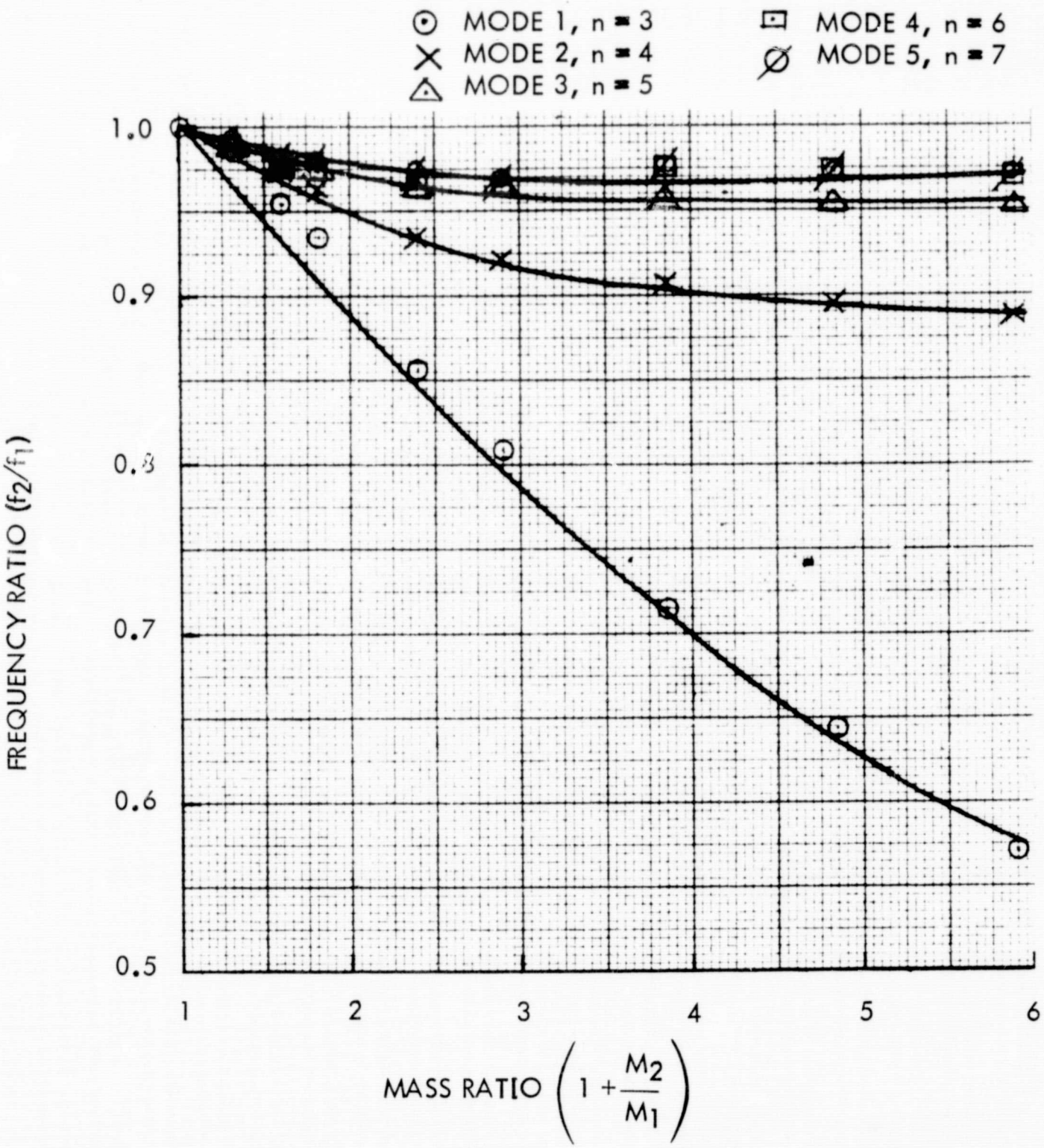


Figure 48. Mass-Loading Effect on Natural Frequencies of Shell II

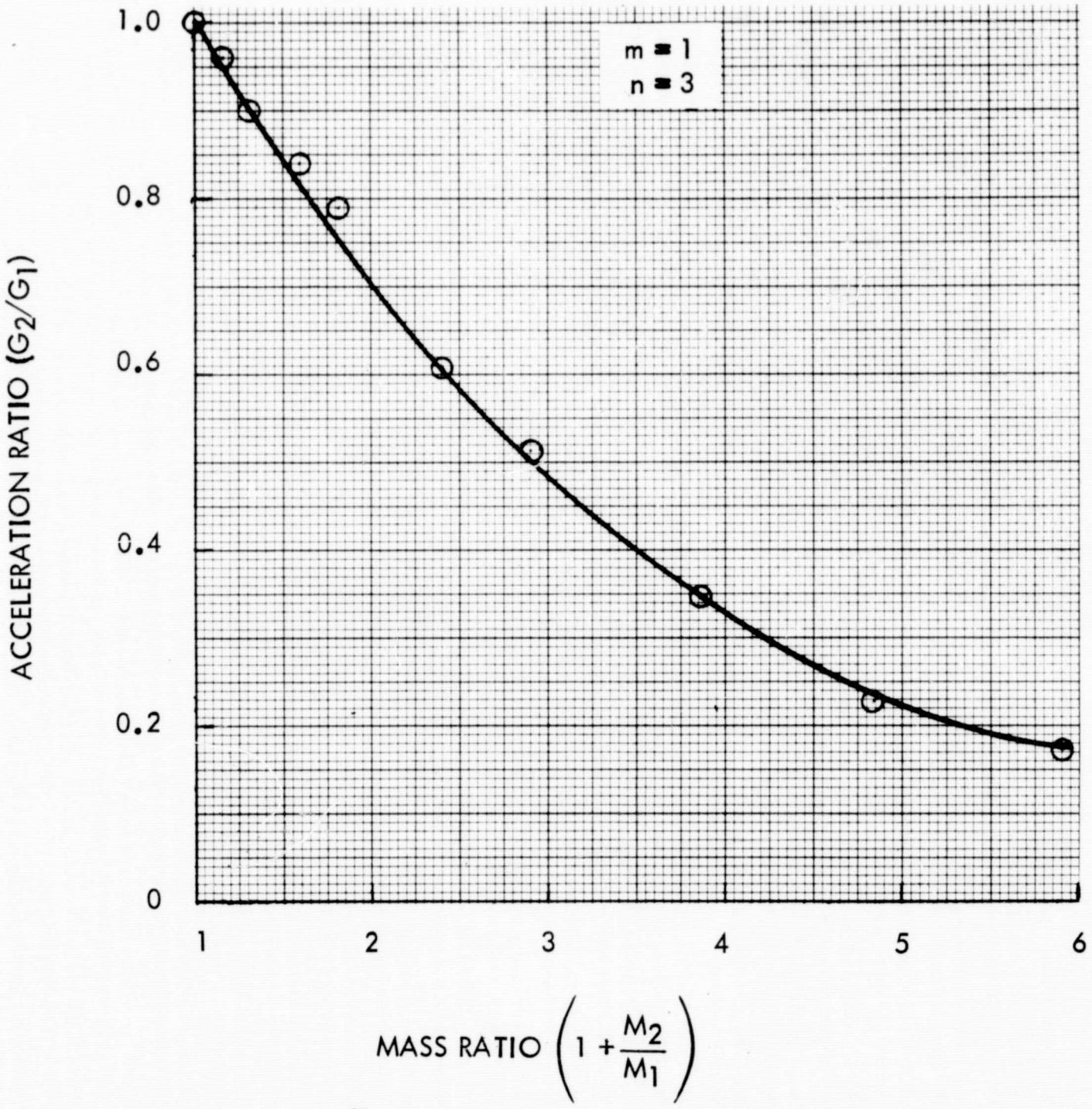


Figure 49. Mass-Loading Effect on Acceleration Response of Shell I, Mode 1

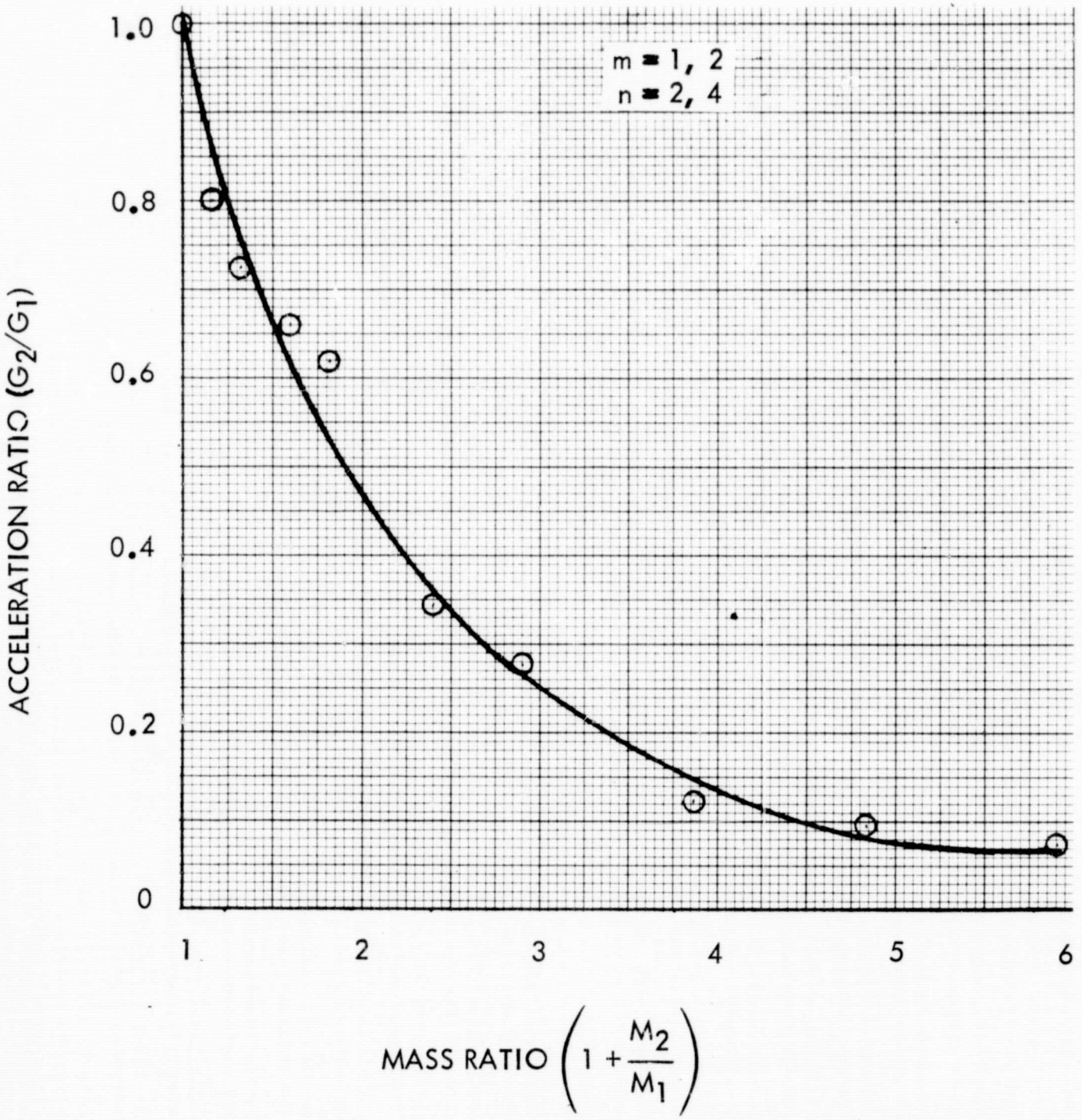


Figure 50. Mass-Loading Effect on Acceleration Response of Shell I, Mode 2

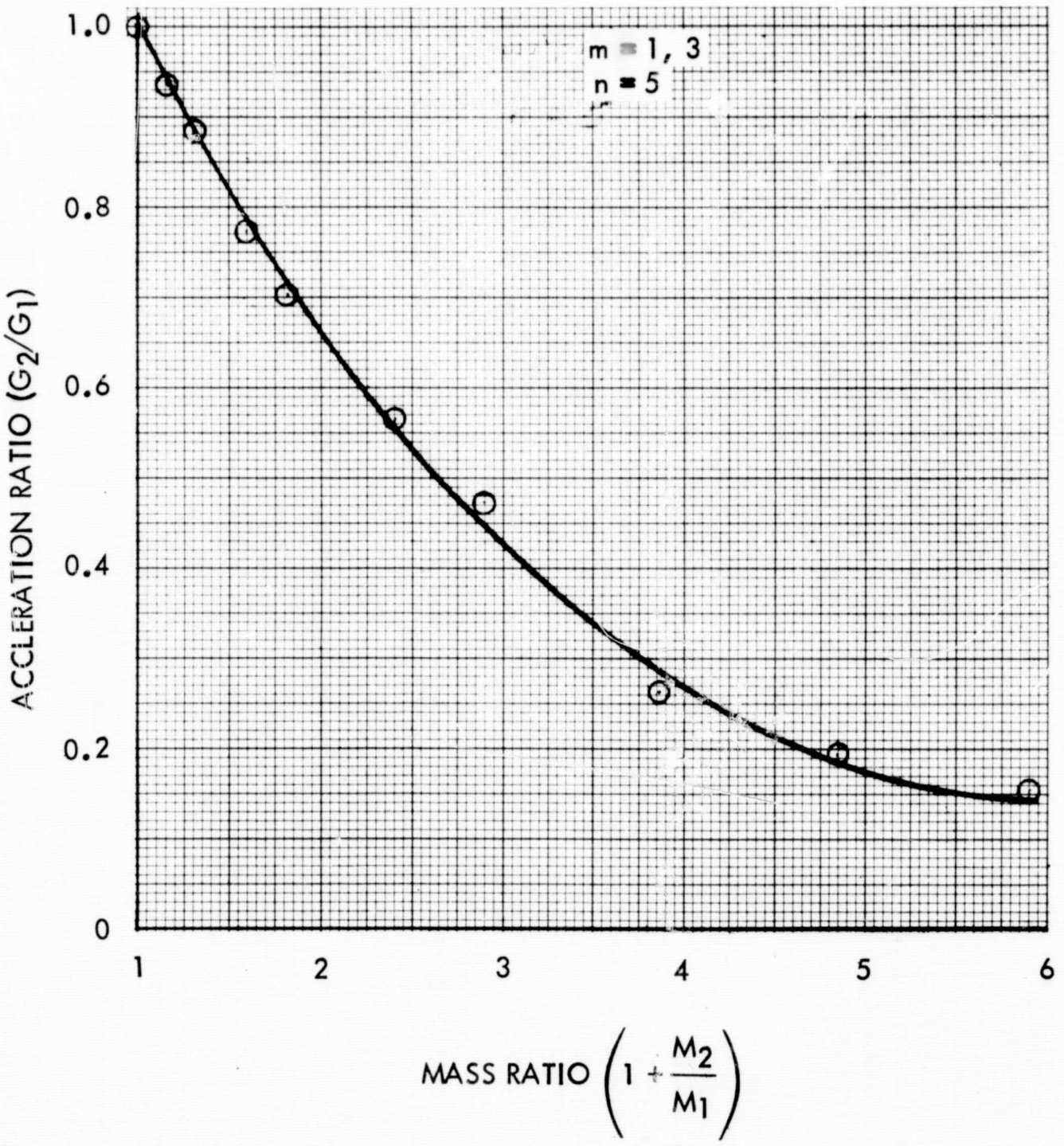


Figure 51. Mass-Loading Effect on Acceleration Response of Shell I, Mode 3

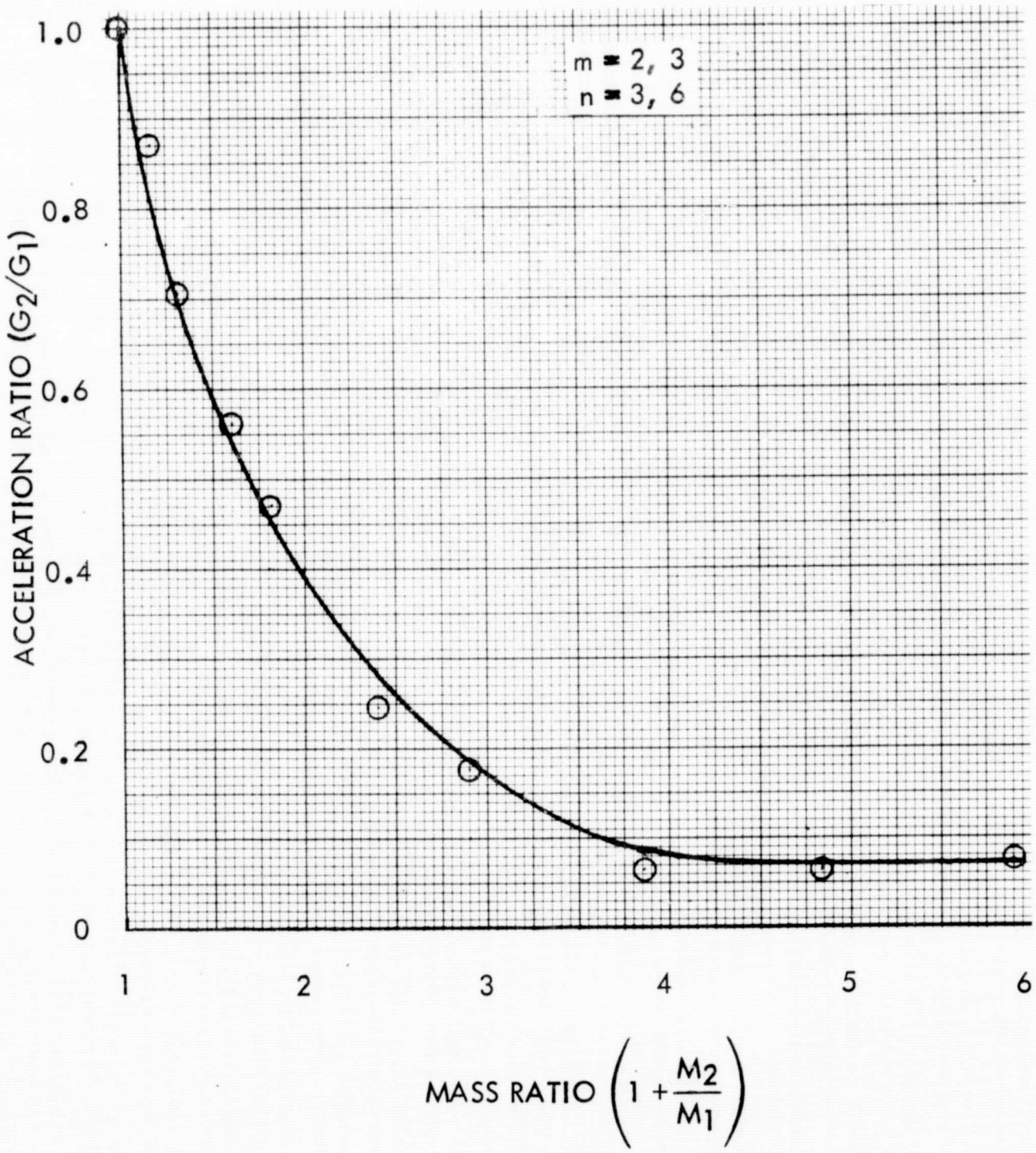


Figure 52. Mass-Loading Effect on Acceleration Response of Shell I, Mode 4

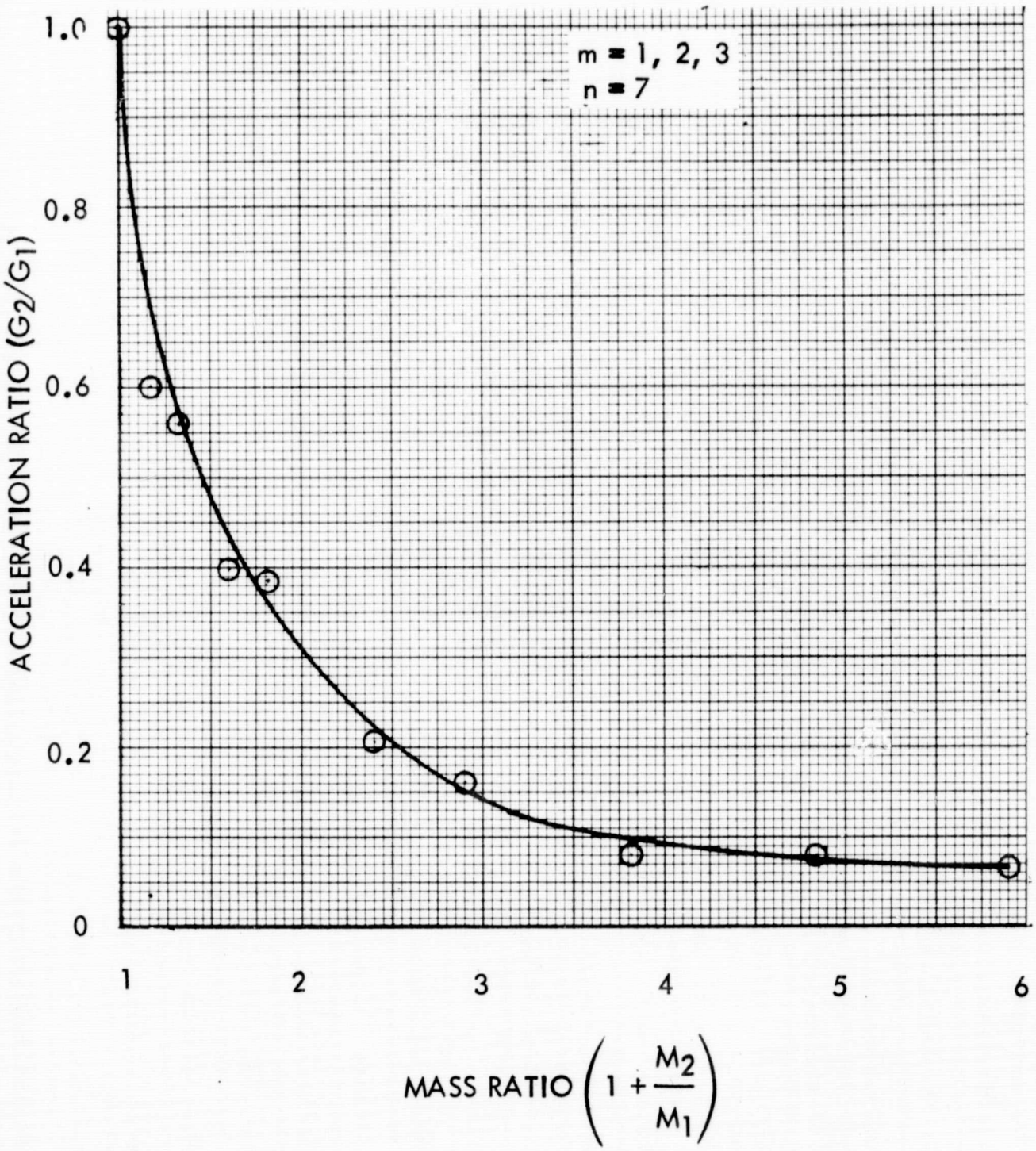


Figure 53. Mass-Loading Effect on Acceleration Response of Shell I, Mode 5

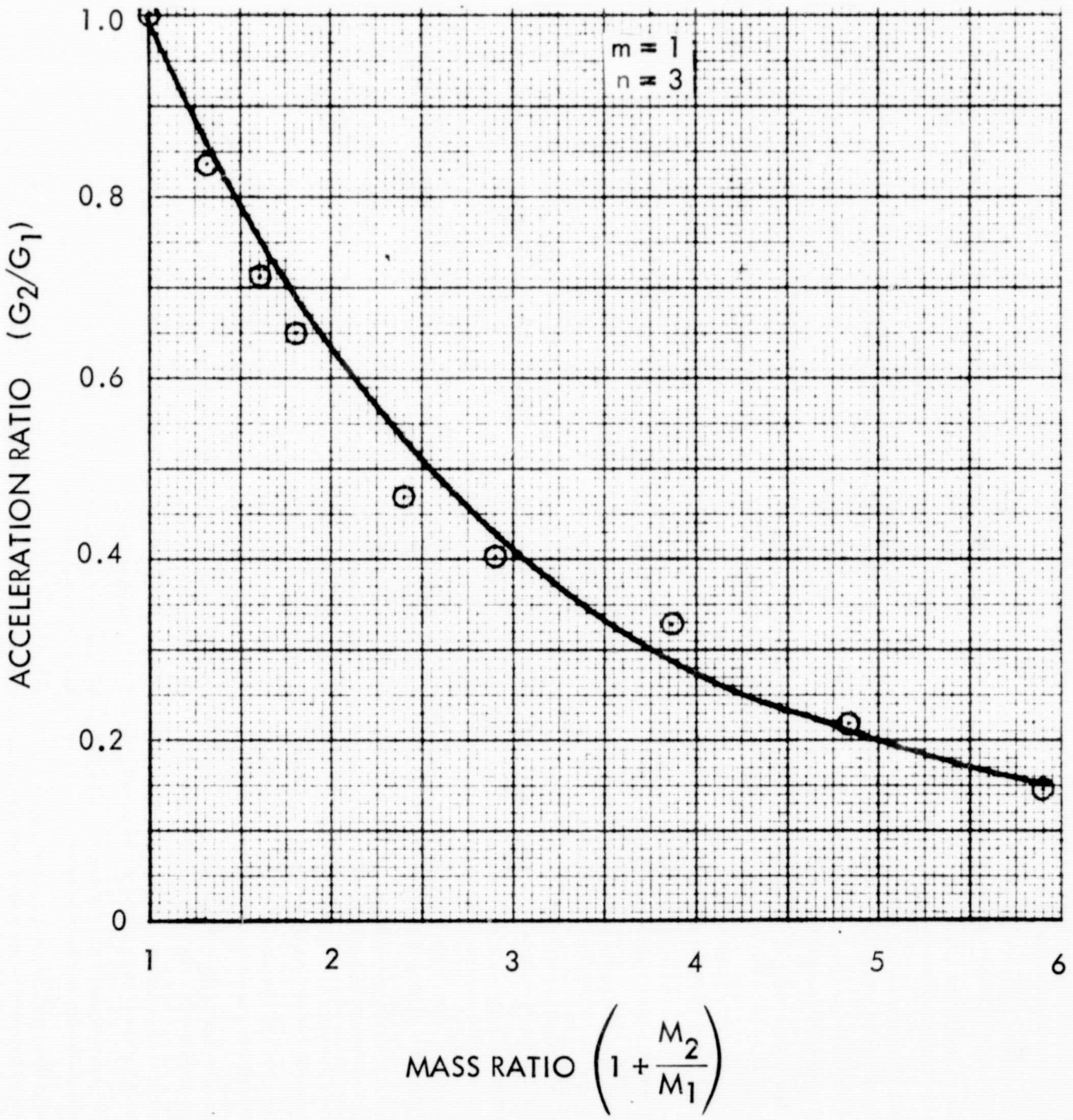


Figure 54. Mass-Loading Effect on Acceleration Response of Shell II, Mode 1

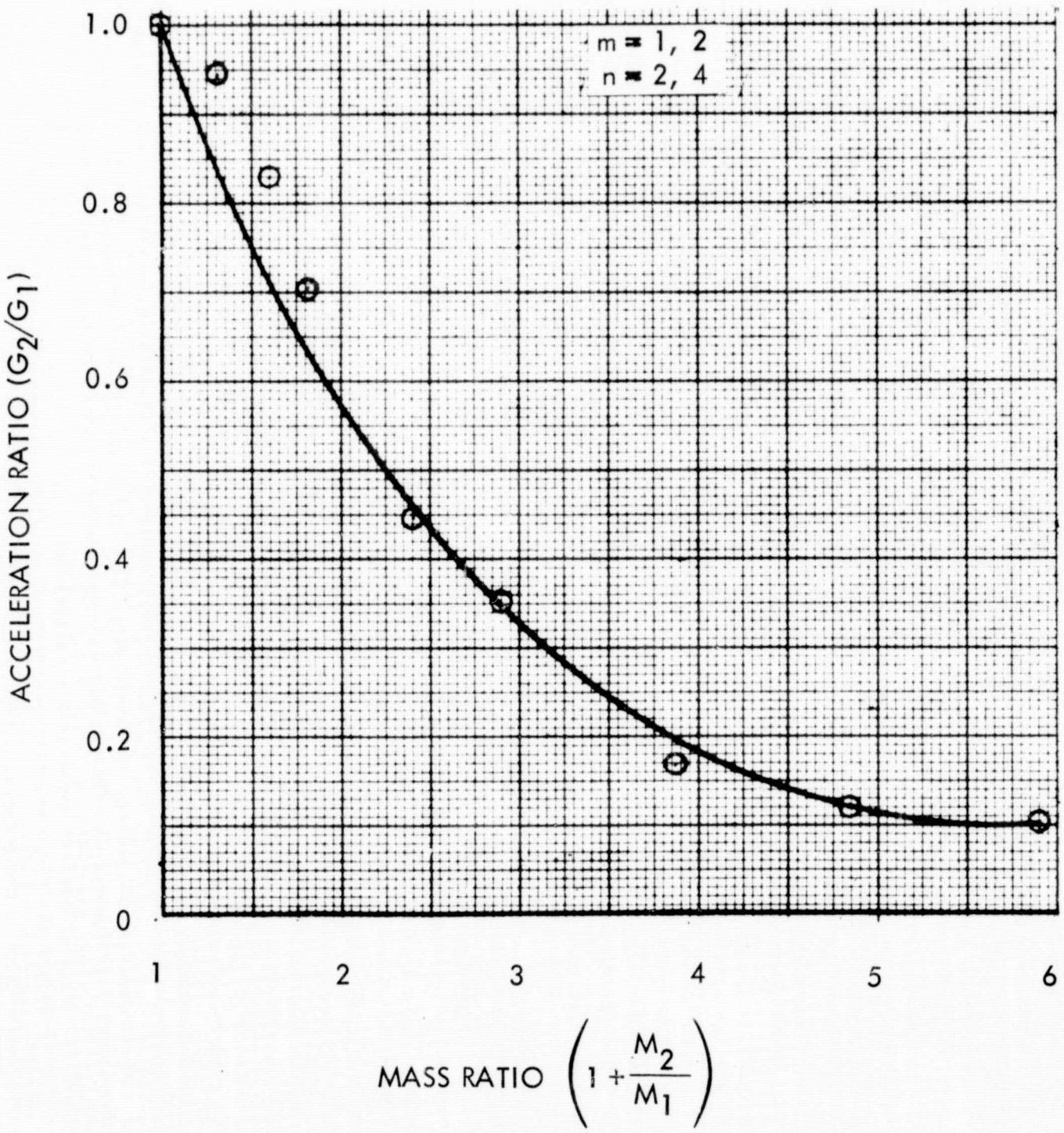


Figure 55. Mass-Loading Effect on Acceleration Response of Shell II, Mode 2

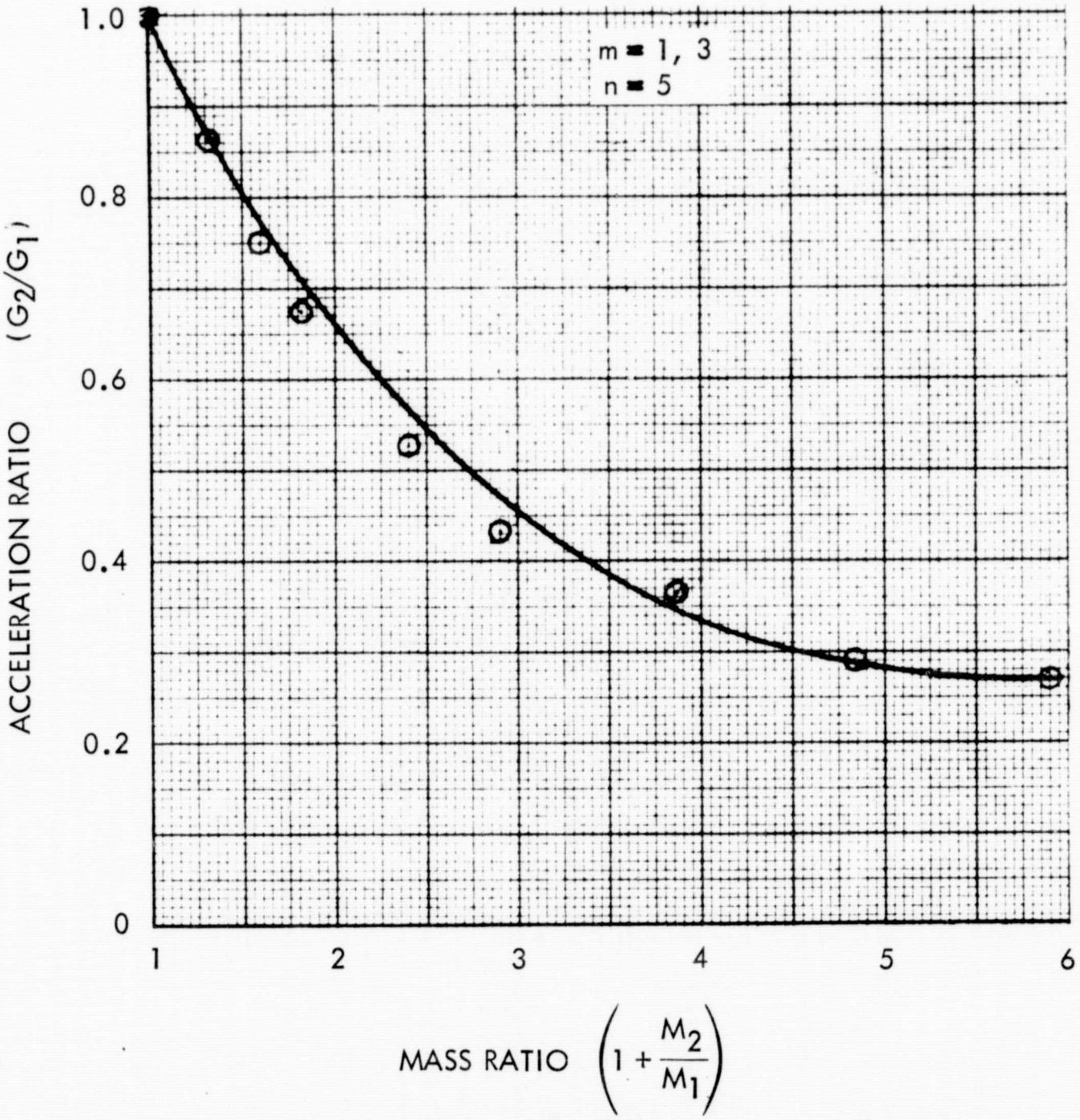


Figure 56. Mass-Loading Effect on Acceleration Response of Shell II, Mode 3

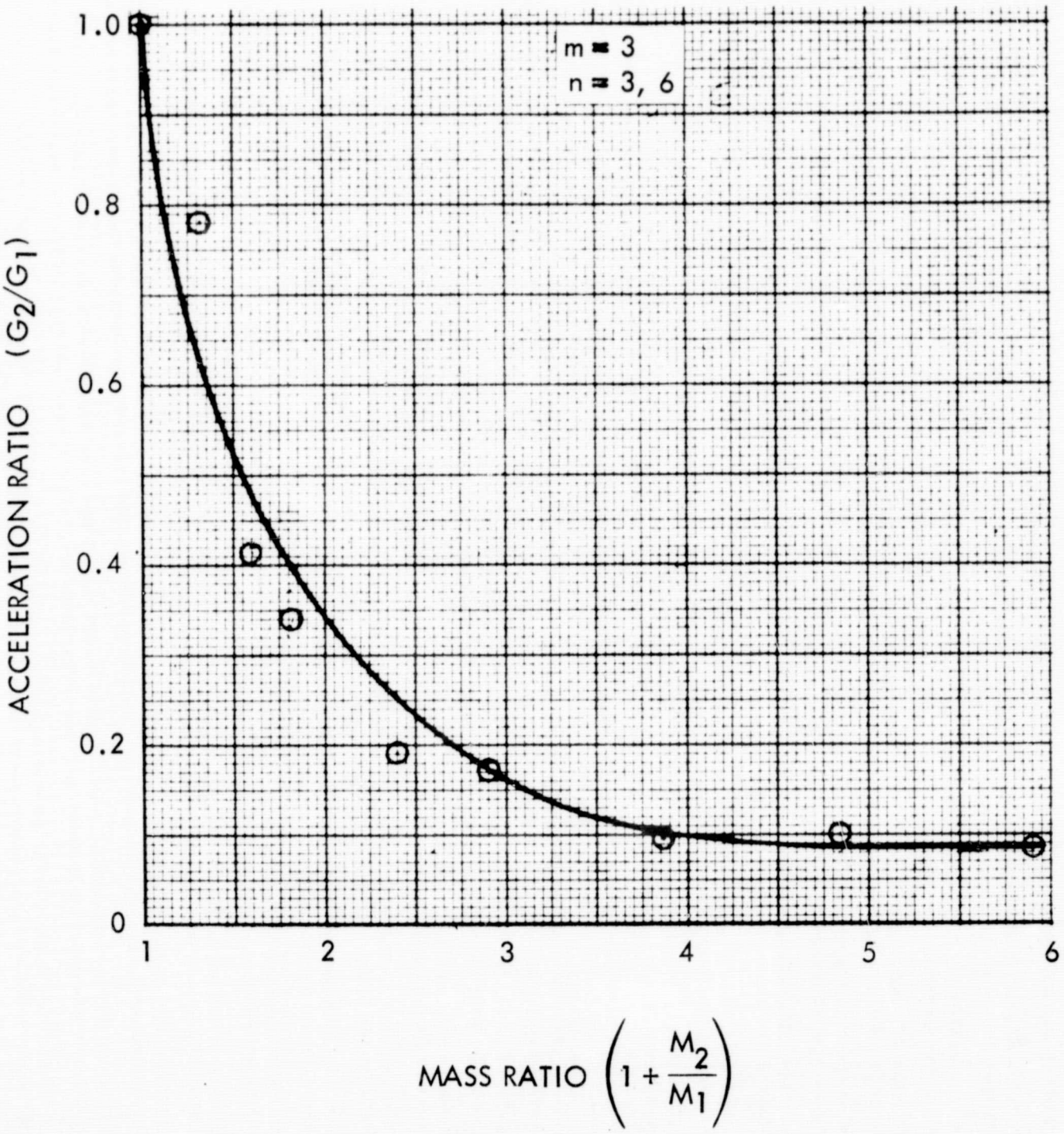


Figure 57. Mass-Loading Effect on Acceleration Response of Shell II, Mode 4

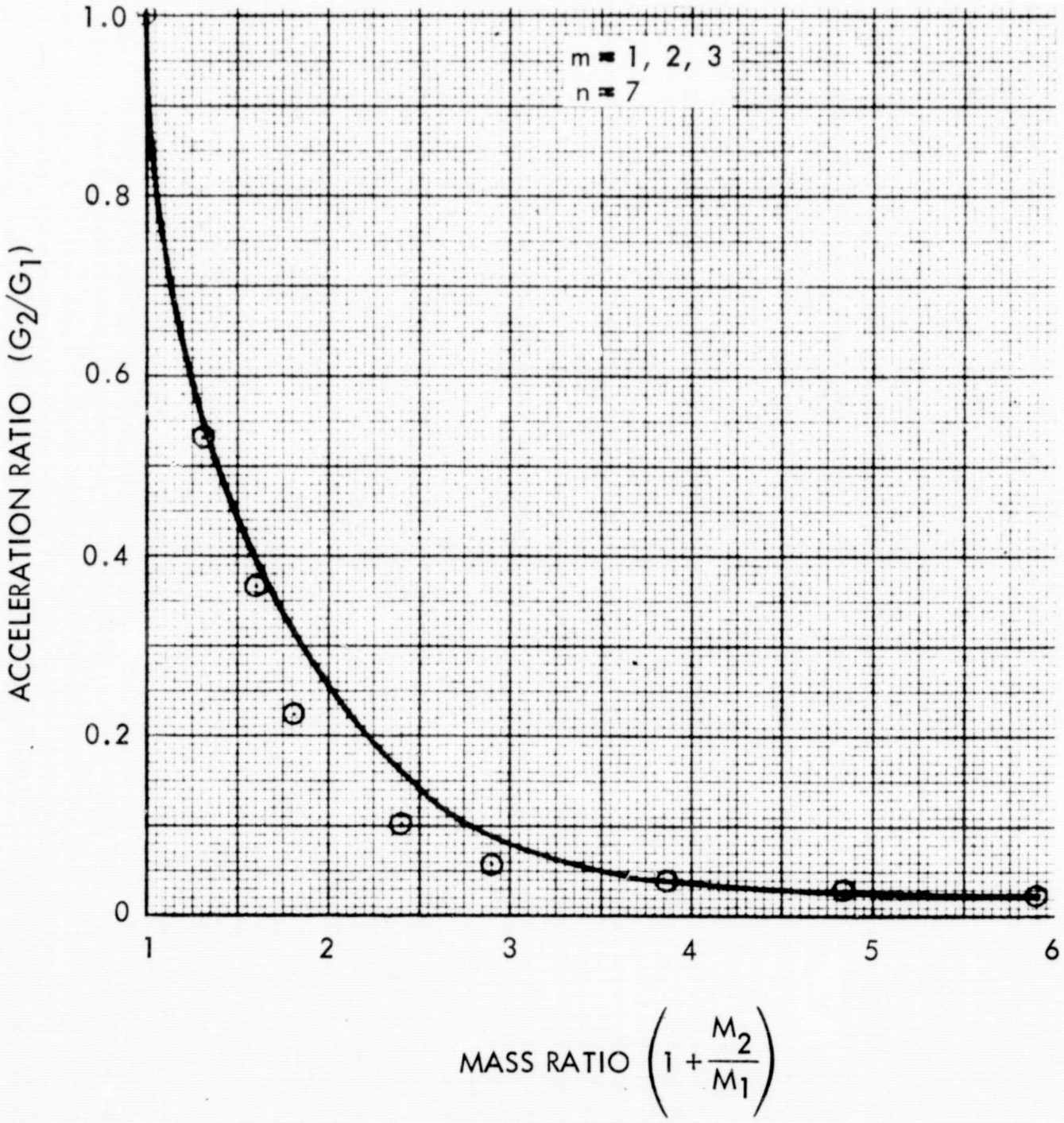


Figure 58. Mass-Loading Effect on Acceleration Response of Shell II, Mode 5

7.0 CONCLUSIONS

The analytical and experimental studies of the mass-loading effects on vibration of rings and shells can be summarized as follows:

1. Efficient methods have been developed for analyzing vibration of mass-loaded ring and shell structures.

2. Analytical results closely agreed with test data.

3. Frequency-shifts for mass-loaded rings and shells differed somewhat from those previously obtained in the Phases I and II of this program for the cases of beams and plates. Because of the motion of the mass interacted with the two- or three-dimensional motions of the support structures, the effect of mass loading on rings and shells caused a decrease in natural frequencies; however, for the higher modes, the frequency shifts became less significant as the attached mass increases. This information was presented in this report in the form of equations, tables, plots, and nondimensional graphs for various applications.

4. Transmissibilities and attenuations followed a trend similar to that of beams and plates, but possessed special characteristics. The results followed the equation $y = A + \frac{B}{Xn}$ which was previously established in Phases I and II of this program. The coefficients A, B, and n can be determined from the transmissibility plots in conjunction with firing test data and some consideration for design safety.

5. Mass loading also caused changes in mode shapes and disappearance of some modes at the mass mounting location; however, these phenomena of rings and shells deviated from that of beams and plates and were demonstrated by test data and computer solutions in this report.

6. The free vibration characteristics of mass-loaded shells can be solved analytically by the Fourier series-expansion technique,

which gives closed-form and nearly exact solution. This method required the use of four summations of the m n i j terms instead of only two summations of m n terms to describe the interacted motion.

7. Transfer matrix methods were efficient in calculating the lower frequencies of ring structures, while the finite-element method was good for both lower and higher frequencies. The transfer matrix method, however, offered a simple direct solution which provided a step-by-step insight into the solution and was helpful in the study of response characteristics.

8. The developed experimental and instrumentation techniques permitted continuous plotting of mode shapes and produced meaningful data for immediate evaluation during the test.

9. Sufficient data had been obtained for smaller mass ratios to better define the mass-loading phenomena.

As a general conclusion to the study, the trend of mass-loading effects on vibration of ring and shell structures has been established and the prediction methods have been developed; however, some refined studies and investigations for applications are needed and recommended as follows:

1. Refine the closed-form exact-solution technique for shell vibration analysis.

2. Further define the analysis of mass-loading effects on modal characteristics of shell structures.

3. Investigate the finite-element technique for obtaining an approximate solution for shell vibration.

4. Apply results to solve bracketry problems, definition of support structures, design of local structures, and test and evaluation of components.

5. Further refine the experimental technique.

6. Simplify the analytical solution, and reduce the mathematical complexity for further development in the definition of the basic mass-loading mechanism.

7. Extend the developed method to solve vibration problems of complicated shell structures loaded with bulkheads, propellants, ring frames, longerons, and a variety of discrete masses.

REFERENCES

1. Lee, S. Y. Shock and Vibration Analysis of Structures. Mechanical Engineering Department, University of Southern California, Research Report ME 590 (1959).

2. Lee, S. Y. Sonic Induced Vibration and Control for Advanced Spacecraft. Presented at the 65th Meeting of Acoustical Society of America, May 15-18, 1963, New York.

3. Lee, S. Y. Vibration Environment and Design Development Program. North American Rockwell Space Division, Report SD 62-74 (May 1962).

4. Lee, S. Y. Test Results of Mass-Loading and Coupling Investigation. North American Rockwell Space Division, Dynamic Sciences Internal Report (June 1963).

5. Lee, S. Y. and M. Chapman. Technical Proposal for a Study of Mass Loading Effects on Localized Vibratory Environments of Rocket Vehicles. North American Rockwell Space Division, Report SID 64-2180-1 (December 1964).

6. Lee, S. Y. The Mass-Loading and Mass-Coupling Effects on Vibration Response. University of Southern California, Research Report AE590 (1959-1962).

7. Lee, S. Y. Extension of Study of Mass Loading Effects on Localized Vibratory Rocket Vehicle Environments. North American Rockwell Space Division, Report SID 66-319 (March 1966).

8. Lee, S. Y. Further Study of Mass-Loading Effects of Localized Vibratory Rocket Vehicle Environments. North American Rockwell Space Division, Report SID 66-1284 (5 August 1966).

9. Lee, S. Y. Analytical and Experimental Determination of Localized Structure to be Used in Laboratory Testing of Shell Structure Mounted Components. North American Rockwell Space Division, Report SID 64-2081 (7 December 1964).

10. Lee, S. Y. A Study of Axial Transmissibility Characteristics for Typical Rocket Vehicle Structures. North American Rockwell Space Division, Report SID 63-1496 (7 January 1964).

11. Lee, S. Y. Mass Loading Effects on Vibration of Honeycomb Plates. North American Rockwell Space Division, Report SD 67-605 (21 June 1967).

12. Lee, S. Y. and S. S. Tang. Mass Loading Effects on Localized Vibratory Environments of Rocket Vehicles. North American Rockwell Space Division, Report SID 66-1201 (20 July 1966).

13. Lee, S. Y., Tang, S. S. and J. G. Liyeos. Axial Transmissibility Characteristics of Typical Multi-Stage Rocket Vehicle Structures. North American Rockwell Space Division, SID 67-604 (28 June 1967).

14. Mahaffey, P. T. and Smith, K. W. Methods for Predicting Environmental Vibration Levels in Jet Powered Vehicles, Noise Control. (July-August 1960).

15. Eldred, K., Roberts, W., and R. White. Structural Vibrations in Space Vehicles. WADD TR 61-62 (December 1961).

16. Franken, P. "Sound Induced Vibration of Cylindrical Vehicles," J. Acou. Soci. of America, Vol. 34, No. 4 (April 1962).

17. MIL-STD-810 Dynamic Conference; USAF-ASD Wright-Patterson Air Force Base, Ohio (September 1960).

18. Schock, R. W., et al. Vibration, Acoustic, and Shock Environmental Specifications for Saturn Vehicles. NASA Internal Notes (1964-1966).

19. Barrett, R. E. Statistical Techniques for Describing Localized Vibratory Environments of Rocket Vehicles. NASA/MSFC, NASA TN D-2158 (July 1964).

20. Jewell, R. E. "A Technique for Predicting Localized Vibration Environments in Rocket Vehicles and Spacecraft," Shock and Vibration Bulletin No. 33, Part II (March 1964), pp. 26-33.

21. Lifer, C. E. "Design of Space Vehicle Structures for Vibration and Acoustic Environments," Shock and Vibration Bulletin No. 33, Part IV (March 1964), pp. 201-207.

22. Barrett, R. E. Techniques for Predicting Localized Vibratory Environments of Rocket Vehicles. NASA TN D-1836 (Oct. 1963).

23. MAC Staff. Summary of Random Vibration Prediction Procedures. NASA-CR, NASA/MSFC, Huntsville, Alabama, 1968.

24. Pestel, E. C., F. A. Leckie. Matrix Methods in Elasto Mechanics. McGraw-Hill Book Co. (1963).

25. Martin, H. C. Introduction to Matrix Methods of Structural Analysis. McGraw-Hill Book Company (1966).

26. Zienkiewicz, O. C. The Finite Element Method in Structural and Continuum Mechanics. McGraw-Hill Book Company (1967).

27. Przemieniecki, J. S. Theory of Matrix Structural Analysis. McGraw-Hill Book Company (1968).

28. Guyan, R. J. "Reduction of Stiffness and Mass Matrices," J. AIAA, 3, No. 2 (1965) p. 380.

29. Arnold, R. N. and G. B. Warburton. "Flexural Vibrations of the Walls of Thin Cylindrical Shells Having Freely Supported Ends," Proc. Roy. Soc. A197 (1949).

30. Arnold, R. N. and G. B. Warburton. "The Flexural Vibration of Thin Cylinders," Proc. Inst. Med. Engr. A 167 (1953).

31. Weingarten, V. I. "Free Vibration of Thin Cylindrical Shells," AIAA J., V2N4 (April 1964).

PRECEDING PAGE BLANK NOT FILMED.

APPENDIX

PROPERTIES OF THE RING ELEMENT AND ATTACHED MASS

MASS OF RING ELEMENT (FIGURE A-1)

$$m = R \Psi A \frac{\gamma}{g}$$

$$= R \Psi h L \frac{\gamma}{g}$$

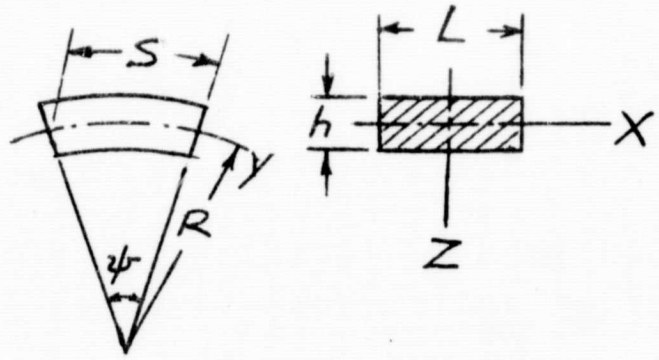


Figure A-1. Geometry of Ring Element

MASS MOMENT OF INERTIA OF RING ELEMENT

$$I_X = \int_V \left(y^2 + z^2\right) dm$$

$$= \frac{\gamma}{g} \int_V \left(y^2 + z^2\right) dx\, dy\, dz$$

$$= \frac{\gamma L h s}{12 g} \left(h^2 + s^2\right)$$

$$= \frac{m}{12} \left(h^2 + R^2 \Psi^2\right)$$

AREA MOMENT OF INERTIA OF RING ELEMENT

$$J_x = \frac{L}{12} h^3$$

MASS MOMENT OF INERTIA OF ATTACHED MASS

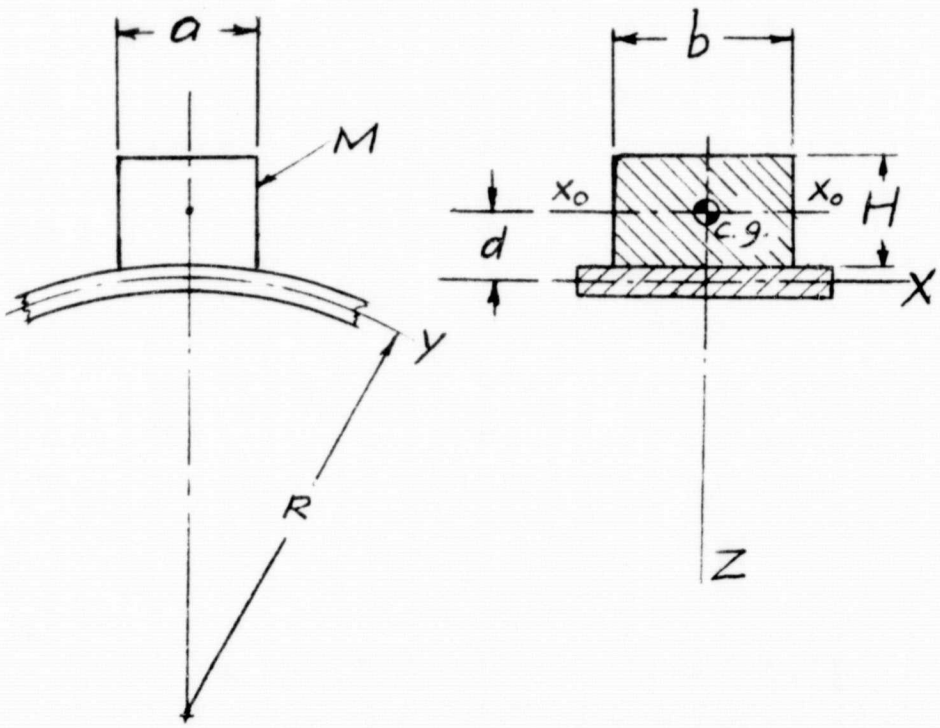


Figure A-2. Geometry of Attached Mass

$$I_{x_o} = \bar{I} + M d^2$$

where I = mass moment of inertia of M about x_o x_o, an axis through c. g. and parallel to x-axis. (Figure A-2)

d = distance between c. g. and x-axis.

For a rectangular solid mass of size a x b x H,

$$\bar{I} = \frac{M}{12}\left(H^2 + a^2\right)$$

$$d = \frac{1}{2}(H + h)$$

Hence,

$$I_{x_o} = \frac{M}{12}\left(H^2 + d^2\right) + \frac{M}{4}\left(H + h\right)^2$$

$$= \frac{M}{12}\left(H^2 + a^2\right) + 3(H + h)^2$$

AREA MOMENT OF INERTIA OF ATTACHED MASS

$$J_{x_o} = \bar{J} + A_o\, d^2$$

where J = area moment of inertia about $x_o\, x_o$ Figure
For a rectangular solid mass,

$$A_o = b\,H, \qquad d = \frac{(H + h)}{2}, \qquad \bar{J} = \frac{b\,H^3}{12}$$

then

$$J_{x_o} = \frac{b\,H^3}{12} + b\,H\left(\frac{H + h}{2}\right)^2$$

$$= \frac{b\,H}{12}\left[\, H^2 + 3(H + h)^2 \,\right]$$